

The Age and Origin of the Western Ethiopian Shield

Thesis submitted in accordance with the requirements of the
University of Adelaide for an Honours Degree in Geology

Morgan Blades

November 2013



THE UNIVERSITY
of ADELAIDE

THE AGE AND ORIGIN OF THE WESTERN ETHIOPIAN SHIELD

ABSTRACT

Western Ethiopia is made up of a range of supra-crustal and plutonic rocks. The Precambrian exposures of the Western Ethiopian Shield are positioned within the juvenile Neoproterozoic crust of the Arabian Nubian Shield and the older, predominately gneissic Mozambique Belt (Woldemichael et al. 2010). The age and origin of the Western Ethiopian Shield are still largely unidentified. The aim of this paper is to constrain the age and origin of the sedimentary and igneous rocks within the Western Ethiopian Shield.

This will be done using isotopic techniques. The detrital zircons have been analysed for U-Pb age (yielding maximum depositional ages and age provenance information) and Hf isotopes (to investigate the nature of zircons). Geochemical analysis on the Thermal Ionisation Mass Spectrometer (TIMS), Inductively Coupled Plasma Mass Spectrometry (ICP-MS) and microprobe has also been undertaken. One of the focuses is the examination of the volcanic and volcanoclastic successions, as well as, the geochemical nature of the ultra-mafic bodies in the Shield. The geochemistry of metavolcanic and meta-volcanoclastic data suggest that the origin of the volcanics formed in an arc-like setting. Relatively low niobium; however, suggest that the mantle source may have been more enriched than that seen in modern volcanic arcs. Detrital zircons, obtained from a meta-sandstone, yielded provenance age peaks at ~2499 Ma, ~1855 Ma and between 1100-800 Ma and a maximum depositional age of 838 ± 13 Ma. Hf Isotopes from the same zircons demonstrated that both the oldest and youngest populations have broadly juvenile Hf isotopic values however; ~1820 Ma age shows significantly evolved Hf isotopic values. A minimum age constraint on the deformation was provided by the U-Pb age of 572.6 ± 7.6 Ma and yielded whole epsilon Nd values of 3.74 and epsilon Hf values of 6.79-7.98, demonstrating a juvenile origin.

A significant aspect of the Arabian-Nubian Shield is the interpretation of the N-S oriented regional shear zones. Concentrically zoned mafic/ultramafic bodies, previously identified as remnants of the oceanic crust, are suggested to be Alaskan-type intrusions. Though chemically different to typical Alaskan-type intrusions these display a subduction affinity and have close associations to shear-zone hosted intrusions elsewhere in the Arabian Nubian Shield. Thus, they have been interpreted as being formed in similar supra subduction intrusive settings.

KEYWORDS

Western Ethiopian Shield, Geochronology, Geochemistry, Chrome Spinel

SUPPLEMENTARY TABLE OF CONTENTS

The age and origin of the Western Ethiopian Shield	1
Abstract	1
Keywords	1
Introduction.....	6
Geological Setting/Background	7
East African Orogen	7
Western Ethiopia:	9
Methods.....	12
U–Pb zircon dating.....	12
Hafnium Isotope determination.....	12
Radiogenic Isotope Geochemistry.....	13
Major Element Geochemistry using the X-Ray Fluorescence (XRF).....	14
Minor trace Element Geochemistry using the XRF	14
Trace element Geochemistry ICP-MS.....	15
Chrome Spinel Analysis	15
⁴⁰ Argon - ³⁹ Argon dating	15
Observations and Results	17
U-Pb Geochronology.....	17
Zircon HF Isotopes	21
Geochemistry.....	22
Radiogenic Isotopes.....	24
Trace Element analysis.....	24
Chrome spinel Analysis	30
⁴⁰ Argon - ³⁹ Argon dating	31
Discussion.....	32
Age and Origin of plutonic sequences in the WES	32
Nature of the rocks of Western Ethiopian Shield	32
Age and Provenance Significance of Metasediment in the Western Ethiopian Shield.	33
Significance of the Yubdo-Tulu Dimtu Ultra-mafics.....	34
Tectonic Setting of the Western Ethiopian Shield.....	37
The Western Ethiopian Shield in the East African Orogen.....	37
Conclusions	39
Acknowledgments.....	40
References.....	41
Appendix A:.....	44

- Figure 1: a) Palaeogeographic reconstruction at 630 Ma. Green represents continental plates delineated from the map. The blue dot shows where the Western Ethiopian Shield is situated. Abbreviations are as follows Amazon=Amazonia; Aus-Maw=Australia/Mawson Block; Az=Azania; Congo=Congo/Tanzania/Bangweulu Block; Kal=Kalahari Block; Laur=Laurentia; RP=Rio de la Plata; SF=São Francisco; WA=West Africa. Adola, Adamastor, Braziliano, Mozambique =oceanic basins. Taken from (Collins and Pisarevsky 2005). b) This is taken from Fritz et al. (2013) shows the location of the Azanian plate in conjunction to Ethiopia.....8
- Figure 2: Simplified geological map of Western Ethiopia. Area of study has been highlighted with the use of a box. Taken and adapted from (Tadesse and Allen 2004) 10
- Figure 3 Location map for samples taken from Ethiopia. The map in the top right hand corner depicts Ethiopia on a country scale showing its proximity to the Afar triple junction, with Gimbi as a reference point on both maps. 11
- Figure 4: U–Pb Concordia graph illustrating zircons analysed from the Ganjii monzogranite (E13.12) collected from the Western Ethiopian Shield. The weighted mean $^{206}\text{Pb}/^{238}\text{U}$ age of all analyses except a single young analysis at 572.6 ± 7.4 Ma, that is interpreted to represent Pb loss in the modern environment. 18
- Figure 5) Probability density plot for sample E13.24a (meta-quartz arenite). $^{206}\text{Pb}/^{207}\text{Pb}$ ages are used when ages are over 1 Ga. $^{206}\text{Pb}/^{238}\text{U}$ ages are used when the age is less than ~1 Ga. The histogram shows the number of analyses per peak for E13-24a. This demonstrates the presence of detrital zircons at ~2499 Ma, ~1855 Ma and between 1100-800 Ma 18
- Figure 6: U-Pb Concordia diagrams constructed with a 2 sigma data point error ellipses. a) U-Pb Concordia of all zircons (n=13), which were sourced from a meta quartz arenite (E13-24a). The colour scale on the right of the graph depicts uranium concentration of individual zircons. (b-c) focuses on individual clusters. b shows that there are rocks in the source region with ages at ~820 Ma and ~1000-1100 Ma. c demonstrates that there is a population of detrital zircons at ~1850. 19
- Figure 7 CL images for E13.12, a Ganji Granite and E13.24a, a meta-quartz-arenite, taken from Western Ethiopia. E13.12 They have a prismatic shape typical of igneous zircons. The low response (dark) suggests a higher uranium content. Zircons show oscillatory zoning typical of formation in a magma chamber. E13.24a These have a typical irregular and partially rounded detrital shape. The low response (dark) suggesting higher uranium content. s. Apatite and titanate are abundant within this sample. 20
- Figure 8: ϵHf_t versus age plot. The purple dots represents sample E13.12, a monzogranite. The green line along the x-axis represents CHUR. The red line represents the depleted mantle. The blue dots represent zircons from E13.24a meta quartz-arenite. This shows three distinct populations the oldest and youngest being of juvenile nature. The population at ~1800 Ma is more evolved suggesting that addition of a continental influence..... 22
- Figure 9 a) E13.11 taken from Daleti Quarry. Note the alignment of the chrome/magnetite spinel grains. b) Sample location of E13.12 the Ganjii Granite c) represents the Abshala Mélange where E13.18 and 19 were sampled from. 23
- Figure 10 ϵNd_t -T diagram for samples, 12 (granite), 19 (basalt), 18(basalt), 23 (volcaniclastic) and 27 (dolorite). The sample numbers are shown next to their perspective data point. The blue dotted line illustrates the isotopic evolution of the granite (E13.12) with a depleted mantle model age (953 Ma) located along the depleted mantle line. The samples have a positive value, indicating a juvenile nature..... 24
- Figure 11 N-MORB normalised spider plot for the samples collected from the WES. Figure a and b are normalised to the Nmorb (Sun and McDonough 1989). a contains igneous and volcaniclastic samples. b) Contains basalts taken from Abshala Mélange. c) Is a dunite taken from Daleti Quarry

and has been normalised to the chondrite. The REE pattern is relatively flat with minor anomalies. However, geochemical data must be treated carefully due to low concentrations.	25
Figure 12 Four different basalt discrimination diagrams used for identifying the tectonic environment during the emplacement. The two basalts were taken from the Abshala Mélange. Whilst the other two samples; volcanoclastic and dolerite were collected in close proximity to the Sayi River. The mélange basalt (E13.19) plot in the ‘within-plate’ field for all diagrams (a-d). Similarly the mélange basalt (E13.18) and volcanoclastic (E13.27) consistently plot in the MORB (a-d). The dolerite however, does vary, plotting in both MORB and ‘within plate’ basalt.	26
Figure 13 Elemental maps constructed on the microprobe for a chrome spinel grain from sample E13.26 a dunite from the WES. Figure 3 A depicts the Fe concentrations across the given grain. This shows that they have magnetite rims around chromite cores. The magnetite could have formed during serpentinization. Figure B illustrates the Mg concentrations across the grain. Figure C and D show the Al and Cr variations within the same grain. Figure C and D illustrate that there is depletion in Al and Cr at the rims. Figure A and B define an inversely proportional relationship between the Fe and Mg, suggesting an elemental exchange.	27
Figure 14 Photos taken from E13.11 and E13.26. a-b Dunite taken from Daleti Quarry. The apparent grain size of the olivine in these dunites has been affected by serpentinisation. This is seen by the mesh textured serpeninite grains. The small grains of olivine are relics of what would have been coarse grained olivine. c-d Is sample E13.26 taken from Tulu Dimtu Hill showing the same mesh texture however, serpentinisation is more extensive than Daleti Quarry.	28
Figure 15:a) Cr# (Cr/Cr+Al) against Mg# (Mg/Mg+Fe ²⁺) show the spinels from Daleti, Yubdo plot in the Alaskan Type intrusion field. b) a plot of Cr# against Mg# in spinels. Fields for various types of complexes are from Irvine (1967). Symbols are represented on the right side of the diagram. Taken and adapted from (Helmy and El Mahallawi 2003) c) Al ₂ O ₃ vs TiO ₂ compositional relationship in chrome spinel grains. Discrimination between mid ocean basalt (MORB), ocean-island basalt (OIB), Large igneous province (LIP) and island arc magmas (arc). The spinels plot with in the arc tectonic setting after hydration and serpetinisation. d) TiO ₂ vs Cr# analyses plot in the boninitic field suggest that the rocks are sourced from the deeper mantle as the residual after a boninitic magma has been taken out. This is characteristic of a subduction system.	29
Figure 16 Al-Cr-Fe ³⁺ depicting the alteration of samples. Sample E13.11 taken from Daleti Quarry displays a Fe ³⁺ enrichment suggesting alteration of the chrome spinels.	30
Figure 17 ⁴⁰ Argon - ³⁹ Argon dating of muscovite grains from schists sampled from the Western Ethiopian Shield. This was done using the total fusion method. , showing the interpreted age of the greenschist metamorphism.	31
Figure 18 The set up for the separation of zircons via the use of heavy liquids.	61

Supplementary Table 1: Trace and major element analysis of 6 samples conducted on the XRF	44
Supplementary Table 2: SHRIMP U-Pb-Th analytical data for zircons and determined ages for the igneous and meta-sedimentary rocks of Western Ethiopia.....	45
Supplementary Table 3: Hf results conducted on the Laser at Waite Campus Adelaide University. E13.12 Ganji Granite and E13.24a is meta quartz-arenite.....	46
Supplementary Table 4: ICP-MS REE analysis of 7 samples. These samples are E13.12 (granite), E13.19 (basalt), E13.18 (basalt), E13.23 (volcaniclastic) and E13.27 (dolorite). Some samples contain duplicates indicated as following E13.18.1 and E13.18.2.	47
Supplementary Table 5: Sm-Nd isotopic compositions of igneous and metavolcanic rocks of the WES	48
Supplementary Table 6: Chrome spinel analyses on the microprobe at Adelaide Microscopy. Samples are dunites taken from Yubdo and Tulu Dimtu WES	49
Supplementary Table 7 Microprobe analysis of olivine in association with Chrome spinel with in the dunites for E13.26 and E13.11.....	56
Supplementary Table 8 Microprobe analysis of olivine in association with Chrome spinel with in the dunites for E13.26 and E13.11.....	57
Supplementary Table 9 ⁴⁰ Argon - ³⁹ Argon results from the total fusion of muscovites (E13.14) sampled from the Western Ethiopian Shield	58
Supplementary Table 10 ⁴⁰ Argon - ³⁹ Argon results from the total fusion of muscovites (E13.13) sampled from the Western Ethiopian Shield	59
Supplementary Table 11: This demonstrates the estimated concentrations of Sr, Nd and Sm used to calculate the respective weights. The recorded weight and addition of spike is also depicted in this Supplementary Table.	64
Supplementary Table 12 This shows the parameters that the mass spectrometer operated for the Sr acquisition of each sample.	74
Supplementary Table 13 This shows the parameters that the mass spectrometer operated for the Nd and Sm acquisition of each sample.	74

INTRODUCTION

The Western Ethiopian Shield lies within the East African Orogen (Stern, 1994), a major Gondwana-forming collisional zone (Collins and Pisarevsky, 2005). It contains poorly dated and poorly geochemically characterised terranes that host significant ore systems (Tadesse and Allen 2005, Tadesse and Allen 2004, Yibas et al. 2003, Mogessie et al. 2000). The Western Ethiopian Shield lies close to the Western cratonic margin of the East African Orogen, and forms a transition between lower crustal rocks found in the southern East African Orogen (known as the Mozambique Belt), and upper crustal rocks of the northern Arabian-Nubian Shield (Stern 1994, Johnson et al. 2011, Fritz et al. 2013). Despite linking these regions together, being well exposed, and accessible, it has received little modern geological work.

The aim of this paper is to constrain the age and origin of the Neoproterozoic sediments and igneous rocks within the western Ethiopian Shield. The maximum depositional age and provenance of the protoliths to meta-sedimentary units are constrained, by obtaining the U-Pb age of detrital zircons. The age of post-tectonic granites are derived by U-Pb dating magmatic zircons and the petrogenesis of magmatic rocks are investigated using, mineral and whole rocks elemental and isotopic chemistry. Finally, the age of the greenschist metamorphism has been derived from ^{40}Ar - ^{39}Ar dating of metamorphic muscovites. The paper will focus on constraining the age of volcanic and volcanoclastic successions in the Western Ethiopian Shield, as well as examining the geochemical nature of the ultra-mafic bodies in the Shield. This will test the hypothesis that the protoliths formed Neoproterozoic volcanic arcs, created as a result of subduction and the closure of the Mozambique Ocean, during the amalgamation of Gondwana.

GEOLOGICAL SETTING/BACKGROUND

East African Orogen

The East African Orogen preserves a complex history of intra-oceanic and continental margin, magmatic and tectonothermal events. The region formed during the Neoproterozoic subduction of the Mozambique Ocean, which separated India from African continents in the Neoproterozoic, and was deformed and amalgamated during the late Neoproterozoic- Cambrian assembly of Gondwana (Grenne et al. 2003). Stern (1994) suggested that the East African Orogen formed the collisional zone between two Neoproterozoic continental masses, East Gondwana (India-Australia- Antarctica) and West Gondwana (Africa-South America). However, a more recent theory has been proposed, suggesting that both East and West Gondwana did not exist as Neoproterozoic super continents, but are both made of smaller continents, which came together during the Neoproterozoic (Meert 2003). Collins and Pisarevsky (2005) amended this with a newly proposed continental block, Azania (Fig 1). This lies within the East African Orogen of Madagascar, Somalia, eastern Ethiopia and Arabia. These authors suggested that Azania collided with the Congo/Tanzania/Bangweulu Block at ~650–630 Ma to form the East African Orogeny (Collins and Pisarevsky 2005, Stern 2002). The complex and prolonged tectonism of the East African Origin resulted from the accretion of volcanic arc and continental terrains during the closure of the Mozambique Ocean and the collision of parts of eastern and western Gondwana in the Neoproterozoic (Meert 2003).

The East African Orogen is subdivided into two along its strike. To the north lies the juvenile (mantle derived) Arabian Nubian Shield, this is dominated by low grade volcano-sedimentary rocks in association with plutons and ophiolitic remnants (Abdelsalam and Stern 1996, Kröner et al. 1991, Shackleton 1996, Stern 1994, Allen and Tadesse 2003). To the south is a tract of older remobilised crust, known as the Mozambique Belt (Meert 2003, Woldemichael and Kimura 2008, Woldemichael

et al. 2010, Yibas et al. 2003). The Western Ethiopian Shield is situated close to the transition between the Arabian Nubian Shield and Mozambique Belt, adjacent and to the east of, ‘Eastern Saharan Meta-craton’. (Abdelsalam and Stern 1996).

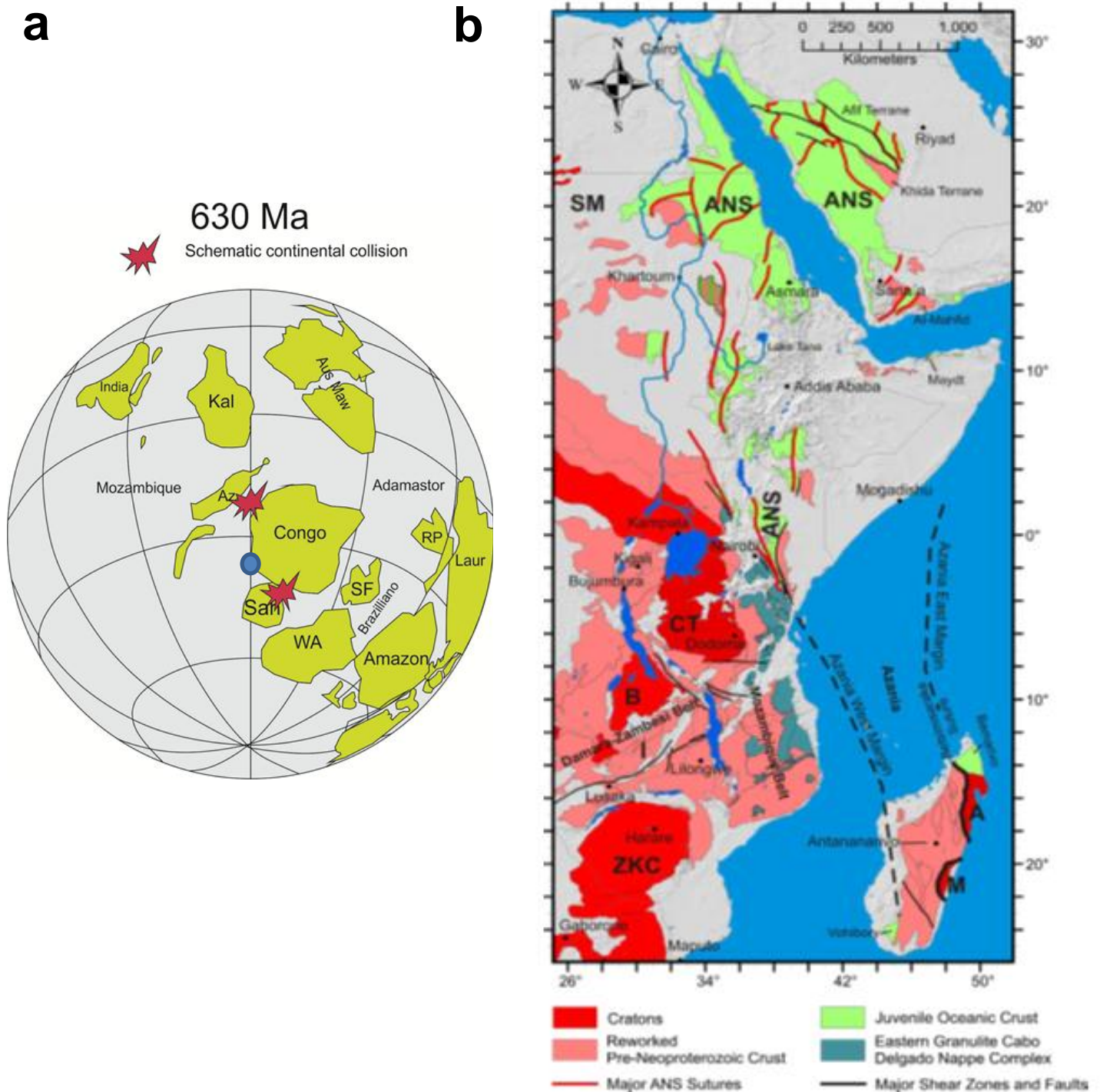


Figure 1: a) Palaeogeographic reconstruction at 630 Ma. Green represents continental plates delineated from the map. The blue dot shows where the Western Ethiopian Shield is situated. Abbreviations are as follows Amazon=Amazonia; Aus-Maw=Australia/Mawson Block; Az=Azania; Congo=Congo/Tanzania/Bangweulu Block; Kal=Kalahari Block; Laur=Laurentia; RP=Rio de la Plata; SF=São Francisco; WA=West Africa. Adola, Adamastor, Brazilliano, Mozambique =oceanic basins. Taken from (Collins and Pisarevsky 2005). b) This is taken from Fritz et al. (2013) shows the location of the Azanian plate in conjunction to Ethiopia.

Western Ethiopia:

Western Ethiopia is made up of a range of supra-crustal and plutonic rocks. The Precambrian exposures of the Western Ethiopian Shield are located between the juvenile Neoproterozoic crust of the Arabian Nubian Shield and the older, predominately gneissic Mozambique Belt (Woldemichael et al. 2010) (Fig 1). There have been numerous divisions proposed (Kazmin et al. 1979, Kebede and Koeberl 2003, Kebede et al. 1999, Mogessie et al. 2000, Tadesse and Allen 2005, Yibas et al. 2003). However, the division outlined by Woldemichael and Kimura (2008) is adopted in this paper. Several lithological and structural domains have been recognised within parts of the Western Ethiopian Shield (Woldemichael and Kimura 2008). The reworked pre-Neoproterozoic and juvenile Neoproterozoic terrane of the Western Ethiopian Shield (Fig 2) consists of three main N-S trending terranes (Woldemichael et al. 2010). These are the Western Migmatitic Gneissic Terrane (WMGT), the Central Volcano Sedimentary Terrane (CVST) and the Eastern Migmatitic Gneissic Terrane (EMGT) (Woldemichael and Kimura 2008). Linear belts of highly deformed mafic-ultramafic bodies, within low-grade terranes, have been interpreted as suture zones containing dismembered ophiolitic rocks (Abdelsalam and Stern 1996, Allen and Tadesse 2003, Ayalew et al. 1990, Stern 2002, Tadesse and Allen 2005). Tadesse and Allen (2005) named this dismembered ophiolite as the Tulu-Dimtu Ophiolite. However, there is a lack of geochemical evidence to support the presence of ophiolites in the Western Ethiopian Shield (Braathen et al. 2001, Grenne et al. 2003, Mogessie et al. 2000, Woldemichael and Kimura 2008, Woldemichael et al. 2010). These ultra-mafic bodies are generally confined to the N-S trending Tulu-Dimtu-Daleti-Yubdo shear zone. A contrasting opinion suggests that the ultra-mafic bodies are Alaskan-type concentrically zoned intrusions, which were emplaced into an extensional arc or back arc environment (Braathen et al. 2001, Grenne et al. 2003, Mogessie et al. 2000).

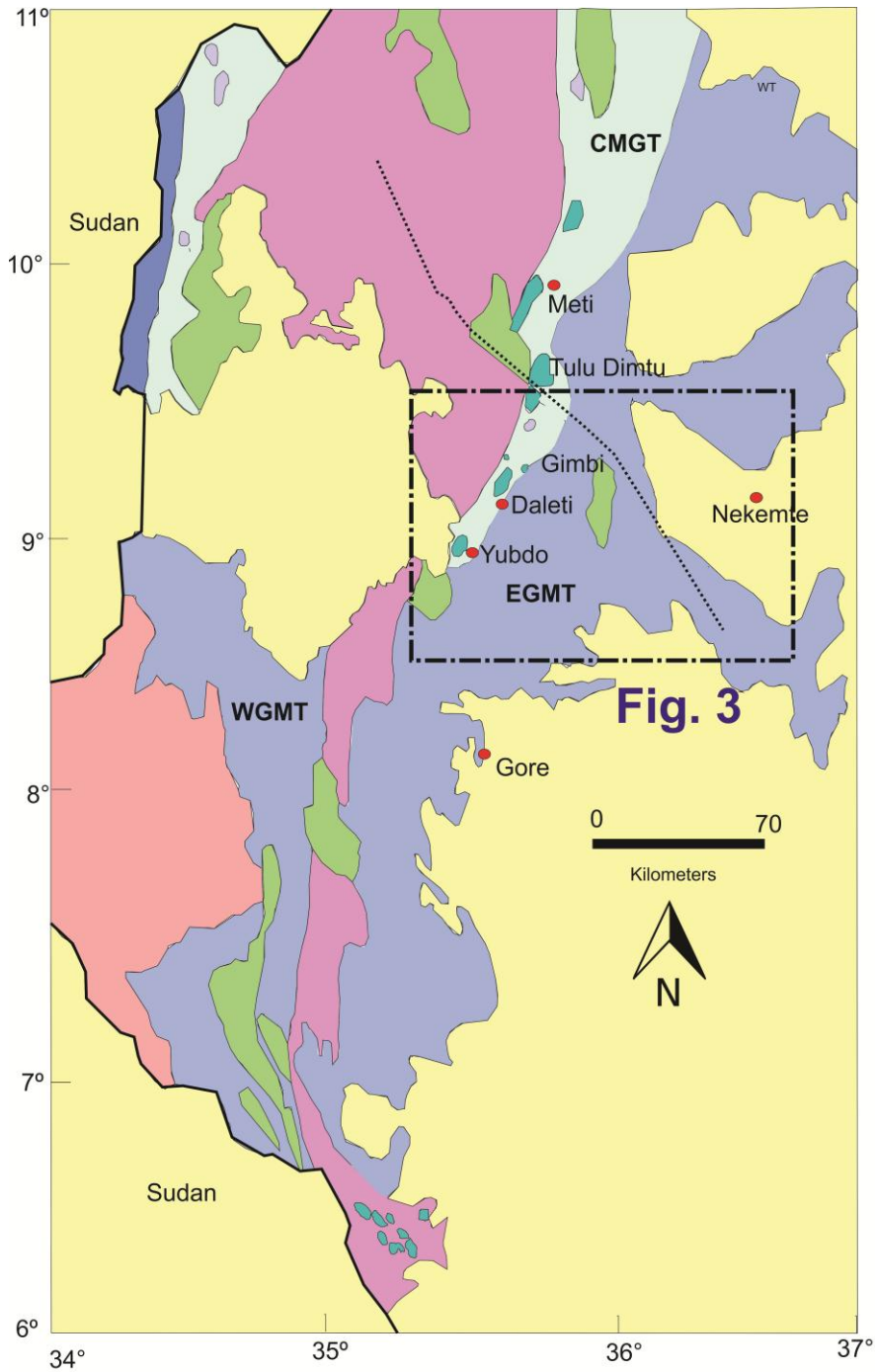


Fig. 3

Legend

- | | |
|---|--|
| <ul style="list-style-type: none"> Quaternary sediments Tertiary volcanics with minor mesozoic sediments Granitoids Low grade volcano-sediments and associated intrusive rocks Ultra-mafics | <ul style="list-style-type: none"> Volcanosedimentary rocks, metavolcanics gabbro and diorite. Gneiss and migmatites Shear zone/fault
1. Surma
2. Didessa Lithological contact International boundary |
|---|--|

Figure 2: Simplified geological map of Western Ethiopia. Area of study has been highlighted with the use of a box. Taken and adapted from (Tadesse and Allen 2004)

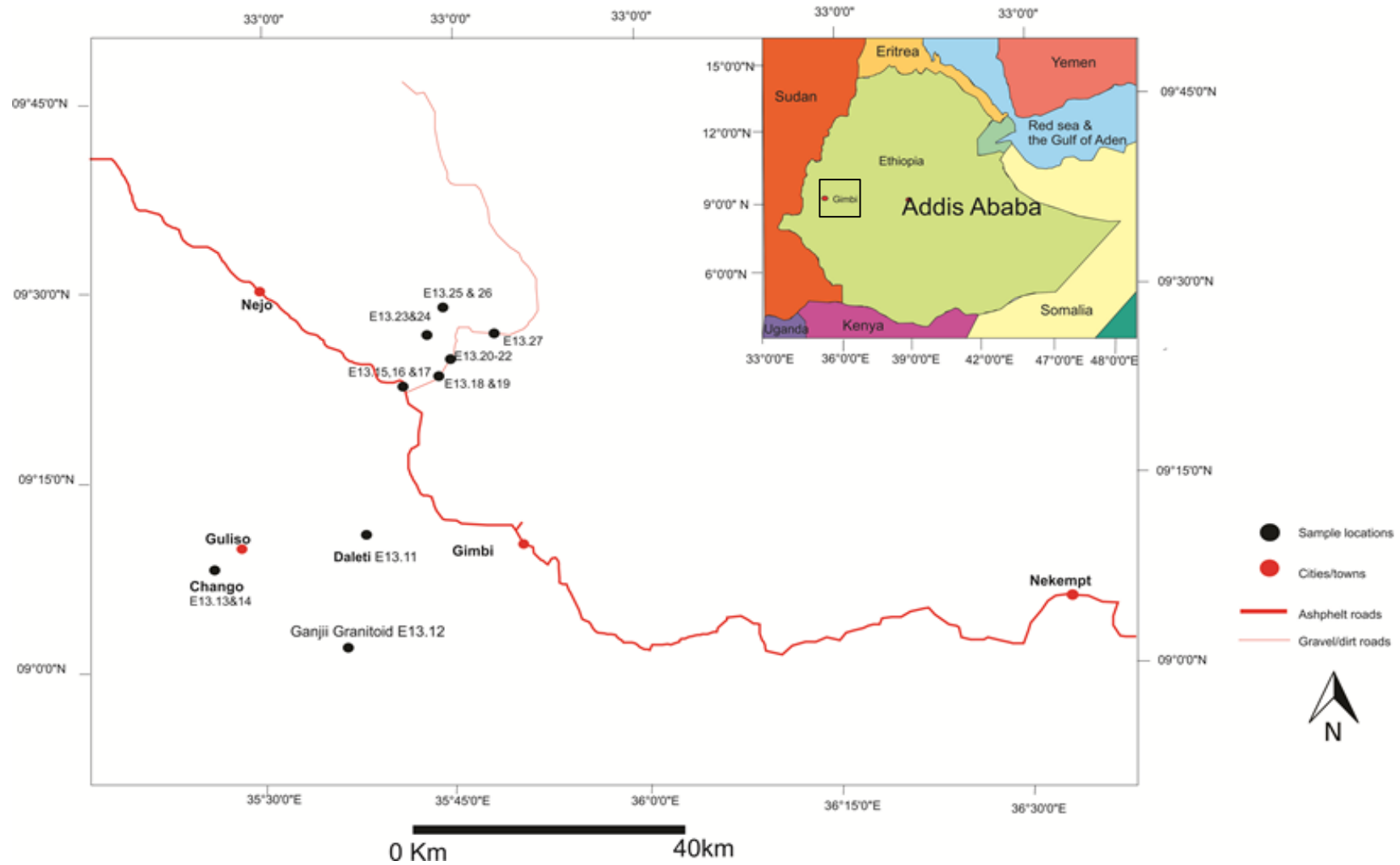


Figure 3 Location map for samples taken from Ethiopia. The map in the top right hand corner depicts Ethiopia on a country scale showing its proximity to the Afar triple junction, with Gimbi as a reference point on both maps.

METHODS

U–Pb zircon dating

The samples were collected from various locations (see figure 3- map of sample locations) within the Western Ethiopian Shield. These are granitic and meta-sedimentary in nature.

Zircons were extracted from crushed rocks using standard magnetic and heavy liquid techniques (Howard et al. 2009). The resulting heavy liquid fraction is washed with acetone and dried. The mineral separates were sent to Curtin University where they were hand-picked and mounted in an epoxy resin. The mounts were polished to expose the minerals; carbon coated and then imaged using a Cathodoluminescence (CL) Detector on a Scanning Electron Microscope at Curtin University in Perth to identify oscillatory-zoned domains in the zircons that were formed as the zircon grew in the magma. These oscillatory-zoned domains were analysed and collected U–Th–Pb isotopic data were collected using a Sensitive High Resolution Ion Microprobe Mass Spectrometer (SHRIMP II) in the John de Laeter Centre of Mass Spectrometry, Perth, Western Australia. The sensitivity for Pb isotopes in zircon using SHRIMP II was 20 cps/ppm/nA, the primary beam current was 2.5–3.0 nA and mass resolution was ca. 5000. Correction of measured isotopic ratios for common Pb was based on the measured ^{204}Pb in each sample and often represented a < 1% correction to the ^{206}Pb counts. Pb/U isotopic ratios were corrected for instrumental discrimination using the observed co-variation between Pb^+/U^+ and UO^+/U^+ (Hinthorne et al., 1979; Compston et al., 1984) determined from interspersed analyses of the standard zircon BR266, a zircon megacryst from Sri Lanka with an age of 559 ± 0.3 Ma, a $^{206}\text{Pb}/^{238}\text{U}$ ratio of 0.09059, and U and Th contents of 909 ppm and 201 ppm respectively (Stern, 2001). Data was reduced using SQUID2 and Isoplot 3.66 (Ludwig, 2001, 2003).

Hafnium Isotope determination

Analytical methods for zircon Hf isotope determination were based upon Payne et al. (2013) and Griffin *et al.* (2006). Analyses were undertaken using a New Wave UP-193 Laser attached to a Thermo-Scientific

Neptune Multi-Collector ICP-MS at Adelaide University. A 193 nm UV ArF excimer Easer Ablation System was used. Ablation times were about 26 s for 200 cycles of each measurement, with a 6 Hz repetition rate, a laser power of 100 mJ/pulse and a spot size of 50 μm . However, for smaller zircons, this was reduced to 30 μm

Data reduction of zircon data was undertaken using a macro-driven Hf isotope data reduction Excel (Microsoft 2007) spreadsheet, Hf TRAX, coded by corresponding author (Payne et al. 2013). The data were normalised to $^{179}\text{Hf}/^{177}\text{Hf} = 0.7325$, using an exponential correction for mass bias. The accuracy of the Yb and Lu corrections has been demonstrated by repeated analysis of standard zircons with a range in $^{176}\text{Yb}/^{177}\text{Hf}$ and $^{176}\text{Lu}/^{177}\text{Hf}$ (Griffin et al. 2006). Before and during the analysis of unknowns, standards were analysed to check instrument performance and stability. The measured $^{176}\text{Lu}/^{177}\text{Hf}$ ratios of the zircons have been used to calculate initial $^{176}\text{Hf}/^{177}\text{Hf}$ ratios. These age corrections are very small, and the typical uncertainty on a single analysis of $^{176}\text{Lu}/^{177}\text{Hf}$ (+1%) contributes an uncertainty of $<0.05 \epsilon_{\text{Hf}}$ unit (Payne et al. 2013).

Radiogenic Isotope Geochemistry

The preparation and analysis of the whole rock Sm and Nd isotopic data are similar to the procedure implemented by Wade et al. (2008) and Payne et al. (2008). The analyses were carried out at the University of Adelaide under the supervision of David Bruce. Samples were spiked with a ^{150}Nd – ^{147}Sm solution. Hydrofluoric acid (HF) was added to the samples in Teflon ‘bombs’ and vials. These were then dried. A further 4 ml HF and 2 ml HNO_3 was added and placed into the metal jackets. Subsequently the samples were oven-heated at 190 $^\circ\text{C}$ for 5 days and evaporated to dry the sample. Hydrochloric acid (6mL/6M) was added and pressure heated at 160 $^\circ\text{C}$ for a further 2 day and evaporated to dryness. The vials follow a similar procedure; however they are heated on the hotplate at 140 $^\circ\text{C}$. Nd (neodymium) and Sm (Samarium) were extracted via column chromatography. Isotopic ratios were measured on a Finigan MAT 262 thermal ionisation mass spectrometer. The neodymium international standard JdNi-1 returned a mean value of 0.5120996 ± 0.0000457 (n=5). The blanks show negligible Nd and Sm. When calculating ϵ_{Nd_t} values, an approximated age of 700 Ma was used as this was when terrane accretion of these rock types was dominant

(Ayalew et al. 1990, Braathen et al. 2001, Grenne et al. 2003, Kazmin et al. 1978, Kebede and Koeberl 2003, Kebede et al. 1999, Tadesse and Allen 2005, Tadesse and Allen 2004, Teklay et al. 1998, Woldemichael and Kimura 2008, Woldemichael et al. 2010, Yibas et al. 2003, Yibas et al. 2002).

Major Element Geochemistry using the X-Ray Fluorescence (XRF)

Major element analysis (SiO_2 , MgO , Fe_2O_3 , MnO , CaO , TiO_2 , Na_2O , and K_2O) was carried out at Adelaide University. A fused disk was prepared from rock powder. Approximately 6 grams of powder was heated to 110°C for four hours to remove any moisture present. The sample was then weighed and ignited at 960°C for 3 hours. Loss of ignition was calculated. Approximately 1 g of the ignited sample was combined with approximately 4 g of a lithium borate flux and fused into a glass disk in a Pt/Au crucible and mold. The resulting glass disk was analysed on the Phillips PW 1480 XRF spectrometer using a dual-anode (Sc-Mo) X-ray tube, operating at 40 kV, 75 mA. The samples were analysed with a Philips PW 1480 X-ray Fluorescence Spectrometer, using an analysis program calibrated against several international and internal Standard Reference Materials (SRM's).

Minor trace Element Geochemistry using the XRF

About 5-10 g of sample powder was combined with 1 ml of binder solution (Poly Vinyl Alcohol) and pressed to form a pellet. This was allowed to dry in air and was heated for a further 1 to 2 hours in a 60°C oven to ensure that the pellet was completely dry before analysis. The samples were analysed using a Philips PW 1480 XRF Spectrometer, using several analysis programs covering suites of 1 to 7 trace elements, with conditions optimised for the elements being analysed. The programs were calibrated against internal and international SRM's. The dual-anode Sc-Mo and an Au tube were used for the analyses. Matrix corrections are made using either the Compton Scatter peak, or mass absorption coefficients calculated from the major element data.

Trace element Geochemistry ICP-MS

Rock samples were cut using a diamond bladed rock saw. Samples were crushed and milled using the procedure outlined above. Approximately 0.1 g of rock powder was weighed into a cleaned Teflon bomb/vial. The same dissolution process used for the radiogenic geochemistry. The resulting precipitate was dissolved in 2ml of 7.5M HNO₃ and split into two 5 mL aliquots at 1000 and 5000 times dilution. Standards and procedural blanks are prepared (BHV-02, BCR-2 and G2) in the same manner and diluted accordingly to create a calibration curve. The resulting solutions were analysed on an Agilent 7500 ICP-MS. The element counts per second (CPS) were converted to a concentration (ppm). This is done by fitting the measured CPS to a calibration curve constructed from a series of multi element standard solutions. Corrections to measured CPS were made using indium as an internal standard and the bracketing of samples by the BCR-2 as well as the use of BHV-01 (Basalt Hawaiian Volcanic Observatory) and G2 (Granite)

Chrome Spinel Analysis

The chemical compositions of the chrome spinels and olivine were determined using an Electron Microprobe Cameca SX5 at Adelaide Microscopy, Adelaide University. Thin sections of six representative samples were made at Adelaide Petrographic Laboratories Pty Ltd and were analysed. Spot analyses were conducted using a beam current of 20 nA and an accelerating voltage of 15 kV, with a defocused beam of 5 micron. Representative mineral compositions are given in Supplementary Table 6. Calibration was made based on natural and synthetic mineral standards.

⁴⁰Argon / ³⁹Argon dating

Two samples were analysed for ⁴⁰Ar / ³⁹Ar dating. The minerals separated were unaltered, optically transparent, 150 µm-size, muscovite. These minerals were separated using a Frantz magnetic separator, and then carefully hand-picked under a Binocular Microscope Olympus SZ51. The muscovites were further leached in diluted HF for one minute and then thoroughly rinsed with distilled water in an ultrasonic cleaner.

The samples were loaded along with samples of the Fish Canyon sanidine (FCs) used as a neutron monitor for which an age of 28.305 ± 0.036 Ma (1σ) was assigned based on the calibration by Jourdan and Renne (2007). The discs are irradiated in the Hamilton McMaster University Nuclear Reactor (Canada). The correction factors for interfering isotopes were $(^{39}\text{Ar}/^{37}\text{Ar})_{\text{Ca}} = 7.30 \times 10^{-4}$ ($\pm 11\%$), $(^{36}\text{Ar}/^{37}\text{Ar})_{\text{Ca}} = 2.82 \times 10^{-4}$ ($\pm 1\%$) and $(^{40}\text{Ar}/^{39}\text{Ar})_{\text{K}} = 6.76 \times 10^{-4}$ ($\pm 32\%$). The samples were fusion heated using a 110 W Spectron Laser Systems, with a continuous Nd-YAG (IR; 1064 nm) laser. Ar isotopes were measured in static mode using a MAP 215-50 mass spectrometer (resolution of ~ 500 unit; sensitivity of 4×10^{-14} mol/V) with a Balzers SEV 217 electron multiplier mostly using 9 to 10 cycles of peak-hopping. ^{40}Ar blanks range from 1×10^{-16} to 2×10^{-16} mol. (Jourdan and Renne 2007).

OBSERVATIONS AND RESULTS

U-Pb Geochronology

Sample E13.12 was collected from the undeformed, post-tectonic Ganjii granitoid in order to provide a minimum age of deformation and amalgamation in the area. This is primarily a monzogranite, with subordinate monzodiorite. The monzogranite is porphyritic, with K-feldspar megacrysts. The granitoid is affected by NE-trending sub-vertical fractures and joints. These joints are filled by micro granite dykes. The Ganjii monzogranite shows the chemical and mineralogical characteristics of within-plate granite and has been interpreted to have been emplaced in an extensional tectonic environment (Kebede and Koeberl 2003). A $^{207}\text{Pb} - ^{206}\text{Pb}$ zircon age of 622 ± 7 Ma has been previously reported as reflecting crystallisation of the intrusion (Kebede et al. 1999).

Extracted zircons are prismatic and show oscillatory zoning in CL, characteristic of formation within a magma chamber (Corfu et al. 2003)(Fig. 7). Twenty two analyses of 19 zircon grains were conducted. A majority of the analyses' were targeted at the rims. The few core analyses showed no discernible age difference with the rims. The data are displayed on a Wetherill Concordia plot (Fig. 4). This yields a concordant $\text{Pb}^{206}/\text{U}^{238}$ age of 572.6 ± 7.4 , with 95% confidence and a MSWD of 1.7. This suggests a crystallisation age during the Ediacaran and ~50 Ma younger than previously interpreted.

Sample E13.24a was sourced from a meta-quartz-arenite located along the Sayi River (Fig 3). There were thirteen zircons analysed due to the paucity of recoverable zircon in the sample. The CL images show that the grains are sub-rounded to rounded (Fig. 7). The U-Pb Concordia plot (Fig. 6a-c) and probability density plot (Fig. 5) demonstrates the presence of detrital zircons at ~2499 Ma (Fig. 6a), ~1855 Ma (Fig. 6b) and between 1100-800 Ma (Fig. 6c). The limited number of zircons available are too few to statistically characterise the source region (Vermeesch 2004). However, the zircons can be used to reveal ages present within the source region. The population at ~2499 Ma is slightly discordant, thus suggesting that the zircons have not remained in a completely closed system. The four zircons that yield an age of ~1855 Ma (Fig. 6b) have a mean average of 1852 ± 7.9 Ma with an MSWD of 0.35, suggesting that these come from the same-aged source.

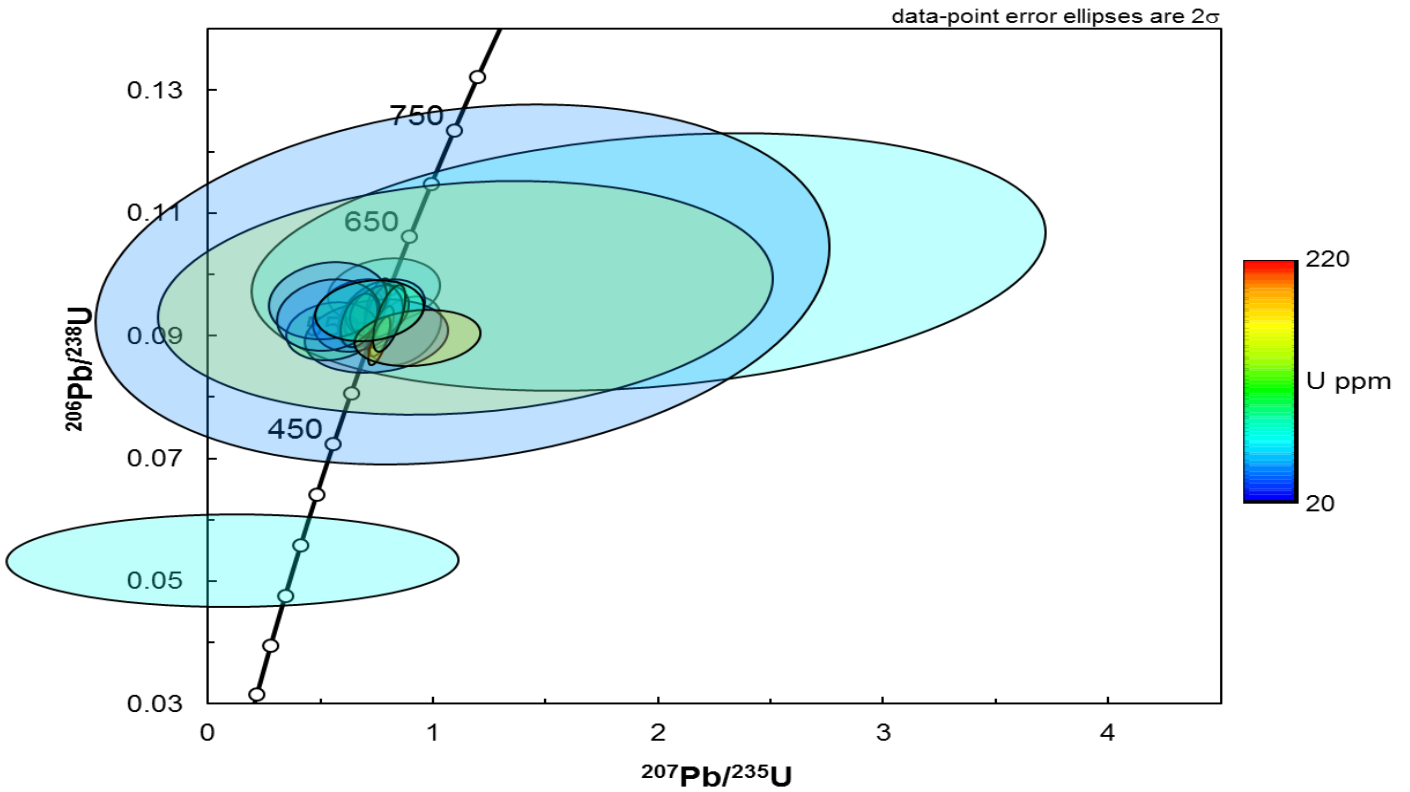


Figure 4: U–Pb Concordia graph illustrating zircons analysed from the Ganjii monzogranite (E13.12) collected from the Western Ethiopian Shield. The weighted mean $^{206}\text{Pb}/^{238}\text{U}$ age of all analyses except a single young analysis at 572.6 ± 7.4 Ma, that is interpreted to represent Pb loss in the modern environment.

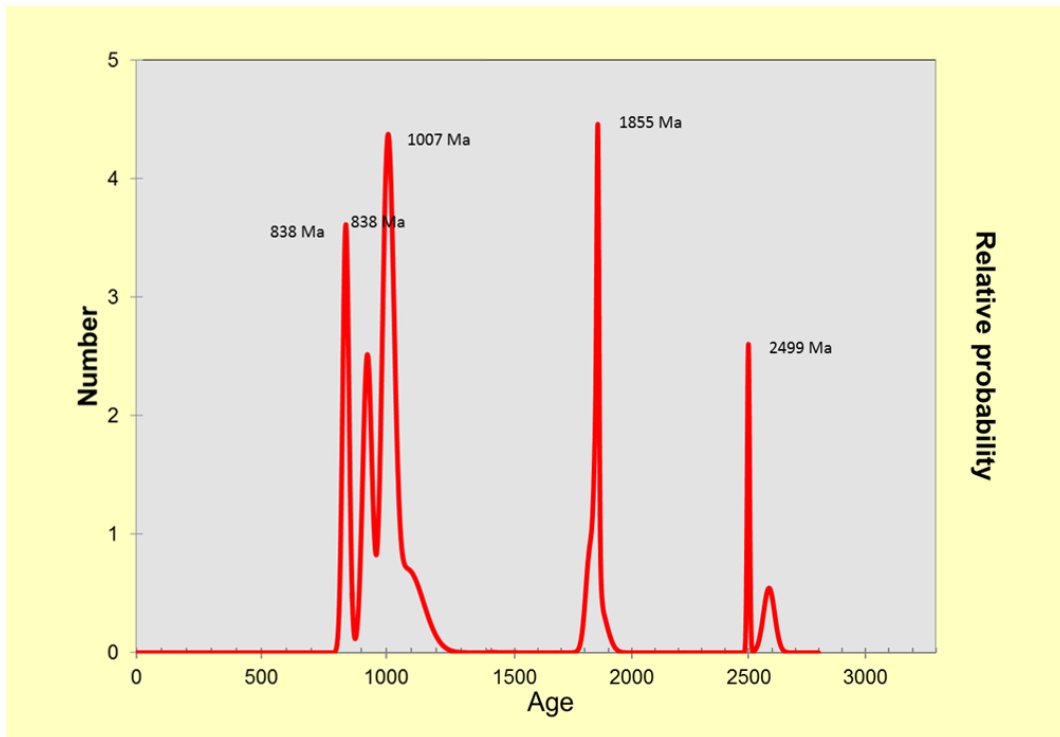


Figure 5) Probability density plot for sample E13.24a (meta-quartz arenite). $^{206}\text{Pb}/^{207}\text{Pb}$ ages are used when ages are over 1 Ga. $^{206}\text{Pb}/^{238}\text{U}$ ages are used when the age is less than ~1 Ga. The histogram shows the number of analyses per peak for E13-24a. This demonstrates the presence of detrital zircons at ~2499 Ma, ~1855 Ma and between 1100-800 Ma

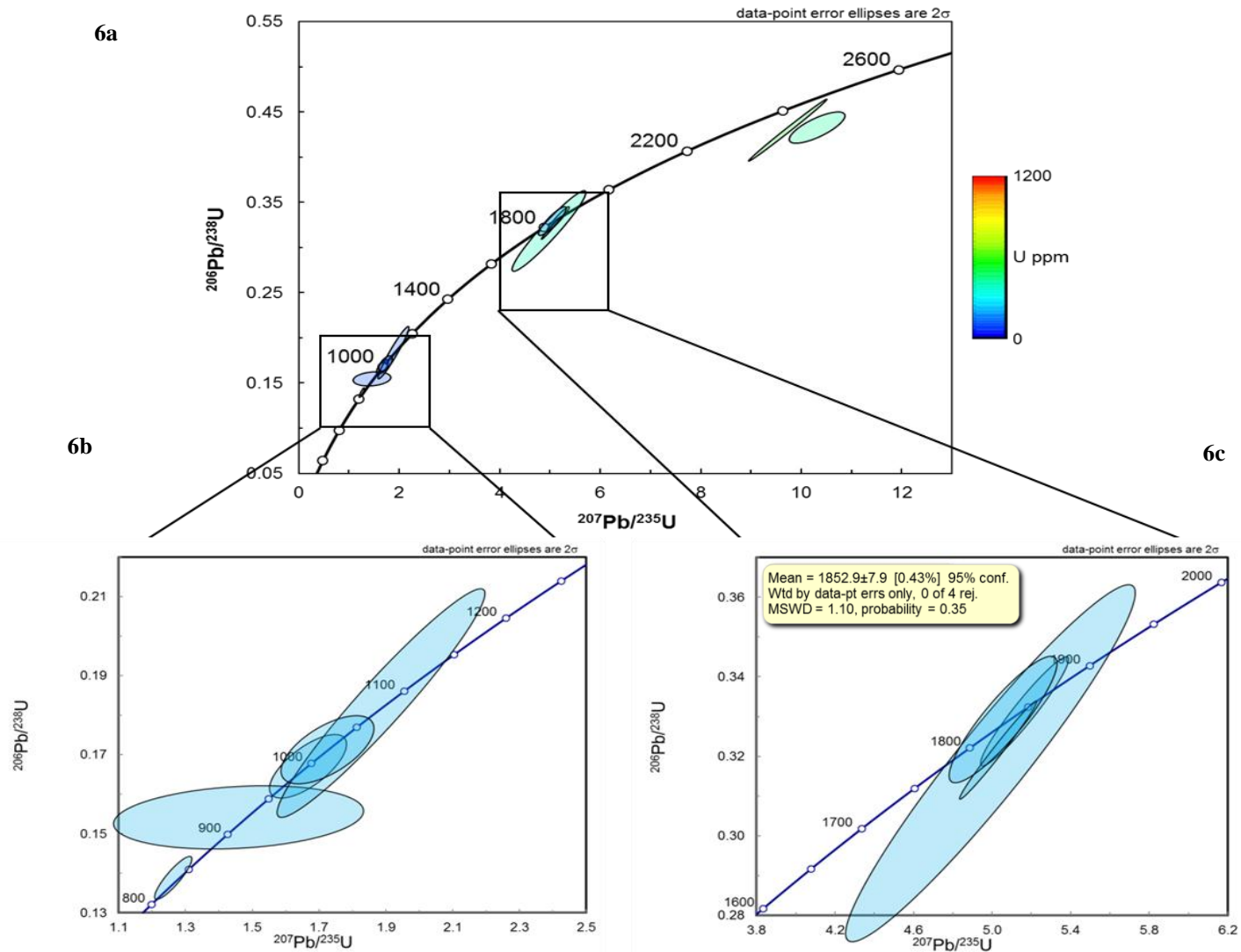


Figure 6: U-Pb Concordia diagrams constructed with a 2 sigma data point error ellipses. a) U-Pb Concordia of all zircons (n=13), which were sourced from a meta quartz arenite (E13-24a). The colour scale on the right of the graph depicts uranium concentration of individual zircons. (b-c) focuses on individual clusters. b shows that there are rocks in the source region with ages at ~820 Ma and ~1000-1100 Ma. c demonstrates that there is a population of detrital zircons at ~1850.

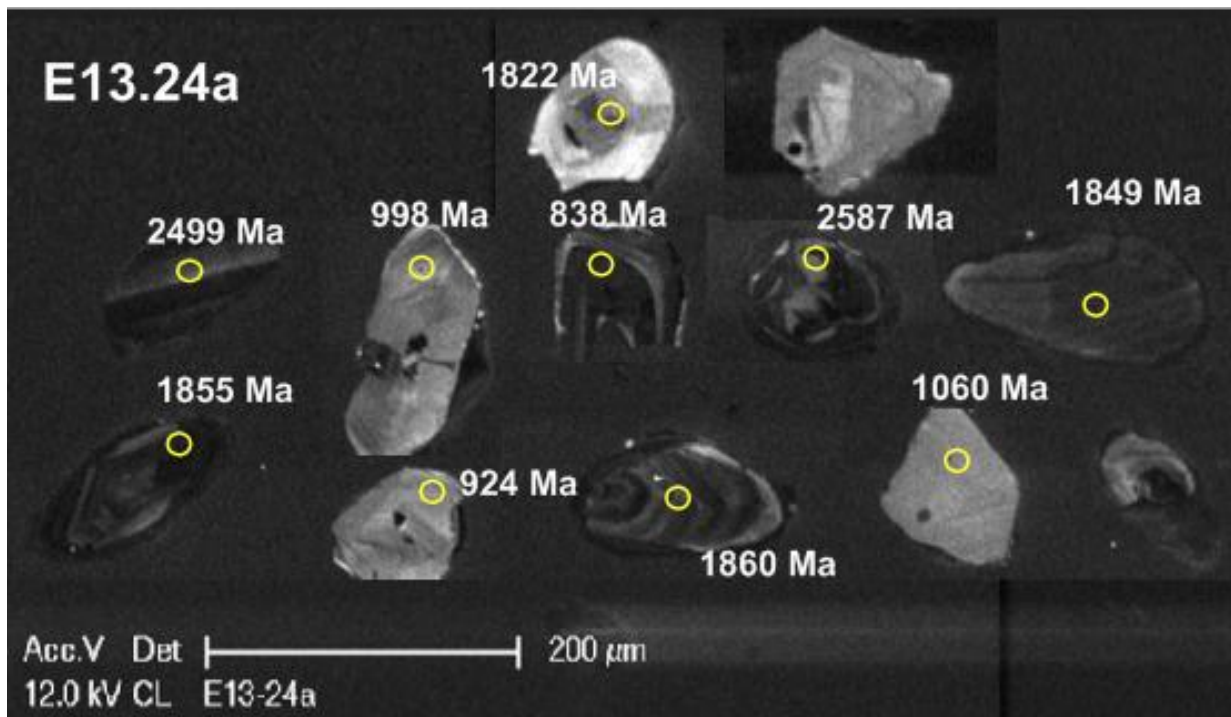


Figure 7 CL images for E13.12, a Ganji Granite and E13.24a, a meta-quartz-arenite, taken from Western Ethiopia. E13.12 They have a prismatic shape typical of igneous zircons. The low response (dark) suggests a higher uranium content. Zircons show oscillatory zoning typical of formation in a magma chamber. E13.24a These have a typical irregular and partially rounded detrital shape. The low response (dark) suggesting higher uranium content. s. Apatite and titanate are abundant within this sample.

Zircon Hf Isotopes

The Lu–Hf isotope system can be used to track the history of chemical differentiation of the silicate Earth (crust and mantle) by virtue of the fact that fractionation of Lu from Hf occurs during magma generation. Zircon effectively preserves the initial $^{176}\text{Hf}/^{177}\text{Hf}$ ratio of the magma from which it grew, providing an enduring record of the Hf isotopic composition of the source environment, at the time of crystallization. Hf isotope analysis was undertaken on the zircons from the monzogranite and meta-quartz-arenite. These have been plotted on separate ϵHf vs. time plots (Fig. 8). The Hf isotopic data was obtained by overlapping the laser pit over the pre-existing SHRIMP analysis spot. Sample E13.12 (Ganjii granite) yielded positive ϵHf values with a range of 6.79–7.98 (Fig. 8), suggesting that the granite crystallised from a magma derived from depleted sources in the mantle.

The Hf isotopic data for detrital zircons from sample E13.24a (meta-quartz-arenite) illustrates that the detrital zircons at ~2499 Ma grains have positive ϵHf_t values ranging from 1.79 to 2.08. Zircons at ~1855 Ma conversely, have negative ϵHf_t values ranging from -2.29 to -12.41 (Fig. 8). This suggests that they are not juvenile in nature; the magma from which the zircons grew from contained a significant input of older continental crust. Lastly, the population between 1100–800 Ma yielded positive ϵHf_t values ranging from 1.25 to 7.84.

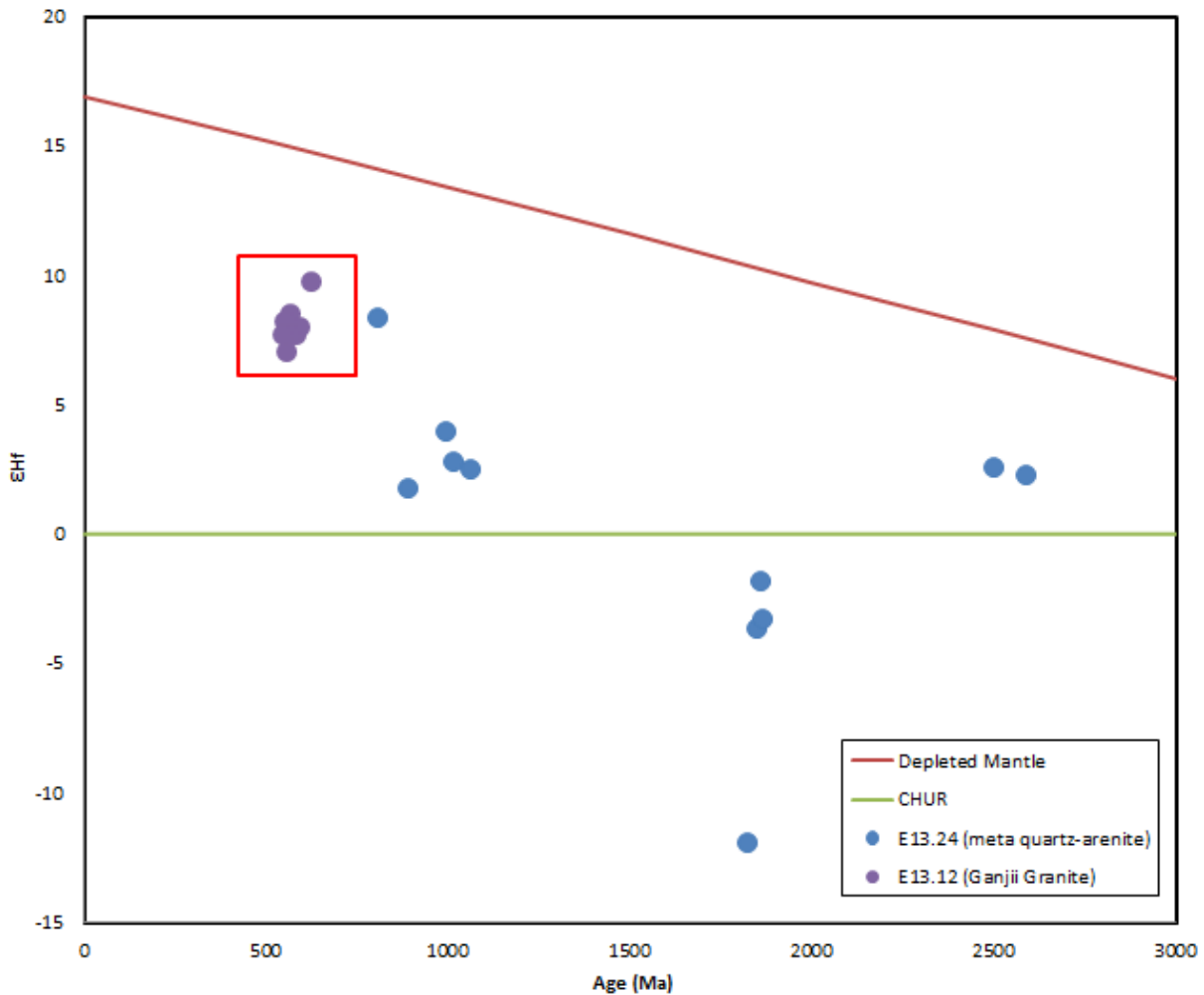


Figure 8: ϵHf_t versus age plot. The purple dots represents sample E13.12, a monzogranite. The green line along the x-axis represents CHUR. The red line represents the depleted mantle. The blue dots represent zircons from E13.24a meta quartz-arenite. This shows three distinct populations the oldest and youngest being of juvenile nature. The population at ~1800 Ma is more evolved suggesting that addition of a continental influence.

Geochemistry

Geochemical analysis was undertaken on six samples; E13.12, a post-tectonic Ganjii granitoid, volcaniclastic and dolerite. The volcaniclastic rock and dolerite were collected in close proximity to the Sayi river (Fig. 3)

Figure 11b depicts E13.18 and 19, which were sampled from the Abshala Mélanges. These are exposed in the Abshala stream. The Abshala Mélange is internally complex, containing rocks of disparate histories. It is comprised of tectonically mixed rock types; metabasalt/amphibolite, ultra-mafics and quartzite/chert. The mechanism responsible for the juxtaposition of the tectonically different fragments has been interpreted to be thrust imbrication (Alemu and Abebe, 2000)

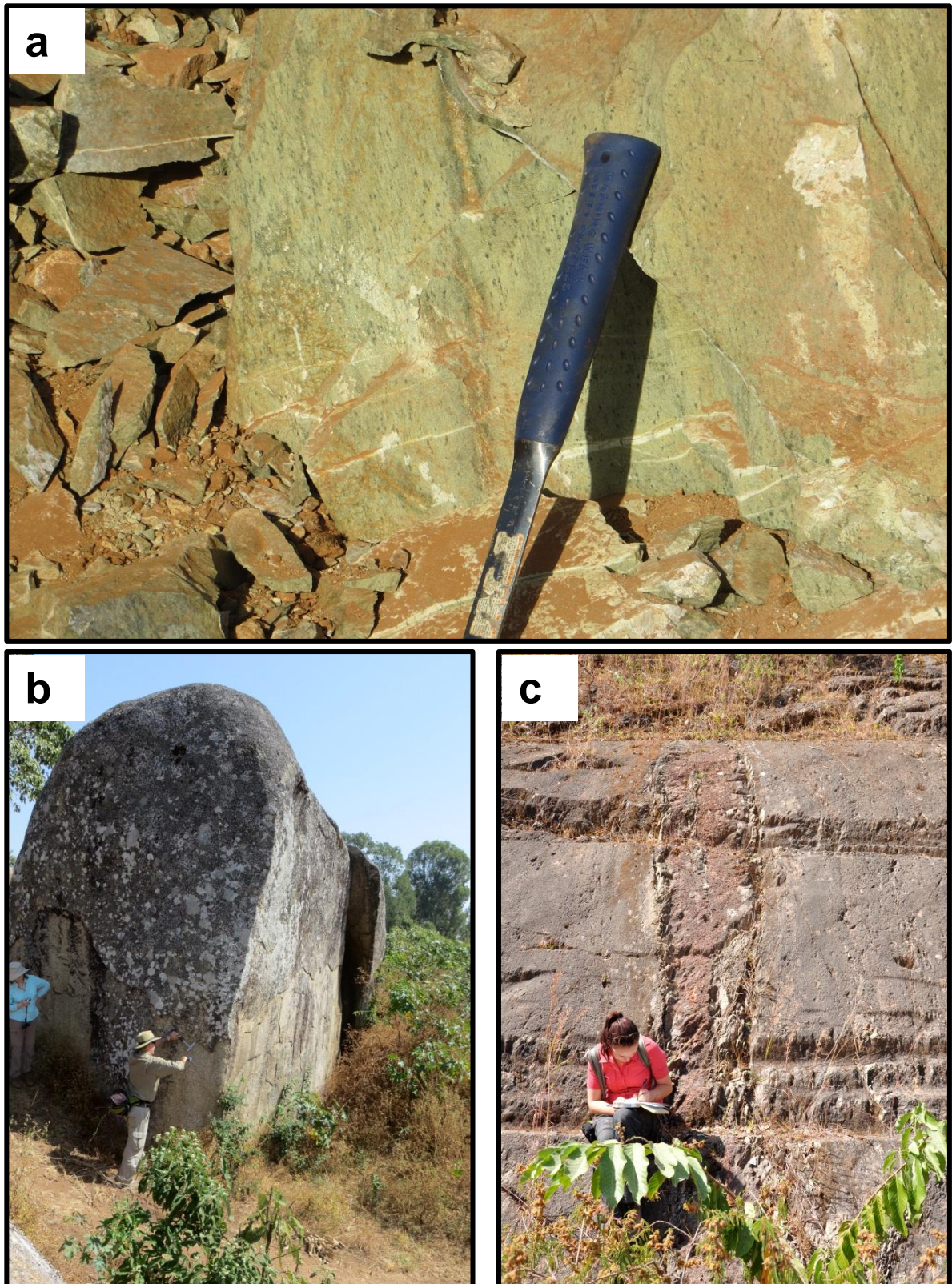


Figure 9 a) E13.11 taken from Daleti Quarry. Note the alignment of the chrome/magnetite spinel grains. b) Sample location of E13.12 the Ganjii Granite c) represents the Abshala Mélange where E13.18 and 19 were sampled from.

RADIOGENIC ISOTOPES

A set of six representative samples of metavolcanic and plutonic rocks have been analysed for Nd and Sm isotopes. In the ϵ_{Nd} v. T diagram, the data plot between the Depleted Mantle and Chondritic Unfractionated Reservoir (CHUR) lines, suggesting that these rocks are juvenile in nature and have only been weakly contaminated by older crustal material (Fig. 10). This is illustrated in the relative similarity of the U-Pb age and Nd model ages of the samples. For example, E13.12 provides a depleted mantle model age of 953 Ma and a $\text{Pb}^{206}/\text{U}^{238}$ age of 572.6 ± 7.4 Ma (Fig. 4). The ϵ_{Nd} values for the post-tectonic granite are similar to those of the pre-tectonic mafic and intermediate rocks. This suggests a similar source.

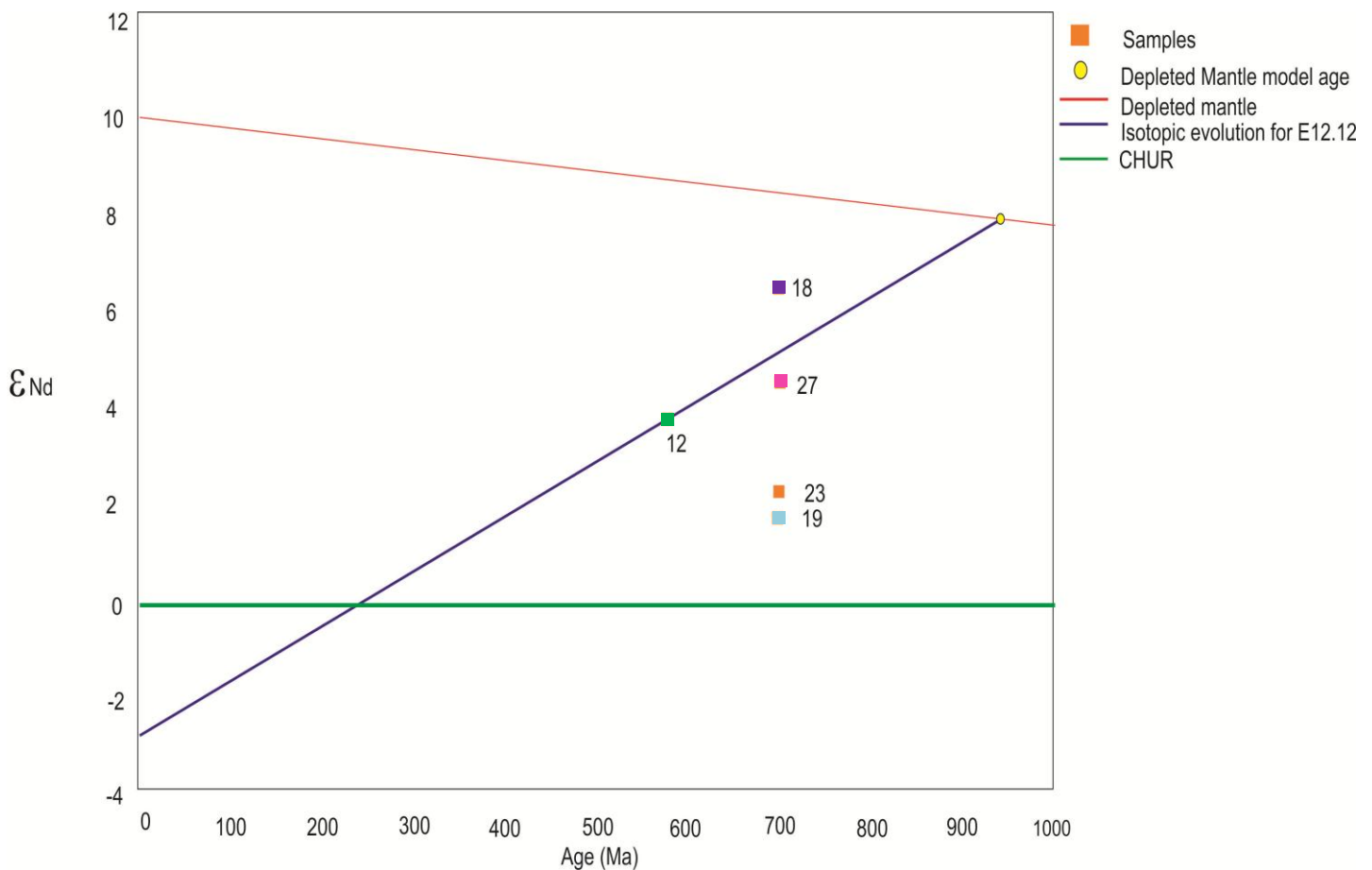


Figure 10 ϵ_{Nd} -T diagram for samples, 12 (granite), 19 (basalt), 18 (basalt), 23 (volcaniclastic) and 27 (dolorite). The sample numbers are shown next to their respective data point. The blue dotted line illustrates the isotopic evolution of the granite (E13.12) with a depleted mantle model age (953 Ma) located along the depleted mantle line. The samples have a positive value, indicating a juvenile nature.

TRACE ELEMENT ANALYSIS

The MORB-normalised multi-element diagrams (Fig. 11) show enrichment relative to MORB, the sequences are generally enriched in most of the compatible trace elements especially the Large Ion

Lithophile Elements (LILEs). Less incompatible high strength field elements are consistent and much less enriched when compared to MORB. These compositions are similar to those seen in basalts from arc environments. The trace element patterns for the basalts taken from the Abshala Mélange is relatively flat lying with a negative anomaly in strontium. Discrimination plot (Fig. 12 b) for the basalt E13.18 (basalt) from the Abshala Mélange, E13.23 (dolerite) E13.27 (volcaniclastic), all plots within the MORB field/ocean. Conversely, E13.19 also sampled from the mélange, suggests a within plate basalt. This is consistent throughout all plots (Fig.12 a, b, c, d). The dolerite (E13.23) whilst plotting in MORB field for (Fig. 12 b d), plots in the field of within plate basalt in figure 10a.

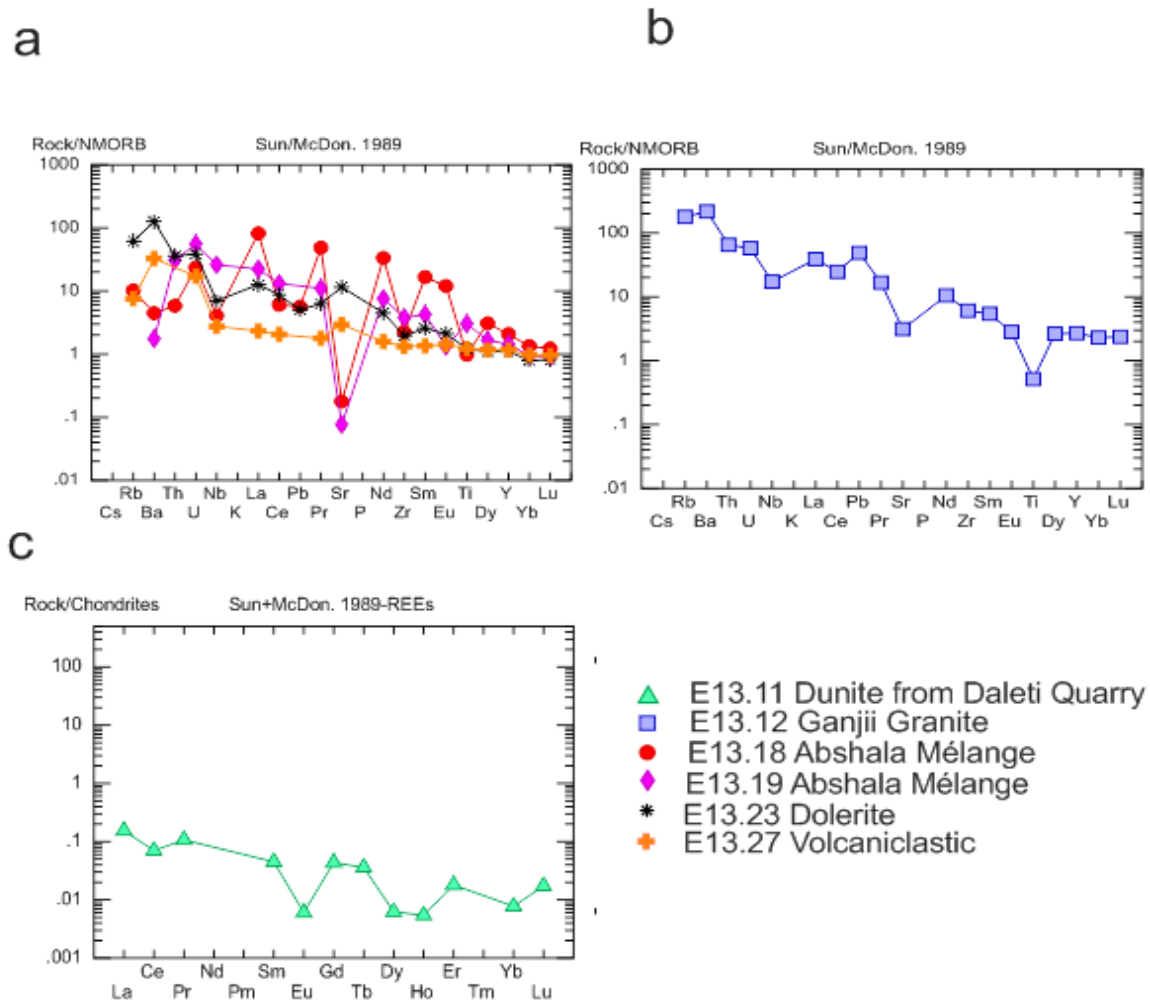


Figure 11 N-MORB normalised spider plot for the samples collected from the WES. Figure a and b are normalised to the Nmorb (Sun and McDonough 1989). a contains igneous and volcaniclastic samples. b) Contains basalts taken from Abshala Mélange. c) Is a dunite taken from Daleti Quarry and has been normalised to the chondrite. The REE pattern is relatively flat with minor anomalies. However, geochemical data must be treated carefully due to low concentrations.

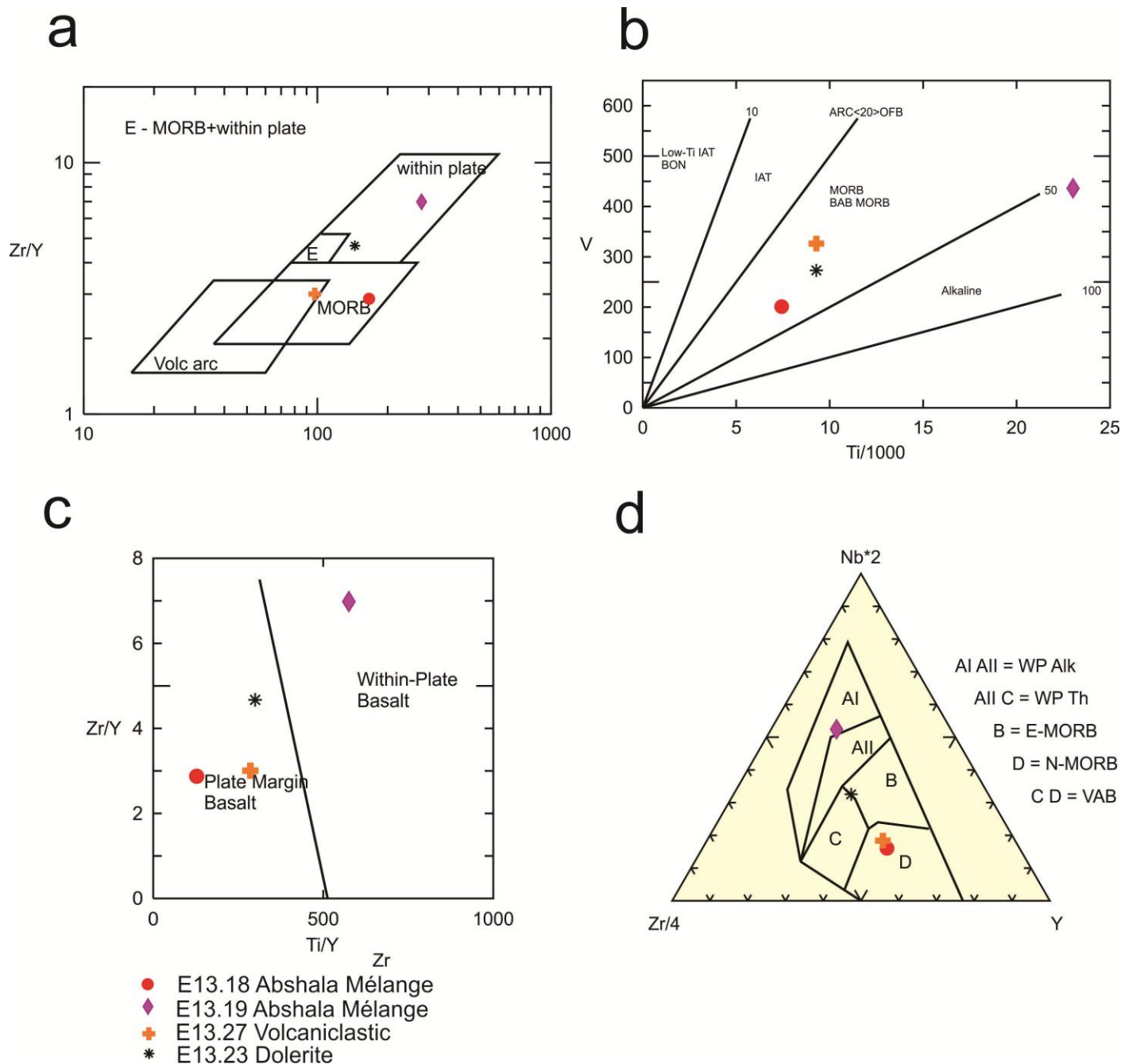


Figure 12 Four different basalt discrimination diagrams used for identifying the tectonic environment during the emplacement. The two basalts were taken from the Abshala Mélange. Whilst the other two samples; volcaniclastic and dolerite were collected in close proximity to the Sayi River. The mélange basalt (E13.19) plot in the ‘within-plate’ field for all diagrams (a-d). Similarly the mélange basalt (E13.18) and volcaniclastic (E13.27) consistently plot in the MORB (a-d). The dolerite however, does vary, plotting in both MORB and ‘within plate’ basalt.

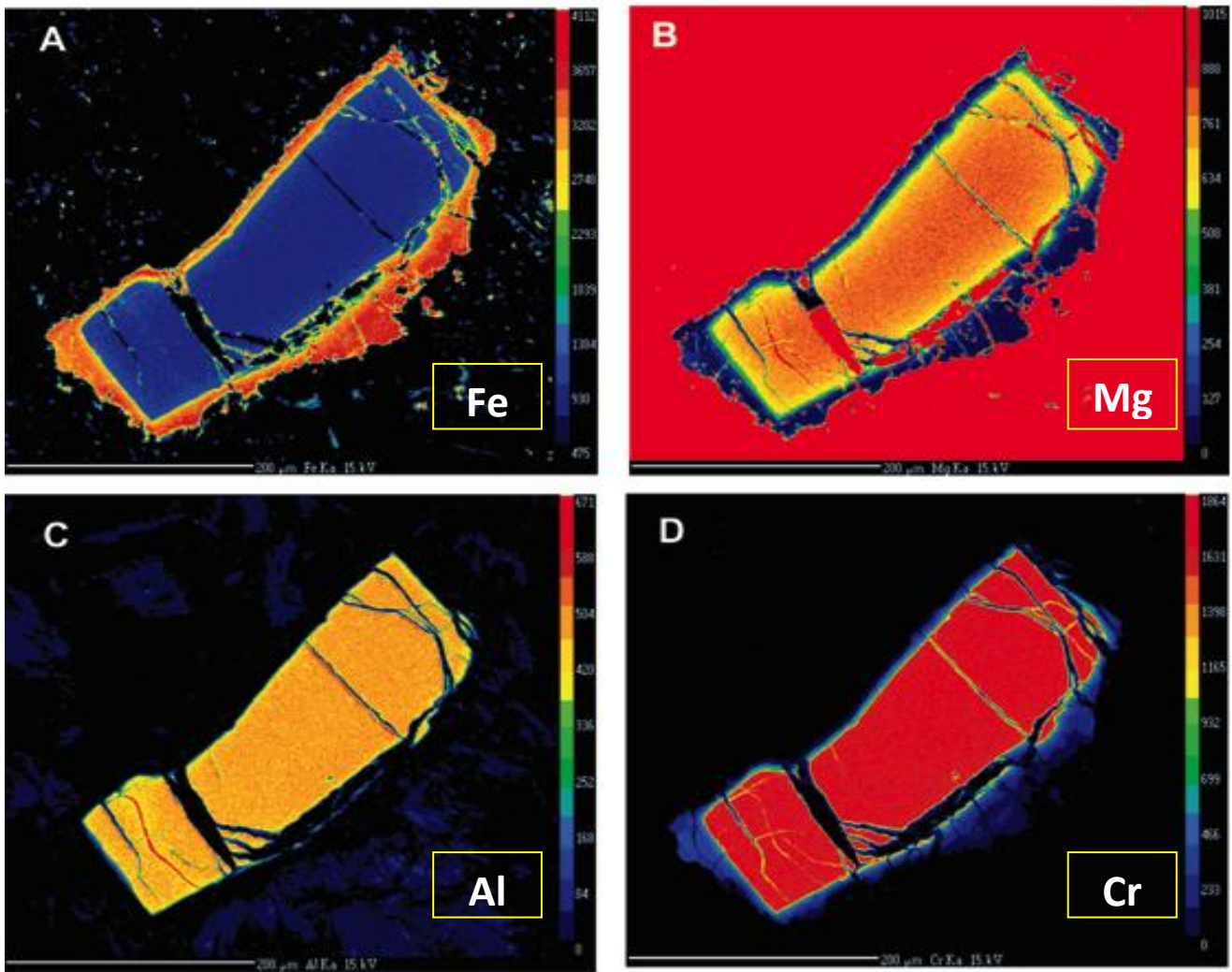


Figure 13 Elemental maps constructed on the microprobe for a chrome spinel grain from sample E13.26 a dunite from the WES. Figure 3 A depicts the Fe concentrations across the given grain. This shows that they have magnetite rims around chromite cores. The magnetite could have formed during serpentinization. Figure B illustrates the Mg concentrations across the grain. Figure C and D show the Al and Cr variations within the same grain. Figure C and D illustrate that there is depletion in Al and Cr at the rims. Figure A and B define an inversely proportional relationship between the Fe and Mg, suggesting an elemental exchange.

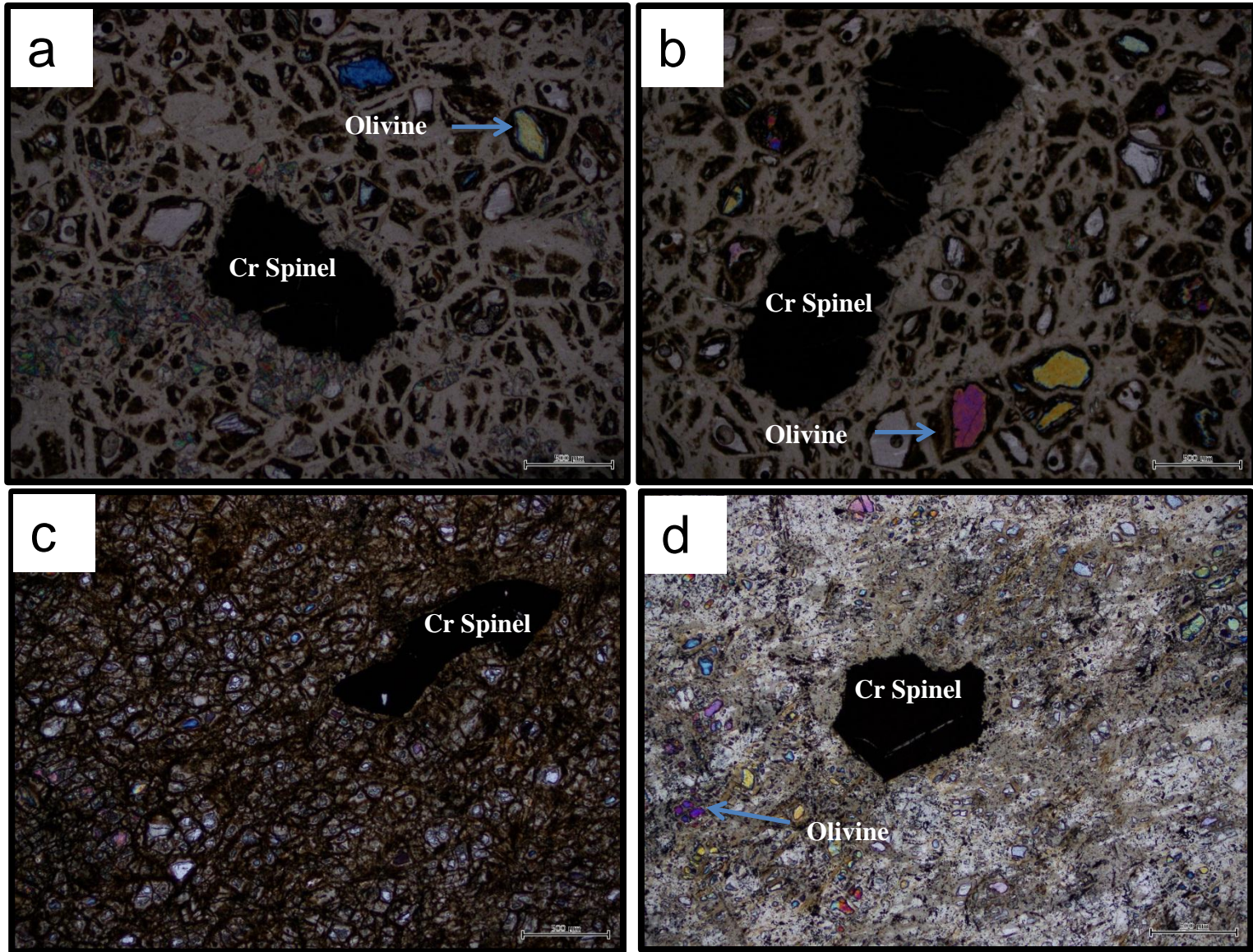


Figure 14 Photos taken from E13.11 and E13.26. a-b Dunite taken from Daleti Quarry. The apparent grain size of the olivine in these dunites has been affected by serpentinisation. This is seen by the mesh textured serpeninite grains. The small grains of olivine are relics of what would have been coarse grained olivine. c-d Is sample E13.26 taken from Tulu Dimtu Hill showing the same mesh texture however, serpentinisation is more extensive than Daleti Quarry.

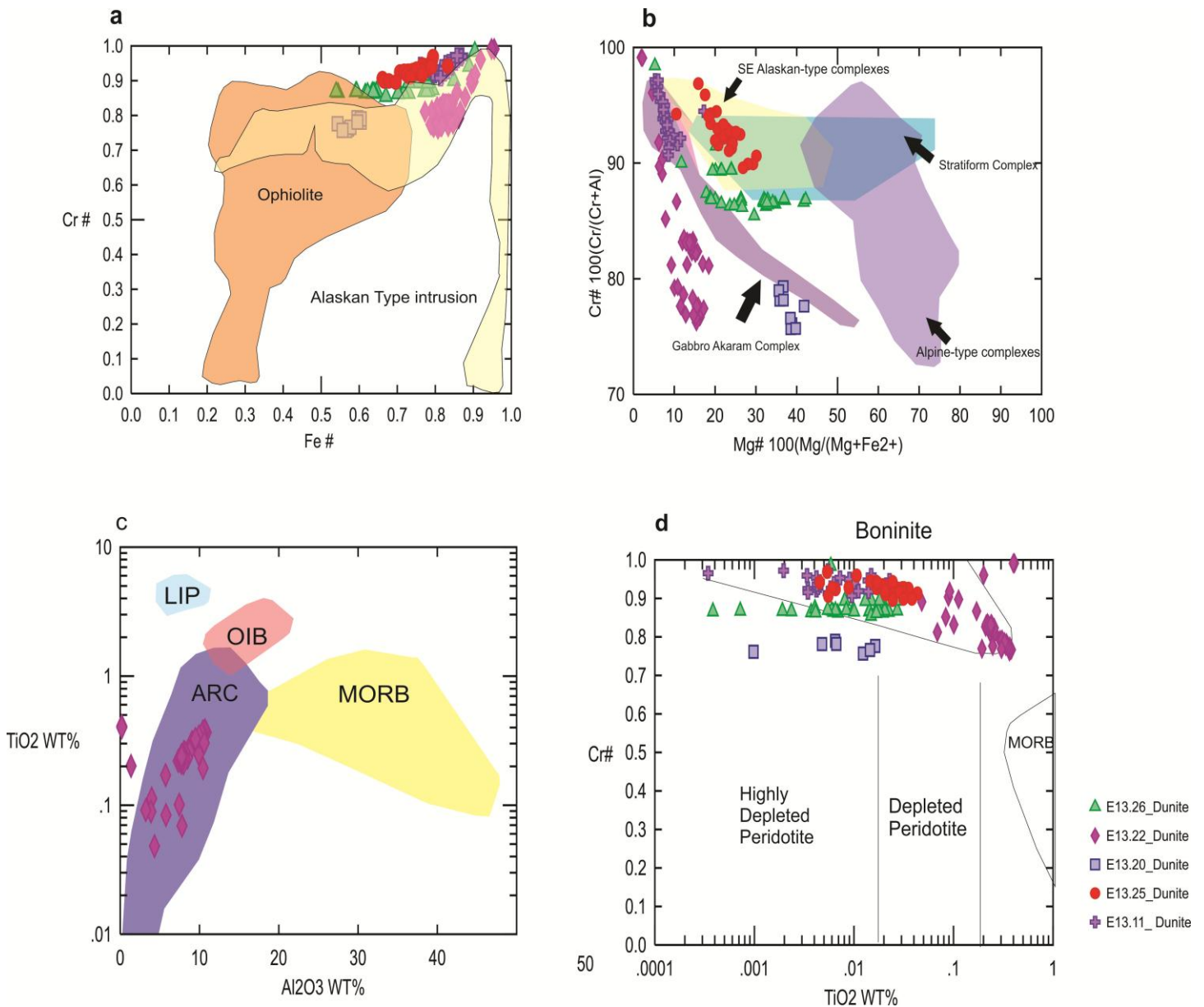


Figure 15: a) Cr# (Cr/Cr+Al) against Mg# (Mg/Mg+Fe²⁺) show the spinels from Daleti, Yubdo plot in the Alaskan Type intrusion field. b) a plot of Cr# against Mg# in spinels. Fields for various types of complexes are from Irvine (1967). Symbols are represented on the right side of the diagram. Taken and adapted from (Helmy and El Mahallawi 2003) c) Al₂O₃ vs TiO₂ compositional relationship in chrome spinel grains. Discrimination between mid ocean basalt (MORB), ocean-island basalt (OIB), Large igneous province (LIP) and island arc magmas (arc). The spinels plot with in the arc tectonic setting after hydration and serpetinisation. d) TiO₂ vs Cr# analyses plot in the boninitic field suggest that the rocks are sourced from the deeper mantle as the residual after a boninitic magma has been taken out. This is characteristic of a subduction system.

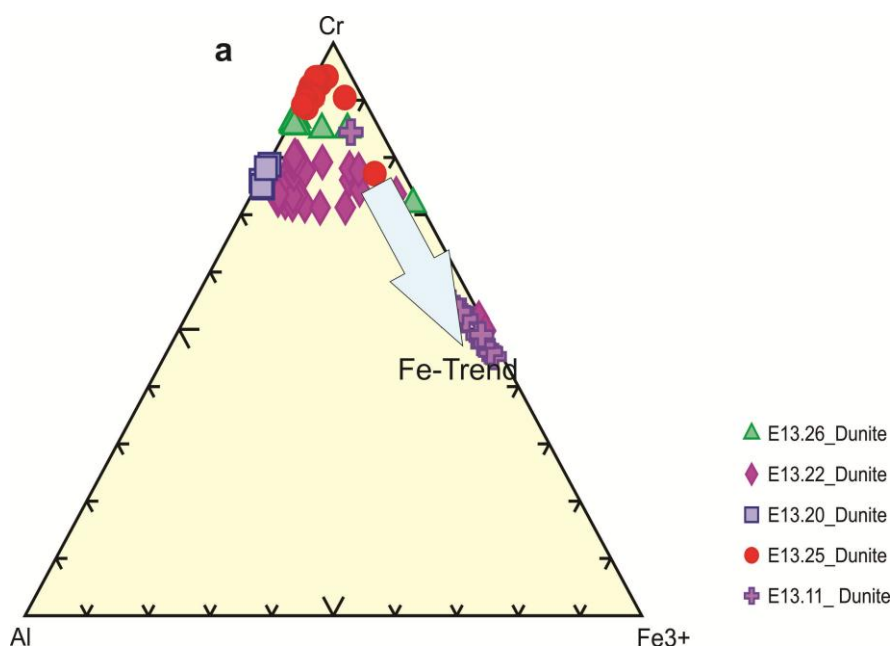


Figure 16 Al-Cr-Fe³⁺ depicting the alteration of samples. Sample E13.11 taken from Daleti Quarry displays a Fe³⁺ enrichment suggesting alteration of the chrome spinels.

CHROME SPINEL ANALYSIS

Chromite, along with scattered relicts of olivine are the only minerals from the original ultramafic rock that routinely retain their original igneous composition (Fig.14). Electron Microprobe analysis has been undertaken on chrome spinels from cumulate ultra-mafics at Daletti, Kemeshi-Gimbi Junction and Tulu Dimtu hill (Fig. 3). Representative chemical analyses of accessory chrome spinels are listed in Supplementary Table 3. The chrome spinels are characterised by high Cr₂O₃ (30.04 wt % 68.76 wt %) and variable TiO₂ content (0.01-0.39), the Cr # (molar Cr/Cr+Al) ranges from 0.757 to 0.991 with an average of 0.882 (Supplementary Table 6). The chrome spinels have a commensurate increase of Fe and decrease of Mg at the rims and are in association with olivine, which has an average Mg # of ~0.93. Fe-rich rims could be related to the Fe-Mg exchange with the olivine during the slow cooling of the mantle (Dick and Bullen 1984). On a Cr-Al-Fe³⁺ diagram (Fig. 15f), the majority of spinels lie at the apex, suggesting only minor loss in Cr₂O₃ and Al₂O₃ during serpentinisation. Sample E13.11 lies along the Cr-Fe join reflecting loss in Cr₂O₃ and Al₂O₃ and the addition of Fe₂O₃, which is likely to have happened during the serpentinisation that pervasively affected the rock. Mapped features and spinel chemistry of the Yubdo ultra-mafics support that

these are Alaskan-type intrusions (Fig. 15 a,b) (Barnes and Roeder 2001, Farahat and Helmy 2006, Helmy and Mogessie 2001, Kamenetsky et al. 2001, Mogessie et al. 2000). Alaskan-type ultra-mafic complexes are formed above active subduction systems, which is supported by the chrome spinel discrimination diagrams that use Ti (Fig. 15 c, d)(Farahat and Helmy 2006). Where the Ethiopian data falls in the fields for bonninites, this suggests the rocks have been formed from a hydrous melt characteristic of subduction environments (Beccaluva and Serri 1988).

$^{40}\text{Ar} - ^{39}\text{Ar}$ dating

Total fusion ages from these muscovites yielded ages ~551 and 545 Ma. As these rocks have been metamorphosed to greenschist facies and presumably hotter than the closure temperature of Ar in muscovite ~350°C (Hames and Bowring 1994), the ages derived from $^{40}\text{Ar}/^{39}\text{Ar}$ are interpreted to be age of cooling after metamorphism (Fig.17).

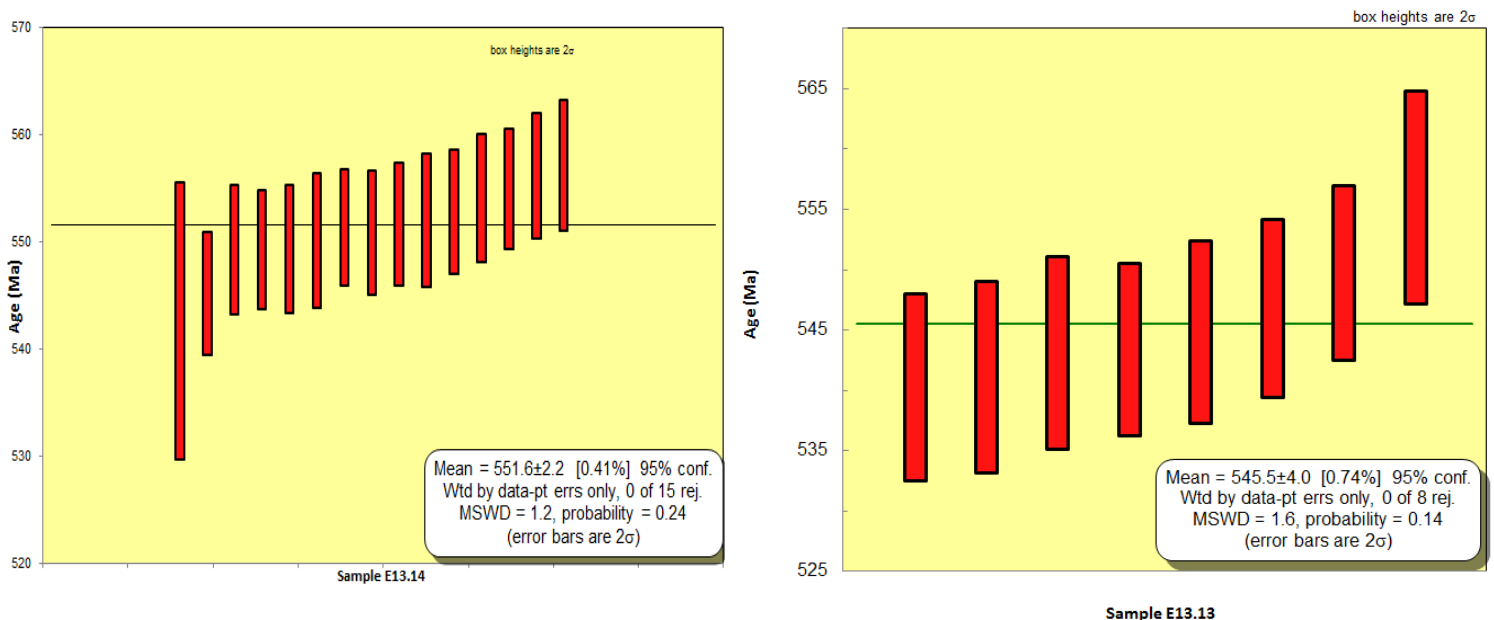


Figure 17 $^{40}\text{Ar} - ^{39}\text{Ar}$ dating of muscovite grains from schists sampled from the Western Ethiopian Shield. This was done using the total fusion method, showing the interpreted age of the greenschist metamorphism.

DISCUSSION

Age and Origin of plutonic sequences in the WES

The Ganjii granitoid yielded a $\text{Pb}^{206}/\text{U}^{238}$ age of 572.6 ± 7.4 Ma which is ~ 50 Ma younger than previously interpreted. It has been previously classified as a monzo-granite (Kebede and Koeberl 2003), and shows the chemical and mineralogical characteristics of within-plate granite, generated and emplaced in an extensional tectonic environment. The Ganjii Granite is undeformed thus forms an age for the final deformation in the area. Nd model ages were calculated assuming derivation of juvenile crust from the depleted mantle following Stern (2002), using the DePaolo Depleted Mantle Model (DePaolo 1988). The sample has a $^{147}\text{Sm}/^{144}\text{Nd} < 0.165$ thus inferring that the results will be more reliable. A high $^{147}\text{Sm}/^{144}\text{Nd}$ value will intercept the mantle curve at a low angle, so that uncertainties in the composition of the mantle source transform into comparatively large variances in model ages (Stern 2002).

The Depleted Mantle model (t) age of the Ganji Granite is ~ 953 Ma (Supplementary Table 5). Model ages are about 300 Ma older than the crystallisation age reported, but younger than the Mesoproterozoic and Archaean ages yielded from detrital zircons in metasedimentary rocks. Zircons from the Ganjii Granite yielded similarly positive ϵ_{Hf} values with a range of 6.79-7.98 (Fig. 8 b). Taken together, the U-Pb, Nd and Hf data suggest that the Ganjii Granite was generated from Neoproterozoic juvenile mantle sources, with any involvement of pre-Neoproterozoic continental crust being minor.

Nature of the rocks of Western Ethiopian Shield

The transitional character of the dolerite and volcanoclastic rocks having partly enriched MORB-like geochemical signatures fits best with continental back-arc or rifted arc paleotectonic settings. The large-ion lithophile elements and light rare earths are considerably enriched relative to MORB. Whilst the HSFE and more immobile elements are enriched; they are less enriched in relation to MORB. This is characteristic of

island arcs (McLennan and Taylor 1981). However, the niobium anomaly is only minor, which is unusual for arc related rocks (Fig. 11). A negative niobium anomaly is characteristic of two things; presence of a subduction zone and the contamination by the crust. This element is highly incompatible during mantle melting and fractional crystallisation. Generally niobium is highly depleted in supra-subduction zone magmas. This has been experimentally shown to be due to the low solubility of niobium in the hydrated and solute-poor fluids in the shallow parts of subduction zones (Baier et al., 2008), suggesting that niobium is not added to the mantle wedge by slab derived fluids. Discrimination diagrams for the basalts derived from the Abshala Mélange (Fig. 12) plot E13.18 as a MORB, suggesting it may have been scrapped off bits of the MORB in an accretionary complex or as an accreted piece of sea-mount. Whereas, the E13.19 data falls in the field of a within plate, alkaline basalt. This is very possible for mélanges as they often form in accretionary prisms where different fragments are scraped off the subducting slab. The volcanoclastic (E13.27) plots in the field of MORB, however dolerite whilst still having a MORB affinity trends towards a within plate basalt. Within out the niobium anomaly the source seems to be more enriched than expected.

Geochemical analysis of radiogenic isotopes from the basalts, dolerite and volcanoclastic rock yield positive ϵ_{Nd_t} values suggesting that they are juvenile in nature, derived from the mantle, with minor continental crust influence (Fig. 10). Therefore, the relatively juvenile nature together with the subduction affinity interpreted from the REE spider-plots (Fig. 11), suggests that the Neoproterozoic terrane was, in part, formed as the result of the closure of a Neoproterozoic ocean (Mozambique Ocean) and the formation of an arc.

Age and Provenance Significance of Metasediment in the Western Ethiopian Shield.

Meta-quartz-arenite are sourced from Stenian -Tonian (1.15 – 0.8 Ga), late Palaeoproterozoic (~1.8 Ga), Palaeoproterozoic – Neoarchaeon (2.4 – 2.8 Ga). The maximum depositional age of the protolith to this metasediment is 838 ± 13 Ma based on the age of the youngest zircons grain. These populations can be

traced back to orogenic events present in African crust to the west. Tonian - Stenian magmatism and metamorphism have been found from the granitoids and gneisses in the north-central Bayunda Desert in Sudan (Küster et al. 2008). This peak defines the largest and youngest population of zircons. The positive ϵ_{Hf_t} of these zircons suggest that the source rocks were juvenile. The populations of the late Palaeoproterozoic zircons at ~1820 Ma yield a negative ϵ_{Hf_t} value. These zircons could have been sourced from the tract of older remobilised crust to the south of the Arabian Nubian Shield, the Mozambique Belt (Meert 2003, Woldemichael and Kimura 2008, Woldemichael et al. 2010, Yibas et al. 2003).

Palaeoproterozoic - Neoproterozoic rocks are common in the cratonic Africa, and these form the potential sources from the couple of similar-aged zircons found here (Muhongo et al. 2001). Ages derived from $^{40}\text{Ar}/^{39}\text{Ar}$ are assumed to be age of metamorphism. These rocks have been metamorphosed to greenschist facies at ~551 and 543 Ma (Fig.17). When combined with the igneous geochemistry discussed in the previous section, the detrital zircon data suggest that although the greenschist-facies terrane in the Western Ethiopian Shield formed as a Neoproterozoic arc, it was depositionally connected to the African continent, as sandstones were sourced from there.

Significance of the Yubdo-Tulu Dimtu Ultra-mafics.

The Western Ethiopian Shield has a tectonically complex history, beginning with early rifting and associated sedimentation, subsequent subduction and island arc formation, arc accretion and lastly continent-continent collision. A significant aspect of the Arabian-Nubian Shield is the interpretation of the N-S oriented regional shear zones. The Barunda-Tulu Dimtu zone stretches through Ethiopia and connects with the Barka zone in Eritrea. It is one of the major structures of this type within the Arabian- Nubian Shield. These are host mafic and ultra-mafic rocks, which have been suggested to be of similar nature to an ophiolite (Tadesse and Allen 2005, Tadesse and Allen 2004). Braathen et al. (2001) questioned this, and pointed out that the components essential for the identification of ophiolites such as, tectonised mantle harzburgite, sheeted dyke complex, or basaltic pillow lavas with associated pelagic sediments, have not been recognised as being directly

associated with the complexes found in Ethiopia. Braathen et al. (2001) proposed an alternate theory stating that the zoned mafic and ultra-mafic bodies along the shear zone, as well as isolated bodies along the shear zone, were originally emplaced as solitary magma chambers with mafic and ultra-mafic cumulates similar to so-called 'Alaskan-Type intrusions' (Mogessie et al. 2000). This was interpreted to be a result of limited dilation within the back-arc basin without the development of true oceanic crust (Braathen et al. 2001, Grenne et al. 2003).

The mineral chromite has been used to determine the petrogenetic conditions of evolving mafic magmas since the establishment of Irvine's papers in 1965 and 1967. In recent times it has also been documented that chromites formed in mafic melts of differing tectonic environments have compositional differences. Therefore, the use of chromite can help to establish the tectonic setting of mafic and ultramafic rocks (Kamenetsky et al. 2001). Chrome spinel compositions are used to test the two main theories for the formation of the Tulu Dimtu and Yubdo ultra-mafic complexes. Firstly, that the complexes are ophiolites, remnants of the Mozambique Ocean. Secondly, that they form as intrusive rocks above subduction zones, similar to Alaskan-type intrusions. Ophiolitic peridotites, commonly have a spinel Cr#s that exceed 0.55, suggesting mantle melting considerably beyond the exhaustion of clinopyroxene. This is attributed to the role of water in the mantle melting above a subduction zone (Dick and Bullen, 1984). This is similar to the Cr# values obtained from spinels in this study. Figure 15d shows that the associated spinels have a boninitic affinity. Boninites define a field of exceptionally high Cr/(Cr+Al), low Fe³⁺ and exceptionally low TiO₂ lavas, formed in a supra-subduction zone (Barnes and Roeder 2001). Although the mafic-ultramafic complexes are concentrated along the shear-zones, their existence outside this zone is problematic for the ophiolite suture model. Generally enclosed in meta-sediments, may also suggest that they represent solitary intrusions, rather than being tectonic fragments of oceanic crust which have been caught up in the suture zones (Braathen et al. 2001).

Recently Mogessie et al. (1999, 2000) mapped the Yubdo and Tulu-Dimtu ultra-mafic bodies and showed them to have concentric zoning typical of Alaskan-type intrusions. Alaskan-type zoned mafic-ultramafic complexes are characterized by a concentric arrangement of rock types. Such complexes have been described from Alaska, the Urals of Russia, Australia, Canada and Columbia (Farahat and Helmy 2006, Barnes and Roeder 2001, Dick and Bullen 1984, Helmy and El Mahallawi 2003, Helmy and Mogessie 2001, Himmelberg and Loney 1995, Jackson et al. 2005). Alaskan-type intrusions are small in size, elliptical or rounded in shape and located along lineaments. One can distinguish Alaskan-type intrusions by; 1) the gradation from dunite to gabbros, 2) Fe³⁺ - Ti- rich spinels, 3) depletion of CaO in olivine 5) evidence of crystal accumulation such as scarce graded layers (Dick and Bullen 1984, Farahat and Helmy 2006, Helmy and El Mahallawi 2003, Helmy and Mogessie 2001, Himmelberg and Loney 1995). The Tulu-Dimtu and Yubdo zones have similar characteristics to Alaskan- type deposits. The main rock units of the Yubdo area are dunites at the core, surrounded by peridotite and hornblende-clinopyroxenite; similar to the Abu Hamamid Neoproterozoic Alaskan-type complex in Egypt (Farahat and Helmy 2006). However, there are chemical differences, when compared to typical Alaskan-type intrusions. Samples collected from the Tulu-Dimtu and Yubdo region display chrome spinel chemistry with considerably lower TiO₂ and low Fe³⁺ concentrations (Supplementary Table 6). (Barnes and Roeder 2001, Dick and Bullen 1984, Farahat and Helmy 2006, Helmy and El Mahallawi 2003, Helmy and Mogessie 2001, Himmelberg and Loney 1995, Kamenetsky et al. 2001, Proenza et al. 2007).

The spinel chemistry supports the subduction - related (island-arc) environment, from sources that are enriched in the slab component in the presence of a hydrous melt. This is characteristic of supra-subduction zone peridotites (Fig. 15C), where the data falls in the field of arc related peridotites. However, the ultra-mafic rocks of Yubdo have analogous map features and close chemical affinities to shear-zone hosted intrusions elsewhere in the Arabian-Nubian Shield (Farahat and Helmy 2006). Therefore, this suggests that these are not remnants of the Mozambique Oceanic crust, rather intrusions formed in a similar supra–

subduction zone to those seen in Egypt. However, differences in the spinel chemistry of Yubdo and Tulu Dimtu rocks, from other typical Alaskan-type intrusions, suggest that further study is warranted.

Tectonic Setting of the Western Ethiopian Shield

The tectonic history of the Western Ethiopian Shield can be interpreted in terms of Gondwana assembly and the closure of the Mozambique Ocean during the Neoproterozoic East African orogen.

Data supports the formation of the Western Ethiopian Shield over a subduction zone and the formation of an arc. However, it wasn't an intra-oceanic arc as sediments clearly show sources that are consistent with being derived from cratonic Africa. During this time, the emplacements of large mafic/ultra-mafic Alaskan-type intrusions occurred (Tulu Dimtu-Daleti-Yubdo Belt), as well as the generation of calc-alkaline basalts with a subduction affinity. The calc-alkaline basalts, a part of the tectonically complex and lithologically diverse mélangé, have been suggested to have formed as the result of thrust imbrication.

Towards the late Neoproterozoic the Ganjii granitoid was emplaced at ~572 Ma, generated from Neoproterozoic juvenile mantle sources, with minor continental crust involvement. Being relatively undeformed this represented the age for final deformation. The area was affected by late stage metamorphism; the rocks of the Western Ethiopian shield were affected by hydrous greenschist facies fluid at ~551 Ma and ~543 Ma.

The Western Ethiopian Shield in the East African Orogen

Comprehensive and systematic studies of felsic and granitic intrusions in the Western Ethiopian Shield (Ayalew et al. 1990, Grenne et al. 2003, Kebede and Koeberl 2003) have recognised three generations of magmatism (~830-810 Ma; ~780-700 Ma and ~620-550 Ma) in a subduction-related island-arc and intra-plate post collisional environment (Braathen et al. 2001, Grenne et al. 2003, Woldemichael and Kimura 2008, Woldemichael et al. 2010). The Gore-Gambella region contains nearly concordant zircons of igneous origin (Fig. 2). These yield intrusion ages for the pre-kinematic Birbir quartz-diorite and Goma granodiorite,

of $828 \pm 9/-2$ Ma and 814 ± 2 Ma (Ayalew et al. 1990). A major magmatic event around this time (ca. 815 Ma) is recognised in the Gimbi area (Kebede and Koeberl 2003). Studies on the Ganjii granite has placed the age 50 Ma earlier, (~ 572 Ma) than previously reported.

There has been little research conducted on metamorphism in the Western Ethiopian Shield. However, there have been two regional metamorphic events that have been identified (Ayalew 1990). Mineral assemblages in the meta-basic rocks indicate that there is a maximum of greenschist to epidote-amphibolite facies within the juvenile domains (ANS). ^{40}Ar and ^{39}Ar dating of muscovite has placed metamorphism at ~ 551 Ma and ~ 541 Ma. Within the gneissic domains mid-upper amphibolite facies are primarily seen, however there are occurrences where the gneissose rocks, that have preserved E-W orientated fabrics, have recorded granulite facies conditions. Studies have been conducted on metapelitic rocks from Gore-Gambella area (Fig. 3). These studies indicated that there was a peak P-T condition of around 520°C and 7kbar for the Birbir and Baro domains. This suggests steep metamorphic gradient at domain transition. Yibas et al. (2002) reported a number of tectonothermal events in southern Ethiopia throughout the Neoproterozoic and related them to subduction/accretion processes. The youngest is associated with granulite-facies metamorphism, which post-dates a 540–520 Ma granite (Genzebu et al., 1994) and has been interpreted as being related to the amalgamation of Gondwana (Yibas et al. 2002).

Positive ϵNd values have been collected for a series of rocks ranging from plutonic to metavolcanic. These range from 1.79 to 10.45. The two intrusive groups with differing magma chemistry and ages suggest that the earliest magmatism was tholeiitic and associated with the passive margin system followed by continental breakup to form the Mozambique Ocean (Ayalew et al. 1990, Braathen et al. 2001, Grenne et al. 2003, Kebede and Koeberl 2003, Stern 1994, Woldemichael and Kimura 2008, Woldemichael et al. 2010). The combination of tholeiitic and calc-alkaline magmatism is related to arc and back-arc basin formation and later terrane accretion.

Therefore it has been interpreted that the Western Ethiopian Shield has a tectonically complex history, beginning with early rifting and associated sedimentation, subsequent subduction and island arc formation, arc accretion and lastly continent-continent collision (Abdelsalam and Stern 1996). A general lack of evidence for Archean ages and scarcity of granulite-facies metamorphic relicts suggest that the relationship between the gneissic terrains in the Western Ethiopian Shield and those of the Mozambique Belt in the complex, making way for further study in the future.

Conclusions

Conclusions have been made about the geochronological and geochemical evolution of the Western Ethiopian Shield. The age yielded by the post tectonic Ganjii Granite have an age of ~572 Ma, this is 50 Ma younger than previously dated zircons. The Ganjii Granite has a positive ϵ_{Hf} and ϵ_{Nd} suggesting that the granite is relatively juvenile with minor crustal influence. Metasediments yielded a maximum deposition age of ~ 838 Ma. There are three distinct populations; hafnium isotopes reveal that sources are not all juvenile. The few zircons available are too few to statistically characterise the source region. However, zircons present, reveal ages of parts of the source region, one being perhaps the Bayunda Desert in Sudan. Radiogenic isotopes suggest that the terranes are largely juvenile; with minor continental crust interaction. Trace element diagrams are supportive of this demonstrating enrichment of large-ion lithophile elements with regard to MORB. The high strength field elements, more immobile, show slight enrichment, however not to the degree of the more mobile elements. This is characteristic of an arc environment. However, the minor negative niobium anomaly differs from typical island arc environments. The spinel chemistry of the ultra-mafic bodies supports the presence of an arc/subduction zone. They have mapped features similar to Alaskan-type intrusions and have close chemical affinities to shear-zone hosted intrusions elsewhere in the Arabian Nubian Shield for example the Abu Hamamid Complex. There these intrusions have been

interpreted to have been formed in a similar supra-subduction setting. The Western Shield of Ethiopia is interpreted as forming in a Neoproterozoic arc attached to the margin of Africa. It was metamorphosed to green-schist-facies at ~570 Ma and intruded by post-tectonic granites.

ACKNOWLEDGMENTS

I would like to thank my primary supervisor Dr. Alan Collins for his continual help and support throughout the year. Dr. John Foden and Dr. Justin Payne have also been invaluable throughout the process.

Gebremedhin Tadesse and Tesfaye Kebede need to be acknowledged for their extensive knowledge of the Western Ethiopia Shield, as well as for all the logistical support that they provided during the stay in Ethiopia. Many thanks need to go to David Bruce for all his help throughout the year with the geochemical analyses and John Stanley for his guidance in running samples through the XRF. I would like to express gratitude to Dr. Chris Clark and Dr. Richard Taylor from Curtin University for their help in analysing zircons on the SHRIMP. A huge thanks to Dr. Fred Jourdan from Curtin University for the Argon-Argon work he conducted on my samples. Many thanks to Aoife McFadden and Dr. Ben Wade from Adelaide Microscopy for all their help and support with ICP-MS and microprobe work. The support and guidance given throughout the year is greatly appreciated.

REFERENCES

- ABDELSALAM M. & STERN R. 1996 Sutures and shear zones in the Arabian-Nubian Shield, *Journal of African Earth Sciences*, vol. 23, no. 3, pp. 289-310.
- ALLEN A. & TADESSE G. 2003 Geological setting and tectonic subdivision of the Neoproterozoic orogenic belt of Tulu Dimtu, western Ethiopia, *Journal of African Earth Sciences*, vol. 36, no. 4, pp. 329-343.
- AYALEW T., *et al.* 1990 U-Pb and Rb-Sr geochronology of the western Ethiopian shield, *Geological Society of America Bulletin*, vol. 102, no. 9, pp. 1309-1316.
- BARNES S. J. & ROEDER P. L. 2001 The range of spinel compositions in terrestrial mafic and ultramafic rocks, *Journal of Petrology*, vol. 42, no. 12, pp. 2279-2302.
- BECCALUVA L. & SERRI G. 1988 Boninitic and low-Ti subduction-related lavas from intraoceanic arc-backarc systems and low-Ti ophiolites: a reappraisal of their petrogenesis and original tectonic setting, *Tectonophysics*, vol. 146, no. 1, pp. 291-315.
- BRAATHEN A., *et al.* 2001 Juxtaposition of Neoproterozoic units along the Baruda–Tulu Dimtu shear-belt in the East African Orogen of western Ethiopia, *Precambrian Research*, vol. 107, no. 3, pp. 215-234.
- COLLINS A. S. & PISAREVSKY S. A. 2005 Amalgamating eastern Gondwana: the evolution of the Circum-Indian Orogens, *Earth-Science Reviews*, vol. 71, no. 3, pp. 229-270.
- CORFU F., *et al.* 2003 Atlas of zircon textures, *Reviews in mineralogy and geochemistry*, vol. 53, no. 1, pp. 469-500.
- DEPAOLO D. J. 1988 Neodymium isotope geochemistry: an introduction. Springer-Verlag Berlin.
- DICK H. J. & BULLEN T. 1984 Chromian spinel as a petrogenetic indicator in abyssal and alpine-type peridotites and spatially associated lavas, *Contributions to Mineralogy and Petrology*, vol. 86, no. 1, pp. 54-76.
- FARAHAT E. & HELMY H. 2006 Abu hamamid neoproterozoic alaskan-type complex, south Eastern Desert, Egypt, *Journal of African Earth Sciences*, vol. 45, no. 2, pp. 187-197.
- FRITZ H., *et al.* 2013 Orogen styles in the East African Orogen: A review of the Neoproterozoic to Cambrian tectonic evolution, *Journal of African Earth Sciences*, no. 0.
- GRENNE T., *et al.* 2003 Neoproterozoic evolution of Western Ethiopia: igneous geochemistry, isotope systematics and U–Pb ages, *Geological magazine*, vol. 140, no. 04, pp. 373-395.
- GRIFFIN W., *et al.* 2006 Comment: Hf-isotope heterogeneity in zircon 91500, *Chemical Geology*, vol. 233, no. 3, pp. 358-363.
- HAMES W. E. & BOWRING S. A. 1994 An empirical evaluation of the argon diffusion geometry in muscovite, *Earth and Planetary Science Letters*, vol. 124, no. 1–4, pp. 161-169.
- HELMY H. & EL MAHALLAWI M. 2003 Gabbro Akarem mafic-ultramafic complex, Eastern Desert, Egypt: a Late Precambrian analogue of Alaskan-type complexes, *Mineralogy and Petrology*, vol. 77, no. 1-2, pp. 85-108.
- HELMY H. M. & MOGESSIE A. 2001 Gabbro Akarem, Eastern Desert, Egypt: Cu–Ni–PGE mineralization in a concentrically zoned mafic–ultramafic complex, *Mineralium Deposita*, vol. 36, no. 1, pp. 58-71.
- HIMMELBERG G. R. & LONEY R. A. 1995 Characteristics and petrogenesis of Alaskan-type ultramafic-mafic intrusions, southeastern Alaska. US Government Printing Office.
- HOWARD K. E., *et al.* 2009 Detrital zircon ages: Improving interpretation via Nd and Hf isotopic data, *Chemical Geology*, vol. 262, no. 3, pp. 277-292.
- JACKSON M., *et al.* 2005 Chrome spinel compositions complexes of the East African bearing Alaskan-type intrusions.
- JOURDAN F. & RENNE P. R. 2007 Age calibration of the Fish Canyon sanidine $^{40}\text{Ar}/^{39}\text{Ar}$ dating standard using primary K–Ar standards, *Geochimica et Cosmochimica Acta*, vol. 71, no. 2, pp. 387-402.

- KAMENETSKY V. S., CRAWFORD A. J. & MEFFRE S. 2001 Factors controlling chemistry of magmatic spinel: an empirical study of associated olivine, Cr-spinel and melt inclusions from primitive rocks, *Journal of Petrology*, vol. 42, no. 4, pp. 655-671.
- KAZMIN V., *et al.* 1979 Precambrian structure of western Ethiopia, *Ann Geol Surv Egypt*, vol. 9, pp. 1-18.
- KAZMIN V., SHIFFERAW A. & BALCHA T. 1978 The Ethiopian basement: stratigraphy and possible manner of evolution, *Geologische Rundschau*, vol. 67, no. 2, pp. 531-546.
- KEBEDE T. & KOEBERL C. 2003 Petrogenesis of A-type granitoids from the Wallagga area, western Ethiopia: constraints from mineralogy, bulk-rock chemistry, Nd and Sr isotopic compositions, *Precambrian Research*, vol. 121, no. 1, pp. 1-24.
- KEBEDE T., KOEBERL C. & KOLLER F. 1999 Geology, geochemistry and petrogenesis of intrusive rocks of the Wallagga area, western Ethiopia, *Journal of African Earth Sciences*, vol. 29, no. 4, pp. 715-734.
- KRÖNER A., *et al.* 1991 Evolution of Pan-African island arc assemblages in the southern Red Sea Hills, Sudan, and in southwestern Arabia as exemplified by geochemistry and geochronology, *Precambrian Research*, vol. 53, no. 1, pp. 99-118.
- KÜSTER D., *et al.* 2008 Zircon geochronology and Sr, Nd, Pb isotope geochemistry of granitoids from Bayuda Desert and Sabaloka (Sudan): Evidence for a Bayudian event (920–900Ma) preceding the Pan-African orogenic cycle (860–590Ma) at the eastern boundary of the Saharan Metacraton, *Precambrian Research*, vol. 164, no. 1, pp. 16-39.
- MCLENNAN S. M. & TAYLOR S. R. 1981 Role of subducted sediments in island-arc magmatism: constraints from REE patterns, *Earth and Planetary Science Letters*, vol. 54, no. 3, pp. 423-430.
- MEERT J. G. 2003 A synopsis of events related to the assembly of eastern Gondwana, *Tectonophysics*, vol. 362, no. 1, pp. 1-40.
- MOGESSIE A., BELETE K. & HOINKES G. 2000 Yubdo-Tulu Dimtu mafic-ultramafic belt, Alaskan-type intrusions in western Ethiopia: Its implication to the Arabian-Nubian Shield and tectonics of the Mozambique Belt, *Journal of African Earth Sciences*, vol. 30, no. 4, p. 62.
- MUHONGO S., KRÖNER A. & NEMCHIN A. A. 2001 Single Zircon Evaporation and SHRIMP Ages for Granulite - Facies Rocks in the Mozambique Belt of Tanzania, *The Journal of Geology*, vol. 109, no. 2, pp. 171-189.
- PAYNE J. L., *et al.* 2008 Temporal constraints on the timing of high-grade metamorphism in the northern Gawler Craton: implications for assembly of the Australian Proterozoic, *Australian Journal of Earth Sciences*, vol. 55, no. 5, pp. 623-640.
- PAYNE J. L., PEARSON N. J. & GRANT K. H., G.P 2013 Reassessment of relative oxide formation rates and molecular interferences on in-situ Lutetium-Hafnium analysis with Laser Ablation MC-ICP-MS. , *Journal of Analytical Atomic Spectrometry* vol. 28, no. 7, pp. 1068-1079.
- PROENZA J. A., *et al.* 2007 Chromian spinel composition and the platinum-group minerals of the PGE-rich Loma Peguera chromitites, Loma Caribe peridotite, Dominican Republic, *The Canadian Mineralogist*, vol. 45, no. 3, pp. 631-648.
- SHACKLETON R. 1996 The final collision zone between East and West Gondwana: where is it?, *Journal of African Earth Sciences*, vol. 23, no. 3, pp. 271-287.
- STERN R. J. 1994 Arc-Assembly and Continental Collision in the Neoproterozoic African Orogen: Implications for the Consolidation of Gondwanaland, *Annual Review of Earth and Planetary Sciences*, vol. 22, pp. 319-351.
- 2002 Crustal evolution in the East African Orogen: a neodymium isotopic perspective, *Journal of African Earth Sciences*, vol. 34, no. 3, pp. 109-117.
- SUN S. & MCDONOUGH W. 1989 Chemical and isotopic systematic of oceanic basalts: implications for mantle composition and processes. . pp. **313-345, 398**. London: **Blackwell Scientific publishing**.
- TADESSE G. & ALLEN A. 2004 Geochemistry of metavolcanics from the Neoproterozoic Tulu Dimtu orogenic belt, Western Ethiopia, *Journal of African Earth Sciences*, vol. 39, no. 3, pp. 177-185.

- 2005 Geology and geochemistry of the Neoproterozoic Tulu Dimtu Ophiolite suite, western Ethiopia, *Journal of African Earth Sciences*, vol. 41, no. 3, pp. 192-211.
- TEKLAJ M., *et al.* 1998 Geochemistry, Pb • Pb single zircon ages and Nd • Sr isotope composition of Precambrian rocks from southern and eastern Ethiopia: implications for crustal evolution in East Africa, *Journal of African Earth Sciences*, vol. 26, no. 2, pp. 207-227.
- VERMEESCH P. 2004 How many grains are needed for a provenance study?, *Earth and Planetary Science Letters*, vol. 224, no. 3-4, pp. 441-451.
- WADE B. P., *et al.* 2008 Origin of metasedimentary and igneous rocks from the Entia Dome, eastern Arunta region, central Australia: a U-Pb LA-ICPMS, SHRIMP and Sm-Nd isotope study, *Australian Journal of Earth Sciences*, vol. 55, no. 5, pp. 703-719.
- WOLDEMICHAEL B. W. & KIMURA J.-I. 2008 Petrogenesis of the Neoproterozoic Bikilal-Ghimbi gabbro, Western Ethiopia, *Journal of mineralogical and petrological sciences*, vol. 103, no. 1, pp. 23-46.
- WOLDEMICHAEL B. W., *et al.* 2010 SHRIMP U-Pb zircon geochronology and Sr-Nd isotopic systematic of the Neoproterozoic Ghimbi-Nedjo mafic to intermediate intrusions of Western Ethiopia: a record of passive margin magmatism at 855 Ma?, *International Journal of Earth Sciences*, vol. 99, no. 8, pp. 1773-1790.
- YIBAS B., *et al.* 2003 Geochemistry of the mafic rocks of the ophiolitic fold and thrust belts of southern Ethiopia: constraints on the tectonic regime during the Neoproterozoic (900-700 Ma), *Precambrian Research*, vol. 121, no. 3, pp. 157-183.
- YIBAS B., *et al.* 2002 The tectonostratigraphy, granitoid geochronology and geological evolution of the Precambrian of southern Ethiopia, *Journal of African Earth Sciences*, vol. 34, no. 1, pp. 57-84.

APPENDIX A:

Supplementary Table 1: Trace and major element analysis of 6 samples conducted on the XRF

Trace and Major Element Analysis

Sample Name	<i>E13.11 Dunite</i>	<i>E13.12 Ganji Granite</i>	<i>E13.18(1)Basalt from Abshala Melange</i>	<i>E13.19 Basalt from Abshala Melange</i>	<i>E13.23 Dunite</i>	<i>E13.27 Dunite</i>
Zr	3.5	446.4	166.6	279.3	144.8	97.6
Nb	0.4	40.1	9.5	60.5	16.2	6.4
Y	0.0	75.3	58.0	40.0	31.0	32.5
Sr	0.5	280.5	16.0	6.9	1036.2	264.0
Rb	0.5	99.7	5.7	0.0	34.3	4.2
U	0.8	2.7	1.1	2.6	1.8	0.8
Th	0.0	7.8	0.7	3.7	4.3	0.0
Pb	0.8	14.6	1.7	0.0	1.5	0.0
Ni	4573	1	314	578	38	76
Zn	34	89	86	63	102	80
Cu	6	0	7	1	82	58
Ga	1.3	22.5	20.6	13.0	17.4	14.2
Ba	16	1360	28	11	797	206
Sc	3.4	9.7	30.8	45.0	30.6	49.8
Co	123	50	64	106	54	61
V	10	20	201	436	273	326
Ce	6	163	40	95	70	23
Nd	-1	65	207	46	27	8
La	0	84	176	53	27	2
Cr	1999	0	412	198	85	333
SiO2 %	43.06	66.33	30.28	26.24	48.97	48.12
Al2O3 %	0.14	14.14	19.12	16.04	15.21	14.64
Fe2O3T %	8.41	4.73	13.15	17.79	11.02	12.08
MnO %	0.08	0.09	0.13	0.16	0.15	0.19
MgO %	34.73	0.73	23.39	25.05	6.32	7.80
CaO %	0.04	2.17	0.32	0.52	9.41	10.56
Na2O %	0.14	3.59	0.32	0.12	3.64	2.53
K2O %	0.01	4.88	0.11	0.00	1.57	0.28
TiO2 %	0.02	0.65	1.24	3.84	1.55	1.55
P2O5 %	0.00	0.21	0.05	0.36	0.60	0.15
SO3 %	0.01	0.04	0.02	0.02	0.23	0.06
LOI %	12.24	0.59	10.26	9.88	1.43	1.95
Total %	98.87	98.16	98.37	100.02	100.09	99.89

Analysis conducted on the XRF

Supplementary Table 2: SHRIMP U-Pb-Th analytical data for zircons and determined ages for the igneous and meta-sedimentary rocks of Western Ethiopia.

Spot Name	4-corr		ppm U	ppm Th	232Th /238U	204corr 206Pb		1s err	207corr 206Pb		1s err	% Dis-cordant	Total 238		% err	Total 207		% err	4corr 207*		% err	4corr 206*		% err	err corr
	% com 206	ppm U				ppm Th	ppm 206*		232Th /238U	Age			1s err	Age		1s err	Total 238 /206		Total 207 /206	4corr 207* /235		4corr 206* /238			
024-1.1	0.05	416	101	0.25	155	2318	32	2253	2587	24	+12	2.3	1.6	0.1734	1.4	10.33	2.2	0.433	1.6	0.8					
024-2.1	0.25	97	52	0.55	14	997	18	997	995	41	-0	6.0	2.0	0.0744	1.4	1.67	2.8	0.167	2.0	0.7					
024-3.1	0.08	296	236	0.82	84	1845	27	1845	1849	10	+0	3.0	1.7	0.1138	0.5	5.17	1.8	0.331	1.7	1.0					
024-4.1	0.20	706	608	0.89	84	838	13	839	806	18	-4	7.2	1.6	0.0677	0.6	1.26	1.8	0.139	1.6	0.9					
024-5.1	0.92	83	28	0.35	11	924	18	925	889	212	-4	6.4	2.1	0.0763	8.6	1.46	10.5	0.154	2.1	0.2					
024-6.1	0.15	89	48	0.56	14	1084	64	1085	1060	39	-2	5.5	6.5	0.0759	1.5	1.89	6.7	0.183	6.5	1.0					
024-7.1	0.05	387	196	0.52	106	1782	90	1772	1860	33	+5	3.1	5.8	0.1142	1.8	4.99	6.0	0.318	5.8	1.0					
024-8.1	0.00	1132	254	0.23	313	1798	25	1790	1855	5	+4	3.1	1.6	0.1135	0.3	5.03	1.6	0.322	1.6	1.0					
024-9.1	0.03	521	153	0.30	192	2307	63	2261	2499	5	+9	2.3	3.3	0.1644	0.3	9.74	3.3	0.430	3.3	1.0					
024-10.1	0.18	111	158	1.47	31	1835	31	1837	1822	19	-1	3.0	2.0	0.1129	0.8	5.06	2.2	0.329	2.0	0.9					
024-11.1	0.39	91	45	0.51	13	1019	19	1019	1015	52	-0	5.8	2.0	0.0763	1.5	1.73	3.3	0.171	2.1	0.6					
012-1.1	0.11	2.30	205	65	17	0.33	586	10	587	10	538	39	-9	10.5	1.7	0.0591	1.4	0.76	2.5	0.095	1.8	0.7			
012-2.1	0.23	3.56	59	22	5	0.39	599	13	600	14	542	280	-11	10.3	2.3	0.0602	12.0	0.78	13.0	0.097	2.3	0.2			
012-3.1	0.78	13.24	83	32	7	0.40	572	12	576	12	343	134	-70	10.7	2.1	0.0596	2.3	0.68	6.3	0.093	2.1	0.3			
012-4.1	-1.07	-13.06	51	24	4	0.49	560	13	553	13	927	146	+41	11.1	2.4	0.0611	3.8	0.88	7.5	0.091	2.5	0.3			
012-5.1	47.56	83.00	70	21	6	0.31	626	50	576	51	2218	620	+75	5.1	7.8	0.5578	3.8	1.96	36.8	0.102	8.4	0.2			
012-6.1	42.66	85.42	153	49	13	0.33	592	46	575	50	1348	926	+59	6.0	7.8	0.4490	4.7	1.15	48.6	0.096	8.1	0.2			
012-7.1	0.25	5.96	174	49	14	0.29	587	10	589	10	503	52	-18	10.5	1.8	0.0593	1.5	0.75	3.0	0.095	1.8	0.6			
012-8.1	0.24	4.55	46	15	4	0.33	576	13	575	13	632	93	+9	10.7	2.4	0.0627	2.9	0.78	4.9	0.093	2.4	0.5			
012-9.1	0.38	6.43	29	10	2	0.35	555	14	554	16	619	366	+11	11.1	2.7	0.0635	15.3	0.75	17.2	0.090	2.7	0.2			
012-9.2	-0.14	-2.95	67	21	5	0.33	581	12	581	12	624	189	+7	10.6	2.1	0.0594	8.7	0.79	9.0	0.094	2.1	0.2			
012-10.1	0.09	1.86	140	42	11	0.31	560	10	558	10	654	45	+15	11.0	1.8	0.0621	1.8	0.77	2.8	0.091	1.8	0.7			
012-11.1	3.97	61.64	105	31	8	0.30	560	11	571	11	-120	366	+593	10.6	2.0	0.0753	1.9	0.55	15.0	0.091	2.1	0.1			
012-12.1	0.00	0.00	120	39	10	0.33	580	10	580	11	562	146	-3	10.6	1.9	0.0589	6.7	0.76	7.0	0.094	1.9	0.3			
012-13.1	1.59	30.42	34	10	3	0.32	575	14	580	14	276	274	-113	10.5	2.5	0.0646	3.2	0.67	12.2	0.093	2.6	0.2			
012-14.1	2.84	62.37	37	10	3	0.29	589	15	603	15	-320	508	+298	10.2	2.5	0.0630	3.2	0.53	20.0	0.096	2.7	0.1			
012-15.1	0.61	6.91	111	63	9	0.58	571	10	575	11	319	103	-83	10.7	1.9	0.0577	2.2	0.67	4.9	0.093	1.9	0.4			
012-16.1	2.57	44.98	41	14	3	0.35	575	14	588	14	-245	441	+350	10.4	2.4	0.0621	3.1	0.54	17.6	0.093	2.6	0.1			
012-17.1	3.29	28.62	44	15	4	0.34	606	70	590	77	1280	1120	+55	9.8	12.2	0.1114	41.1	1.13	58.8	0.098	12.2	0.2			
012-18.1	0.00	0.00	149	49	11	0.34	551	10	549	10	672	36	+19	11.2	1.8	0.0620	1.7	0.76	2.5	0.089	1.8	0.7			
012-19.1	39.07	103.57	69	22	3	0.33	335	19	351	16				11.4	2.3	0.3358	6.2	0.11	361.9	0.053	5.8	0.0			
012-19.2	10.93	54.41	189	98	15	0.54	553	11	543	10	1080	241	+51	9.9	1.8	0.1672	1.1	0.93	12.2	0.090	2.1	0.2			
012-10.2	0.00	0.00	58	29	5	0.52	573	13	570	13	707	62	+20	10.8	2.4	0.0630	2.9	0.81	3.8	0.093	2.4	0.6			
012-12.2	0.83	11.19	92	43	7	0.49	580	12	582	13	433	300	-36	10.5	2.1	0.0622	10.9	0.72	13.6	0.094	2.2	0.2			

Supplementary Table 3: Hf results conducted on the Laser at Waite Campus Adelaide University. E13.12 Ganji Granite and E13.24a is meta quartz-arenite.

Sample N	Hf(i)	Epsilon	1s	T(DM) (Ga)	T(DM) (Crustal)	Hf Chur (T)	Hf DM (T)
<i>Ples_389</i>	0.282445807	-4.52266	0.476676	1.11336399	1.600079	0.282573	0.283009
<i>Ples_390</i>	0.282463647	-3.8899	0.466643	1.08873637	1.560458	0.282573	0.283009
<i>Average Ples Value</i>	0.282454727						
<i>E13.12.1</i>	0.282640749	7.658433	0.974415	0.86164217	1.027518	0.282416	0.282829
<i>E13.12.2</i>	0.282640749	7.943458	0.974415	0.86164217	1.019767	0.282408	0.282820
<i>E13.12.3</i>	0.282670878	8.455499	1.087569	0.81724759	0.966224	0.282425	0.282839
<i>E13.12.4</i>	0.282642767	7.008647	1.173458	0.86813956	1.048074	0.282432	0.282848
<i>E13.12.5</i>	0.282682965	9.703392	1.662483	0.8193999	0.930018	0.28239	0.282800
<i>E13.9.1</i>	0.28267874	8.128568	1.618363	0.819806	0.973491	0.282435	0.282851
<i>E13.10.1</i>	0.28267227	8.15394	1.111555	0.82035648	0.975821	0.282432	0.282848
<i>E13.15.1</i>	0.282667448	7.624583	1.924291	0.86325351	1.017869	0.282425	0.282840
<i>E13.18.1</i>	0.282659771	7.608934	1.179041	0.83230858	1.003148	0.282438	0.282854
<i>E13.24.1</i>	0.281238476	2.277484	1.250878	2.81029015	2.934968	0.281124	0.281353
<i>E13.24.2</i>	0.282303102	3.982977	2.035137	1.37220871	1.578079	0.282156	0.282532
<i>E13.24.3</i>	0.28154202	-3.65433	1.241509	2.40105276	2.709804	0.281606	0.281904
<i>E13.24.4</i>	0.282530626	8.328144	1.518731	1.02926319	1.158591	0.282276	0.282669
<i>E13.24.5</i>	0.282300023	1.73918	2.084194	1.3686106	1.634644	0.282223	0.282609
<i>E13.24.6</i>	0.282219867	2.497691	2.793002	1.48692688	1.720866	0.282114	0.282484
<i>E13.24.7</i>	0.281537723	-3.25307	1.362336	2.39150729	2.694253	0.281599	0.281896
<i>E13.24.8</i>	0.281591291	-1.80149	1.470191	2.33476496	2.603115	0.281602	0.281899
<i>E13.24.9</i>	0.281296039	2.573421	1.349674	2.72170263	2.84772	0.281182	0.281419
<i>E13.24.10</i>	0.281305997	-11.9224	1.359941	2.68375291	3.183378	0.281624	0.281924
<i>13.24.11</i>	0.28223761	2.764318	2.088647	1.42741602	1.669249	0.282143	0.282517

$$Hf_i = {}^{176}\text{Hf}/{}^{177}\text{Hf} \text{ ratio} - ({}^{176}\text{Lu}/{}^{177}\text{Hf} \text{ ratio} * (\text{EXP}(0.0193 * {}^{207}\text{Pb}/{}^{206}\text{Pb} \text{ ratio} / 1000) - 1))$$

CHUR from Bouvier et al. (2008); *Earth and Planetary Science Letters* 273 (2008) 48–57

$$\text{CHUR } {}^{176}\text{Lu}/{}^{177}\text{Hf} = 0.0336 \pm 1 \text{ and } {}^{176}\text{Hf}/{}^{177}\text{Hf} = 0.282785 \pm 11$$

Supplementary Table 4: ICP-MS REE analysis of 7 samples. These samples are E13.12 (granite), E13.19 (basalt), E13.18 (basalt), E13.23 (volcaniclastic) and E13.27 (dolorite). Some samples contain duplicates indicated as following E13.18.1 and E13.18.2.

	<i>E13.27.2</i>	<i>E13.11.1</i>	<i>E13.11.2</i>	<i>E13.12.1</i>	<i>E13.18.1</i>	<i>E13.18.2</i>	<i>E13.19.1</i>	<i>E13.19.2</i>	<i>E13.23.1</i>	<i>E13.23.2</i>	<i>E13.27.1</i>
Zr	102.7157372	0.021556357	0.026599754	523.9385868	173.626909	187.7531065	282.9385604	278.544066	139.769528	141.717412	103.3077191
Nb	4.611170009	0.012715691	0.023075591	37.98597584	8.116052849	8.578720084	59.37973569	59.6701401	14.4040993	14.3484366	4.651461971
La	5.998902362	0.036530776	0.049036522	96.96331309	203.563042	220.5048753	55.55797188	59.8746407	31.5516058	31.7820765	5.812669373
Ce	15.63562376	0.042861947	0.052271667	184.3426151	45.40522135	47.83587331	98.33518023	105.645301	65.0625441	65.9546563	15.36180325
Tb	0.862294142	0.001342682	0.002125007	2.093652612	3.262032691	3.524046706	1.435831572	1.46560403	0.88088629	0.87095557	0.841932149
Pr	2.437586107	0.010175366	0.011359266	21.97022068	63.94796189	68.69276251	14.55087207	15.6085363	8.31846148	8.26097715	2.354869013
Nd	11.56328635	0.023409935	0.030585126	76.50740239	243.2624601	263.6479246	55.34001999	59.4148755	32.7125097	32.1514438	11.51408051
Sm	3.630172482	0.006868349	0.008770399	14.24682914	43.69940331	46.58741712	11.11432924	11.7658554	6.72208159	6.37476087	3.56524952
Eu	1.444678095	0.000350393	0.001996054	2.869396819	12.19363117	13.16815233	1.361190159	1.40466817	2.14969654	2.1420239	1.448629421
Gd	0.370522243	0.008976628	0.005555233	2.137805174	0.681718348	1.126269024	0.330915177	0.69802911	0.35465993	0.20102345	0.599512868
Dy	5.449088582	0.00158028	0.005105655	12.01168495	14.00383987	15.07699472	7.542700802	7.7178093	5.00679554	4.80528384	5.306275349
Ho	1.159012752	0.000307778	0.000688556	2.514767437	2.275929606	2.474434427	1.398268472	1.40727451	0.98053289	0.95684073	1.12776773
Er	3.38687266	0.002981557	0.004036789	7.523711456	5.718595451	6.167767551	3.767484996	3.75997722	2.75643204	2.72220875	3.334697878
Yb	3.063584225	0.00131487	0.002779681	6.990844111	4.071351774	4.346994239	2.886125666	2.8453301	2.41435703	2.3264499	2.95085392
Lu	0.465201572	0.000437674	0.001020929	1.072343598	0.558831425	0.62871242	0.406912303	0.42180364	0.37174433	0.35378342	0.432271288
Hf	2.724394591	0.001168739	0.002624215	13.41753148	4.043924068	4.265724104	7.190277518	6.91086964	3.72003685	3.65388337	2.854466266
Ta	0.334583061	0.009038588	0.011348449	2.589350168	0.514541612	0.525291006	3.42066983	3.38067074	0.78498464	0.75162857	0.364203783
W	86.97988663	4.793520612	6.673196209	309.1956534	27.46836038	28.01049188	5.160999977	5.27172183	101.412826	97.4457669	91.14066296
U	0.156129257	0.213302472	0.244506395	2.305654428	1.105286746	1.104697816	1.326837337	1.3101147	1.59316289	1.51299246	0.15913195

Analysis carried out on the ICP-MS at Adelaide Microscopy

Supplementary Table 5: Sm-Nd isotopic compositions of igneous and metavolcanic rocks of the WES

sample #	E13-11	E13-12	E13-18	E13-19	E13-27	E13-23
input age of rock T (Ma)	700	578	700	700	700	700
Unmixed 143/144Nd	.512192	.512505	.512561	.512454	.512826	.512407
Nd $\mu\text{g g}^{-1}$.0	75.1	216.3	29.5	4.3	97.4
Sm $\mu\text{g g}^{-1}$.0	13.8	38.4	6.7	1.3	19.4
147Sm/144Nd	.1455	.1113	.1074	.1368	.1865	.1205
$\epsilon\text{Nd (T=0)}$	-8.69	-2.60	-1.50	-3.60	3.68	-4.51
143Nd/144Nd (T)	.511524	.512083	.512068	.511826	.511971	.511854
$\epsilon\text{Nd (T)}$	-4.13	3.71	6.49	1.76	4.59	2.31
TDM (Ma)	2109	953	839	1364	1759	1204
TCHUR (Ma)	1329	239	132	470	-2889	464
DM at age of rock (T)	.512166	.512338	.512166	.512166	.512166	.512166
CHUR at age of rock (T)	.511736	.511893	.511736	.511736	.511736	.511736
<i>JNdi-1 reference material measured 3/8/12 to 16/8/12, 143/144Nd = .512074 10(sd), 5 measurements.</i>						
<i>SRM reference material measured 10/8/12 to 16/8/12, 87/86Sr = .710240 6(sd), 4 measurements.</i>						
Nd Model assumptions						
Lambda	6.54E-12	6.54E-12	6.54E-12	6.54E-12	6.54E-12	6.54E-12
143Nd/144Nd CHUR T=0	.512638	.512638	.512638	.512638	.512638	.512638
147Sm/144Nd CHUR T=0	.1966	.1966	.1966	.1966	.1966	.1966
143Nd/144Nd DM T=0	.513150	.513150	.513150	.513150	.513150	.513150
147Sm/144Nd DM T=0	.2145	.2145	.2145	.2145	.2145	.2145
Earth Age	4.615E+09	4.615E+09	4.615E+09	4.615E+09	4.615E+09	4.615E+09
Sample measurements						
Sm Nd spike	F QCD	F QCD	F QCD	F QCD	F QCD	F QCD
sample wt (g)	.49191	.08092	.20203	.20857	.20865	.07747
Sm Nd spike wt (g)	.23911	.44205	.42380	.39794	.46918	.45147
measured 143/144Nd	.515157	.512523	.512564	.512470	.512958	.512422
2 se (x1E-6)	99	9	10	8	10	9
measured 150/144 Nd	13.097149	.321437	.247812	.311875	.838408	.306327
2 se (x1E-6)	3862	57	19	20	151	15
measured 147/149 Sm	98.59845	2.66382	1.30986	2.23165	7.60947	2.29192
2 se (x1E-5)	7231	16	11	20	172	20
measured 152/149 Sm	1.30922	1.91067	1.91801	1.91042	1.87464	1.90789
2 se (x1E-5)	165	16	23	12	69	10

Supplementary Table 7 Microprobe analysis of olivine in association with Chrome spinel with in the dunites for E13.26 and E13.11.

	E13.26	E13.26	E13.26	E13.26	E13.26	E13.26	E13.26	E13.26	E13.26	E13.26	E13.26	E13.26	E13.11	E13.11	E13.11
SiO ₂	40.951	41.560	41.749	41.820	41.890	44.057	41.059	41.152	41.259	41.831	41.175	41.136	42.267	42.081	41.683
TiO ₂	0.000	0.000	0.004	0.000	0.001	0.007	0.001	0.000	0.007	0.014	0.000	0.005	0.001	0.002	0.006
Al ₂ O ₃	0.005	0.003	0.005	0.000	0.000	0.000	0.001	0.000	0.006	0.000	0.000	0.000	0.000	0.003	0.000
Cr ₂ O ₃	0.000	0.000	0.000	0.037	0.002	0.017	0.012	0.000	0.001	0.000	0.017	0.001	0.016	0.015	0.000
FeO	6.904	6.774	6.846	6.993	7.025	6.914	7.096	6.198	6.698	6.834	6.888	7.151	6.118	5.987	5.603
MnO	0.099	0.097	0.095	0.157	0.147	0.110	0.139	0.093	0.124	0.105	0.154	0.131	0.110	0.111	0.105
MgO	49.144	49.931	50.657	50.547	49.778	52.531	48.935	49.960	49.731	51.168	49.686	49.209	48.734	49.256	52.872
ZnO	0.006	0.000	0.011	0.032	0.024	0.023	0.000	0.013	0.015	0.000	0.026	0.022	0.047	0.031	0.064
CaO	0.007	0.012	0.000	0.002	0.007	0.006	0.008	0.027	0.068	0.019	0.011	0.003	0.001	0.009	0.027
Na ₂ O	0.003	0.000	0.001	0.002	0.003	0.021	0.000	0.013	0.021	0.000	0.000	0.000	0.024	0.000	0.015
K ₂ O	0.000	0.000	0.000	0.000	0.000	0.000	0.000	0.000	0.000	0.000	0.000	0.000	0.000	0.000	0.000
NiO	0.428	0.380	0.415	0.410	0.391	0.392	0.406	0.403	0.398	0.386	0.400	0.359	0.388	0.413	0.368
Cl	0.000	0.000	0.000	0.000	0.000	0.000	0.000	0.000	0.000	0.000	0.000	0.000	0.000	0.000	0.000
F	0.000	0.000	0.000	0.000	0.000	0.000	0.000	0.000	0.000	0.000	0.000	0.000	0.000	0.000	0.000
Total	97.55	98.76	99.78	100.00	99.27	104.08	97.66	97.86	98.33	100.36	98.36	98.02	97.71	97.90	100.74
No. Oxygen	4	4	4	4	4	4	4	4	4	4	4	4	4	4	4
Si	1.015	1.016	1.011	1.011	1.020	1.020	1.017	1.013	1.014	1.007	1.012	1.015	1.039	1.032	0.996
Ti	0.000	0.000	0.000	0.000	0.000	0.000	0.000	0.000	0.000	0.000	0.000	0.000	0.000	0.000	0.000
Al	0.000	0.000	0.000	0.000	0.000	0.000	0.000	0.000	0.000	0.000	0.000	0.000	0.000	0.000	0.000
Cr	0.000	0.000	0.000	0.001	0.000	0.000	0.000	0.000	0.000	0.000	0.000	0.000	0.000	0.000	0.000
Fe ²⁺	0.143	0.138	0.139	0.141	0.143	0.134	0.147	0.128	0.138	0.138	0.142	0.148	0.126	0.123	0.112
Mn ²⁺	0.002	0.002	0.002	0.003	0.003	0.002	0.003	0.002	0.003	0.002	0.003	0.003	0.002	0.002	0.002
Mg	1.816	1.820	1.829	1.823	1.806	1.814	1.807	1.834	1.822	1.837	1.821	1.811	1.785	1.801	1.884
Zn	0.000	0.000	0.000	0.001	0.000	0.000	0.000	0.000	0.000	0.000	0.000	0.000	0.001	0.001	0.001
Ca	0.000	0.000	0.000	0.000	0.000	0.000	0.000	0.001	0.002	0.000	0.000	0.000	0.000	0.000	0.001
Na	0.000	0.000	0.000	0.000	0.000	0.001	0.000	0.001	0.001	0.000	0.000	0.000	0.001	0.000	0.001
K	0.000	0.000	0.000	0.000	0.000	0.000	0.000	0.000	0.000	0.000	0.000	0.000	0.000	0.000	0.000
Ni	0.009	0.007	0.008	0.008	0.008	0.007	0.008	0.008	0.008	0.007	0.008	0.007	0.008	0.008	0.007
Cl	0.000	0.000	0.000	0.000	0.000	0.000	0.000	0.000	0.000	0.000	0.000	0.000	0.000	0.000	0.000
F	0.000	0.000	0.000	0.000	0.000	0.000	0.000	0.000	0.000	0.000	0.000	0.000	0.000	0.000	0.000
Total Cation	2.985	2.984	2.989	2.988	2.980	2.980	2.983	2.987	2.987	2.992	2.987	2.984	2.962	2.968	3.004
Mg # mg (m)	0.927	0.929	0.930	0.928	0.927	0.931	0.925	0.935	0.930	0.930	0.928	0.925	0.934	0.936	0.944

Supplementary Table 8 Microprobe analysis of olivine in association with Chrome spinel with in the dunites for E13.26 and E13.11.

	<i>E13.11</i>	<i>E13.11</i>	<i>E13.11</i>	<i>E13.11</i>	<i>E13.11</i>	<i>E13.11</i>	<i>E13.11</i>	<i>E13.11</i>	<i>E13.11</i>	<i>E13.11</i>	<i>E13.11</i>	<i>E13.11</i>	<i>E13.11</i>	<i>E13.11</i>	<i>E13.11</i>
SiO ₂	42.053	42.117	41.645	41.034	40.422	39.855	36.279	41.178	41.250	42.372	42.268	44.264	41.873	41.724	41.986
TiO ₂	0.000	0.000	0.000	0.000	0.000	0.007	0.000	0.005	0.006	0.009	0.008	0.000	0.000	0.000	0.007
Al ₂ O ₃	0.000	0.007	0.004	0.000	0.000	0.000	0.000	0.001	0.000	0.006	0.000	0.016	0.000	0.000	0.000
Cr ₂ O ₃	0.015	0.027	0.000	0.011	0.000	0.005	0.026	0.000	0.000	0.000	0.000	0.001	0.008	0.024	0.003
FeO	5.543	5.585	5.501	5.767	5.761	5.784	5.594	5.838	6.000	6.118	6.097	5.962	6.163	6.643	6.654
MnO	0.161	0.110	0.110	0.135	0.103	0.096	0.087	0.118	0.126	0.101	0.105	0.111	0.141	0.127	0.089
MgO	52.796	52.236	52.897	53.432	53.891	53.865	54.293	53.291	53.416	50.332	50.215	49.286	48.648	51.660	51.605
ZnO	0.000	0.035	0.029	0.007	0.019	0.000	0.015	0.000	0.035	0.000	0.021	0.000	0.026	0.000	0.003
CaO	0.008	0.017	0.000	0.010	0.011	0.004	0.015	0.000	0.001	0.004	0.001	0.004	0.002	0.008	0.000
Na ₂ O	0.000	0.013	0.033	0.015	0.000	0.000	0.011	0.015	0.003	0.001	0.007	0.000	0.000	0.000	0.007
K ₂ O	0.000	0.000	0.000	0.000	0.000	0.000	0.000	0.000	0.000	0.000	0.000	0.000	0.000	0.000	0.000
NiO	0.373	0.367	0.403	0.410	0.391	0.336	0.345	0.340	0.317	0.396	0.416	0.375	0.376	0.357	0.400
Cl	0.000	0.000	0.000	0.000	0.000	0.000	0.000	0.000	0.000	0.000	0.000	0.000	0.000	0.000	0.000
F	0.000	0.000	0.000	0.000	0.000	0.000	0.000	0.000	0.000	0.000	0.000	0.000	0.000	0.000	0.000
Total	100.95	100.51	100.62	100.82	100.60	99.95	96.66	100.79	101.15	99.34	99.14	100.02	97.24	100.54	100.75
No. Oxygen	4	4	4	4	4	4	4	4	4	4	4	4	4	4	4
Si	1.002	1.007	0.996	0.983	0.972	0.965	0.915	0.986	0.985	1.025	1.025	1.058	1.035	1.003	1.006
Ti	0.000	0.000	0.000	0.000	0.000	0.000	0.000	0.000	0.000	0.000	0.000	0.000	0.000	0.000	0.000
Al	0.000	0.000	0.000	0.000	0.000	0.000	0.000	0.000	0.000	0.000	0.000	0.000	0.000	0.000	0.000
Cr	0.000	0.001	0.000	0.000	0.000	0.000	0.001	0.000	0.000	0.000	0.000	0.000	0.000	0.000	0.000
Fe ²⁺	0.110	0.112	0.110	0.115	0.116	0.117	0.118	0.117	0.120	0.124	0.124	0.119	0.127	0.133	0.133
Mn ²⁺	0.003	0.002	0.002	0.003	0.002	0.002	0.002	0.002	0.003	0.002	0.002	0.002	0.003	0.003	0.002
Mg	1.875	1.862	1.886	1.908	1.931	1.944	2.041	1.902	1.901	1.815	1.815	1.756	1.792	1.851	1.844
Zn	0.000	0.001	0.001	0.000	0.000	0.000	0.000	0.000	0.001	0.000	0.000	0.000	0.000	0.000	0.000
Ca	0.000	0.000	0.000	0.000	0.000	0.000	0.000	0.000	0.000	0.000	0.000	0.000	0.000	0.000	0.000
Na	0.000	0.001	0.002	0.001	0.000	0.000	0.001	0.001	0.000	0.000	0.000	0.000	0.000	0.000	0.000
K	0.000	0.000	0.000	0.000	0.000	0.000	0.000	0.000	0.000	0.000	0.000	0.000	0.000	0.000	0.000
Ni	0.007	0.007	0.008	0.008	0.008	0.007	0.007	0.007	0.006	0.008	0.008	0.007	0.007	0.007	0.008
Cl	0.000	0.000	0.000	0.000	0.000	0.000	0.000	0.000	0.000	0.000	0.000	0.000	0.000	0.000	0.000
F	0.000	0.000	0.000	0.000	0.000	0.000	0.000	0.000	0.000	0.000	0.000	0.000	0.000	0.000	0.000
Total Cation	2.998	2.993	3.005	3.018	3.028	3.035	3.085	3.014	3.015	2.975	2.975	2.942	2.965	2.997	2.994
Mg # mg (m)	0.944	0.943	0.945	0.943	0.943	0.943	0.945	0.942	0.941	0.936	0.936	0.936	0.934	0.933	0.933

Supplementary Table 9 ⁴⁰Argon - ³⁹Argon results from the total fusion of muscovites (E13.14) sampled from the Western Ethiopian Shield

Relative Abundances		36Ar [V]	%1σ	37Ar [V]	%1σ	38Ar [V]	%1σ	39Ar [V]	%1σ	40Ar [V]	%1σ	40(r)/39(k) ± 2σ	Age ± 2σ (Ma)	40Ar(r) (%)	39Ar(k) (%)	K/Ca ± 2σ
3M30150D	70 °C	0.0000347	32.641	0.0002464	75.610	0.0001873	4.013	0.0143525	0.626	0.61949	0.074	42.43737 ± 0.71307	540.79 ± 7.85	98.32	0.46	25 ± 38
3M30145D	70 °C	0.0000230	62.254	0.0000802	137.086	0.0023140	1.175	0.1755280	0.366	7.50472	0.020	42.71529 ± 0.31718	543.85 ± 3.49	99.91	5.67	941 ± 2581
3M30156D	70 °C 4	0.0000642	17.565	0.0000559	207.251	0.0023900	1.113	0.1809369	0.385	7.82921	0.019	43.16373 ± 0.33491	548.77 ± 3.67	99.75	5.84	1392 ± 5769
3M30142D	70 °C 4	0.0000346	36.285	0.0000620	191.489	0.0031374	1.341	0.2412252	0.356	10.42413	0.020	43.16980 ± 0.30980	548.84 ± 3.40	99.90	7.79	1674 ± 6411
3M30152D	70 °C 4	0.0000619	19.131	0.0000024	5124.666	0.0027475	0.970	0.2104527	0.381	9.10484	0.021	43.17464 ± 0.33148	548.89 ± 3.63	99.80	6.80	37821 #####
3M30149D~	70 °C 4	0.0001978	13.796	0.0058107	4.113	0.0037206	2.414	0.2853573	0.395	12.40510	0.023	43.26687 ± 0.34735	549.90 ± 3.81	99.53	9.22	21 ± 2
3M30146D	70 °C 4	0.0000608	20.787	0.0000324	404.368	0.0034194	1.119	0.2644019	0.345	11.49256	0.028	43.39692 ± 0.30151	551.33 ± 3.30	99.84	8.54	3508 ± 28368
3M30155D~	70 °C 4	0.0002424	14.861	0.0063013	4.137	0.0048973	1.920	0.3777261	0.363	16.44370	0.029	43.34303 ± 0.32106	550.74 ± 3.52	99.56	12.20	26 ± 2
3M30157D	70 °C 4	0.0000485	25.481	0.0000266	440.141	0.0026241	1.200	0.2007998	0.362	8.73662	0.021	43.43633 ± 0.31706	551.76 ± 3.47	99.83	6.49	3241 ± 28528
3M30141D~	70 °C 4	0.0001042	21.064	0.0040859	4.799	0.0036402	2.608	0.2773192	0.391	12.08605	0.043	43.47056 ± 0.34496	552.13 ± 3.78	99.74	8.96	29 ± 3
3M30140D	70 °C 4	0.0000466	26.280	0.0002051	51.850	0.0020504	0.894	0.1566020	0.365	6.83677	0.026	43.56765 ± 0.32188	553.20 ± 3.52	99.80	5.06	328 ± 341
3M30143D	70 °C 4	0.0000525	25.247	0.0000091	1208.004	0.0022481	1.581	0.1737211	0.377	7.60741	0.026	43.70007 ± 0.33330	554.64 ± 3.64	99.79	5.61	8202 ± 198171
3M30154D	70 °C	0.0000520	26.094	0.0000479	257.190	0.0025515	1.663	0.1971887	0.349	8.65245	0.018	43.79960 ± 0.30932	555.73 ± 3.38	99.82	6.37	1769 ± 9098
3M30147D	70 °C	0.0001242	14.552	0.0001331	89.997	0.0030691	1.145	0.2355544	0.365	10.38760	0.039	43.94045 ± 0.32611	557.27 ± 3.56	99.64	7.61	761 ± 1370
3M30151D	70 °C	0.0000551	21.018	0.0000168	820.930	0.0013711	1.786	0.1051330	0.375	4.64722	0.060	44.04624 ± 0.34084	558.42 ± 3.72	99.64	3.40	2695 ± 44252

Information on Analysis and Constants Used in Calculations	0.480	Results	40(a)/36(a) ± 2σ	40(r)/39(k) ± 2σ	Age ± 2σ (Ma)	MSWD	39Ar(k) (% ,n)	K/Ca ± 2σ
Sample = E14	Age Equations = Min et al. (2000)	Age Plateau		43.36852 ± 0.11343 ± 0.26%	551.02 ± 2.23 ± 0.40%	1.21	76.50	24 ± 2
Material = Msc	Negative Intensities = Allowed				Full External Error ± 4.38	28%	10	
Location = Laser	Decay Constant 40K = 5.531 ± 0.013 E-10 1/a				Analytical Error ± 1.24	1.94	2σ Confidence Limit	
Analyst = Fred Jourdan	Decay Constant 39Ar = 2.940 ± 0.029 E-07 1/h					1.1023	Error Magnification	
Project = ETHIOPIANSHIELD_MB13	Decay Constant 37Ar = 8.230 ± 0.082 E-04 1/h							
Mass Discrimination Law = POW	Decay Constant 36Cl = 2.303 ± 0.046 E-06 1/a	Total Fusion Age		43.41268 ± 0.09035 ± 0.21%	551.50 ± 2.10 ± 0.38%		15	83 ± 6
Irradiation = I17t40h	Decay Constant 40K(EC,β*) = 0.576 ± 0.002 E-10 1/a				Full External Error ± 4.32			
J = 0.00821500 ± 0.00001600	Decay Constant 40K(β-) = 4.955 ± 0.013 E-10 1/a				Analytical Error ± 0.99			
FCs = 28.294 ± 0.037 Ma	Atmospheric Ratio 40/ 36(a) = 298.56 ± 0.30	Normal Isochron	666.42 ± 719.41 #####	43.17748 ± 0.28279 ± 0.65%	548.92 ± 3.61 ± 0.66%	1.24	76.50	
IGSN = Undefined	Atmospheric Ratio 38/ 36(a) = 0.1869 ± 0.0002				Full External Error ± 5.21	27%	10	
Preferred Age = Undefined	Production Ratio 39/ 37(ca) = 0.000706 ± 0.000049				Analytical Error ± 3.10	2.00	2σ Confidence Limit	
Classification = Undefined	Production Ratio 38/ 37(ca) = 0.000023 ± 0.000002					1.1157	Error Magnification	
Experiment Type = Undefined	Production Ratio 36/ 37(ca) = 0.000281 ± 0.000008					1	Number of Iterations	
Extraction Method = Undefined	Production Ratio 40/ 39(k) = 0.000676 ± 0.000068	Inverse Isochron		43.38046 ± 0.28218 ± 0.65%	551.15 ± 3.60 ± 0.65%	1.37	76.50	
Heating = 60 sec	Production Ratio 38/ 39(k) = 0.012400 ± 0.003968	Clustered Points			Full External Error ± 5.21	20%	10	
Isolation = 5.00 min	Production Ratio 36/ 38(cl) = 263.00 ± 13.15				Analytical Error ± 3.09	2.00	2σ Confidence Limit	
Instrument = MAP-215-50	Scaling Ratio K/ Ca = 0.430					1.1705	Error Magnification	
Lithology = Undefined	Abundance Ratio 40K/ K = 1.1700 ± 0.0100 E-04					8	Number of Iterations	
Lat-Lon = Undefined - Undefined	Atomic Weight K = 39.0983 ± 0.0001 g					0.0000299060	Convergence	
Feature = Undefined						1%	Spreading Factor	

Supplementary Table 10 ⁴⁰Argon - ³⁹Argon results from the total fusion of muscovites (E13.13) sampled from the Western Ethiopian Shield

Incremental Heating			36Ar(a) [V]	37Ar(ca) [V]	38Ar(cl) [V]	39Ar(k) [V]	40Ar(r) [V]	Age ± 2σ (Ma)	40Ar(r) (%)	39Ar(k) (%)	K/Ca ± 2σ
3M30176D~	70 °C	4	0.0003954	0.0097655	0.0002619	0.3147336	13.34412	540.36 ± 3.85	99.12	12.06	13.9 ± 0.9
3M30169D~	70 °C	4	0.0003574	0.0096249	0.0002729	0.2781554	11.81391	541.18 ± 3.97	99.10	10.66	12.4 ± 0.7
3M30173D~	70 °C	4	0.0003222	0.0093035	0.0002111	0.2765561	11.79790	543.24 ± 3.98	99.19	10.60	12.8 ± 1.4
3M30171D~	70 °C	4	0.0004261	0.0101010	0.0002244	0.3383509	14.44194	543.50 ± 3.55	99.13	12.96	14.4 ± 0.8
3M30170D~	70 °C	4	0.0004745	0.0093969	0.0003253	0.4538130	19.42842	544.91 ± 3.77	99.27	17.39	20.8 ± 2.1
3M30168D~	70 °C	4	0.0003315	0.0089415	0.0002157	0.3798713	16.33305	546.94 ± 3.68	99.40	14.55	18.3 ± 2.0
3M30175D~	70 °C		0.0003551	0.0095130	0.0001829	0.3045824	13.17575	549.81 ± 3.61	99.20	11.67	13.8 ± 0.9
3M30174D~	70 °C		0.0003647	0.0091887	0.0001690	0.2640791	11.57498	556.08 ± 4.39	99.07	10.12	12.4 ± 1.0

Σ 0.0030269 0.0758349 0.0018633 2.6101419 111.91006

Information on Analysis	Results	40(r)/39(k) ± 2σ	Age ± 2σ (Ma)	MSWD	39Ar(k) (%,n)	K/Ca ± 2σ
Sample = E13 Material = Msc Location = Laser Analyst = Fred Jourdan Project = ETHIOPIANSHIELD_MB13 Mass Discrimination Law = POW Irradiation = I17t40h J = 0.00821500 ± 0.00001561 FCs = 28.294 ± 0.037 Ma	Age Plateau	42.67794 ± 0.17897 ± 0.42%	543.44 ± 2.66 ± 0.49%	1.62 15%	78.21 6	13.8 ± 1.7
			Full External Error ± 4.57 Analytical Error ± 1.97	2.26 1.2713	2σ Confidence Limit Error Magnification	
	Total Fusion Age	42.87509 ± 0.12471 ± 0.29%	545.60 ± 2.25 ± 0.41%		8	14.8 ± 0.4
			Full External Error ± 4.36 Analytical Error ± 1.37			

GEOCHRONOLOGY

Mineral Separation

Crushing

1. Cut the rocks using the rock saw.
2. Make sure that the rocks are dry, clean and fresh. Ensuring that there is no lichen or texta left on the rocks.
3. Clean the jaw crusher before and after use
 - a. This is done using compressed air and ethanol.
4. Line the tray with butcher paper to ensure that the samples are not contaminated.
5. The disc mill is used to achieve the zircon fraction. Clean the machine using compressed air and ethanol.
6. Move the discs until the desired gap is reached. Start at 1mm.
7. Run this through the sieve using $<79\ \mu\text{m}$ and $>479\ \mu\text{m}$ mesh. Place the sieve into the Endcotts EPL2000 Super Shaker and allow for the fractions to separate.
8. Take the course fraction $>479\ \mu\text{m}$ and run it through the disc mill again, changing the spacing between the discs to 0.7mm.
9. Repeat this process again with the spacing at 0.4mm.
10. Put each fraction into the sample bags. Labelling ' $>479\ \mu\text{m}$ ', 'Zircon fraction' and ' $<79\ \mu\text{m}$ '
11. If samples are undergoing geochemistry, after they have been through the jaw crusher they are placed into the ring mill using the tungsten carbide. The ring mill is cleaned with compressed air and ethanol.
12. Quartz blank is first used to ensure contamination is kept at a minimum. The quartz is run for 1.5 minutes.
13. The samples are then placed into the tungsten carbide mill and run for 3 minutes.
14. This fraction is then placed in a sample bag for later requirements.

Separating the zircons from the 'zircon fraction'

The separation was done in the Mawson Building lab B29 at Adelaide University.

Before each use the room is cleaned before each use. The benches are cleaned and the room is vacuumed.

The sample is panned removing the lights from the fraction. The lights are placed into a funnel with filter paper and later dried in the oven.

The heavies extracted by this method are the placed on the hotplate to dry at $50\ ^\circ\text{C}$. To separate the magnetic material the sample is put through the FRANZ.

For the first time the sample is run through at 0.5 amps. This will separate the highly magnetic minerals. This is repeated two more times. The magnet is turned up to 1 amps and 1.7 amps respectively. Each magnetic fraction is placed in a sample bag and clearly labelled.

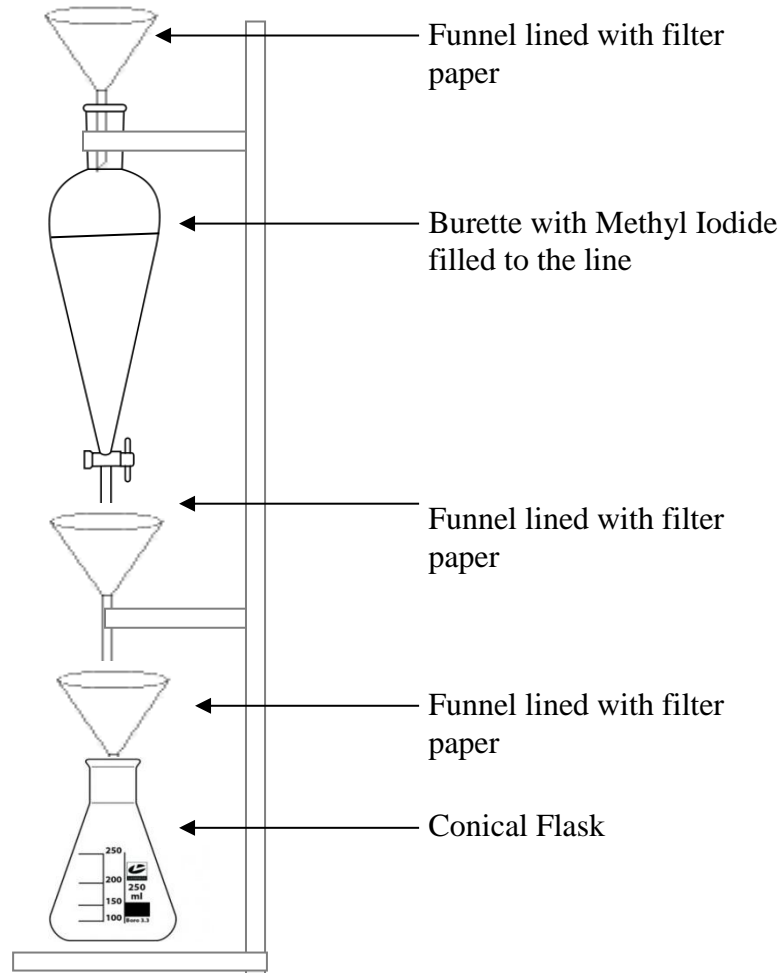
Heavy Liquids

Figure 18 The set up for the separation of zircons via the use of heavy liquids.

Fill the burette with methyl Iodide. The methyl Iodide allows for the zircons to sink to the bottom. Take the top funnel off and pour the remaining fraction of the sample into the burette. Stir it with a stirring rod and allow for the separates to drop to the bottom. Tap off and stir again. This needs to be repeated until there are no more particles sinking. Everything that the heavy liquid touches has to be cleaned 10 times with ethanol. The zircons are then dried on a hot plate with a funnel over the top to stop any from blowing away. The separates remaining are cleaned, dried and placed into a sample bag.

Geochemistry

Cleaning the 7 and 15ml vials Teflon Vials and Bombs

1. Collect sufficient 7 and/or 15 ml PFA Teflon vials and bombs from the recycling container for a batch of samples.
2. Remove labels from the vials with an ethanol moistened tissue in the fume cupboard.
3. Fill with about 5mm of recycled 6M HCl.
4. Heat on hot plate at 140°C for 30 minutes.
5. Discard acid to the waste acid container using jug and funnel.
6. Transfer vials and caps into beaker of deionized (DI) water, and then drain them.
7. Transfer to 3 L glass beaker and cover with 6 M HNO₃ to a maximum two thirds full.
8. Cover with a clock glass.
9. Label the beaker, ie. 6M HNO₃ and also place a yellow Post-It noting the acid and your name in front of a hotplate in fume cupboard FCAMA024.
10. Set hot plate to 170°C and heat overnight.
11. Pour DI water (using DI water jug) into the clock glass to reduce acid loss through evaporation. It pays to mark the HNO₃ level and top up any water losses.
12. Next morning, turn hot plate to maximum. When boiling has commenced, reduce the heat to a gentle boil at approximately 330°C.
13. Add DI water to the clock glass if necessary and boil for 30 minutes.
14. Turn off hot plate and allow to cool.
15. Drain HNO₃ into another beaker or acid storage container.
16. Mark the used acid with the number of uses.
17. Leave the beaker in the fume cupboard and cover the PFA-ware with DI water.
18. Swirl, and drain the PFA-ware.
19. Cover with DI water and drain twice more.
20. Cover with 6M HCl (to a maximum of two thirds full).
21. Label beaker and hot plate.
22. Set hot plate to 170°C and heat overnight.
23. Pour DI water into clock glass. If there are any HCl losses the acid must be topped up with 6M HCl only.
24. Next morning, turn hot plate to maximum. When boiling has commenced, reduce the heat to a gentle boil at approximately 330°C.
25. Add DI water to the clock glass if necessary and boil for 30 minutes.
26. Turn off hot plate and allow cooling for ease of handling.

27. Using gloves and beaker grips, drain HCl into another beaker or acid storage container. This is best done by pouring the acid, first with the clock glass removed then draining the last bit with the clock glass on the beaker. Be careful to pour the acid in a slightly sideways orientation in case of any acid spillage that might drain back towards you.
28. Mark the used acid with the number of uses.
29. Leave the beaker in the fume cupboard and cover the PFA-ware with DI water.
30. Swirl, and drain the PFA-ware.
31. Cover with DI water and drain twice more.
32. Cover with DI water and clock glass.
33. Boil gently for 30 minutes on hot plate (as above).
34. Allow to cool then rinse three times with DI water (as above).
35. Cover a clock glass or tray with cling wrap or tissue and pour the PFA-ware out for reassembly.
36. Carefully separate the vials, (avoid touching the insides or rims) and pour in 5mm distilled 6M HCl and cap them.
37. Place on hot plate in fume cupboard FCAMA022 at 140°C for at least 2 hours.
38. Allow to cool slightly then pour the acid into a jug, then to the 'Recycled 6M HCl' container.
39. Recap vials and store in your large plastic storage container.

Sample Preparation for the vials

Weighing

1. For average composition whole rocks, 100 to 200mg of sample is required.
2. Weighing is carried out on the Mettler Toledo AT201 balance in air lock room b13.
3. The long and short term balance stability is monitored for all weighing sessions. Weigh the 100g weight from the weights box before and after your work and record the weights on the 'balance log sheet'.
4. Label a 15ml vial with black marker pen and record label in the lab book.
5. Holding the uncapped vial with the balance tweezers, use the Zerostat gun to shoot it inside and out from a distance of about 250mm by slowly squeezing then releasing the trigger over about 4 seconds. If you hear a 'crack' sound you are squeezing too quickly. Repeat it more slowly. This neutralizes any static charges.
6. Place vial on the balance and tare to zero.
7. Weigh in the required amounts of spike, trying to limit each spike weight to < .5g and sample to > 50mg. The optimal spike to sample quantities are listed below:
 - 0.2g Sm-Nd spike D per 1 ug Nd
 - 0.14g Rb spike C per 1ug Rb
 - 0.08g Sr spike C per 1ug Sr
8. Next, weigh in sample with a spatula or transfer it via weighing paper.

9. Record all weights, etc. in the Lab book.
10. When running a blank, weigh one drop of the spikes required into a vial. (They can be combined.)
11. Remove from the balance and add approx 2ml of 7M HNO₃ to reduce static build up. Recap vial.

Supplementary Table 11: This demonstrates the estimated concentrations of Sr, Nd and Sm used to calculate the respective weights. The recorded weight and addition of spike is also depicted in this Supplementary Table.

Sample	Estimated Concentration (ppm)			Recorded Powder wt (g)	Recorded SmNd F	
	<i>Sr</i>	<i>Nd</i>	<i>Sm</i>			
<i>E13.11</i>	25	1	0.3	0.23911	0.49191	
<i>E13.12</i>	150	25	5	0.08092	0.44205	
<i>E13.18</i>	250	10	2	0.20203	0.42380	
<i>E13.19</i>	250	10	2	0.20857	0.39794	
<i>E13.23</i>	250	10	2	0.20865	0.46918	
<i>E13.27</i>	150	25	5	0.07747	0.45147	
<i>BHV.02</i>	X	X	X	0.08070	.47230	
<i>Blank #50</i>	X	X	X	X	0.6252	0.16651

Dissolution for vials

12. Add 4ml HF from dispenser.
13. Heat capped vial overnight at 140°C on a hot plate in fume cupboard B-24-18.
14. Next morning, allow to cool then gently tap the vial (at a slight angle) to collect any acid drops from the top or sides to the bottom.
15. Uncap vial and evaporate to dryness at 140°C. This removes silicon as silicon tetrafluoride (SiF₄), but insoluble fluorides can also form as the sample is dried in the presence of excess HF. It can cause Sm and Nd to fractionate and inhomogeneity problems if sample splitting is required for ID analysis.
To reduce the likelihood of insoluble fluorides forming, add approximately 2mL 7M HNO₃ just before the sample dries.
16. Allow to cool, then add 4mL HF + 2mL 7M HNO₃.
17. Recap and heat overnight at 140°C on a hot plate.
18. Again, next morning, allow to cool then gently tap the vial (at a slight angle) to collect any acid drops from the top or sides to the bottom.

19. Uncap vial and evaporate to dryness at 140°C. To reduce the likelihood of insoluble fluorides forming, add 1mL 7M HNO₃ just before the sample dries
20. Cool, and then add 6mL 6M HCl to the solid residue.
21. Heat capped vial on hotplate at 140°C until completely dissolved. (overnight)
22. Allow to cool to room temperature.

Dissolution for the bombs

23. Add 4ml HF from dispenser.
24. Evaporate to dryness at 140°C on a hot plate in fume cupboard. As well as assisting the acid attack, this removes silicon as silicon tetrafluoride (SiF₄), but insoluble fluorides can also form as the sample is dried in the presence of excess HF. It can cause Sm and Nd to fractionate and inhomogeneity problems if sample splitting is required for ID analysis.
25. Allow to cool, and then add 4mL HF + 2mL 7M HNO₃.
26. Recap bomb.
27. Spray inside the metal jacket and on the threads with minimal amount of Ezy Glide (Teflon) spray.
28. Place bomb in the jacket with fittings and screw the top closed tightly.
29. Heat in the oven at 190°C for 4-5 days.
30. After sample has dissolved, remove from the oven and allow to cool on Teflon sheet.
31. Whilst still warm (after about an hour), remove the Teflon bombs from their metal jackets using latex rubber gloves.
32. Using a tissue dampened with de-ionized water, wipe the Teflon bomb exterior to remove any contamination. Repeat with a dry tissue.
33. Gently tap the bomb (at a slight angle) to collect any acid drops from the top or sides into the bottom of the bomb.
34. Carefully remove the bomb top in a fume cupboard.
35. Evaporate to dryness at 140°C on a hot plate in fume cupboard B-24-18. Once again, to reduce the likelihood of insoluble fluorides forming, add 2mL 6M HNO₃ just before the sample dries
36. Cool, and then add 6mL 6M HCl to the solid residue.
37. Recap and place in metal jacket.
38. Heat in the oven at 150°C until completely dissolved (several hours to overnight).
39. Remove from the oven and allow to cool to room temperature.
40. Remove from the metal jacket and clean the bomb surfaces with tissues.

Centrifuge

41. Evaporate to dryness at 140°C on a hot plate in fume cupboard.
42. Cool, and then add 1.5mL 2M HCl to each bomb and leave to dissolve. Swirl gently with minimal heating if necessary but avoid evaporation, which will change the 2M acid concentration required for the ion exchange columns.

43. Rinse 2ml micro centrifuge tube, stored in 6M HCL, three times inside and out with DI water and store in a rack (labelled with your name).
44. Using the Micro centrifuge in Room B14, centrifuge the samples for 5 minutes at 13200 rpm.

Columns

Load the sample

45. Equilibrate with 6mL 2M HCL
46. Load the sample in 1 mL of HCL
47. 1 mL of 2M HCL wash and discard
48. 1 mL of 2M HCL wash and discard

Collecting Sr

49. Discard 8 mL 2M HCL
50. Discard 2 mL 3M HCL
51. Collect 2 mL of 3M HCL in 7mL vials – This is the strontium fraction
52. Place the cap loosely on the vials. Place samples on the hotplate with the vials uncapped. Dry the samples at 140 °C. When the sample is dry add 1mL of HCL, redissolving the sample.

Collecting Sm Nd

53. Discard 1mL of 6M HCL
54. Collect 5mL of 6M HCL in 7mL vials. Place the cap loosely on the vials. Place samples on the hotplate with the vials uncapped. Dry the samples at 140 °C. When the sample is dry add 1mL of HCL, redissolving the sample.

Second pass – Sr

55. 5mL DI water
56. 6mL 2M HCL to equilibrate the columns
57. Load the Sr fraction, which was dried and redissolved in 1mL of HCL
58. 1mL 2M HCL wash and discard
59. 1mL 2M HCL wash and discard
60. Discard 8mL 2M HCL
61. Discard 2mL 3M HCL
62. Collect 2mL 3M HCL – Sr
63. Discard 6mL 6M HCL (Ar grade)

Clean Up

1. 10 mL 6M HCL (Ar grade) repeat step twice
2. 10mL 6M HCL repeat step twice
3. 5mL DI water
4. Rinse tip with 6m HCL

Cleaning source components

(Mass spectrometer and Isotope labs, B14 and B13)

1. Select sufficient shields and support posts for your immediate needs from the 'used components' containers on the middle bench. Please don't hoard excessive quantities.
2. Collect a 2L glass beaker and clock glass from the cupboard under the central bench.
3. Clean the components using a wet scourer on the plastic board at the sink. This should be carried out as quickly as possible to avoid corrosion occurring if they are left wet for any extended length of time.
4. Transfer the cleaned components to a 2L beaker.
5. In the Isotope Lab, cover the components with deionised water and bring to the boil on the hot plates in fume cupboard FCAMA024. Only boil for a few minutes to avoid corrosion.
6. After boiling, turn the hot plate off and allow the beaker to cool slightly.
7. Using the red silicone hand grips and the clock glass, drain the de-ionised water into the sink.
8. Cover the components again with de-ionised water, swirl and drain off the water.
9. Rinse three times with DI water.
10. Dry the beaker of components in the Mass Spectrometer Lab oven at 120°C. Return the dry clock glass to the cupboard.
11. When the components have dried, remove from the oven, allow to cool and then transfer to your clean plastic container using tweezers.

Cleaning filament holders

(Mass spectrometer lab B14, Crushing Room B21b and Isotope lab B13)

12. Select sufficient holders for your work (see Introduction) and a 2L glass beaker (with clock glass cover) as a Supplementary Table container.
13. Use the grinding tool in B21b to very lightly grind the area of the previous weld. I.e. Only grind the outside 2-3 mm at the post end.
Warning: Use safety glasses and be careful not to catch your hair, skin or clothing, etc. in moving grinding bit.
14. In the Isotope Lab, cover the components with deionised water and bring to the boil on the hot plates in fume cupboard FCAMA024. Only boil for a few minutes to avoid corrosion.
15. After boiling, turn the hot plate off and allow the beaker to cool slightly.
16. Use the red silicone hand grips and clock glass to drain the de-ionised water into the sink.
17. Cover the components with de-ionised water again, swirl and drain off the water.
18. Repeat step 7 again. A total of 3 rinses in de-ionised water.
19. Dry the beaker of components in the Mass Spectrometer Lab oven at 120°C. Return the dry clock glass to the cupboard.
20. When dry, remove from the oven and allow it to cool.

Welding new filaments

The welder should be turned on five minutes before use with the switch on the left side of the front control panel. The voltage is normally left at 30V, timing set to 20 and the current to Medium. For best welds the electrodes should be kept polished using very fine wet and dry paper or emery cloth, which is kept in the top drawer. Polishing may be required after several to more than 100 welds. It's quite variable.

21. Screw back the sliding block to the position shown in Figure (a).
22. Clean and straighten a length of filament ribbon with a tissue.
23. Insert the cleaned filament ribbon into the slot between the sliding block and anvil
24. For single filament inserts attach the additional mounting support
25. Attach the carrier plate making sure you have the plate pushed down to the stop pins.
26. Screw the sliding block in to the stop. This will bend the filament ribbon to the desired U-shape and make its ends touch the pins of the filament insert
27. Spot weld the bent ends of the filament ribbon to the pins of the filament
28. Place the 'pin and ribbon' contact point between the electrodes.
29. Press the foot control down as far as it will go.
30. Release the foot control.
31. Repeat this welding process for the other pin.
32. Remove the jig from the spot welder.
33. Screw back the sliding block.
34. Loosen the screw holding the carrier plate in place.

The filaments are then placed in the degasser. This is located at Adelaide University.

Loading sample

Remove the backing paper of a 50mm square of parafilm and place on working surface. Hint. Fold the parafilm diagonally before removing the backing paper so that loading solution won't roll off.

Dispense 1 – 2 drops (depending on the number of samples being loaded) of the loading solution onto middle of the Parafilm. Loading solution on the Parafilm can now be dispensed using the pipettor and a clean tip for each sample. To load a new pipette tip, gently push the pipettor into the clean tip, and then remove the tip. Push in more firmly (at the top only) with your gloved fingers

Nd filaments – The sample is loaded onto a 'double' tantalum filament (evaporation filament) and a 'double' rhenium filament is used for the ionisation filament.

Sm filaments – Sm is run after Nd on the corresponding sample filaments (and shield).

Load sample in 1-3ul Sm Nd loading solution (1% H₃PO₄ in 1M HNO₃) and evaporate to dryness at $\leq 1.2A$.

Slowly raise the filament current to 1.8A and heat for 1 minute.

Raise the current very slowly until the filament 'almost glows' dull red (approx 2.2 – 2.7A). Heat for ~ 5 seconds.

Sr filament – single tantalum.

Evaporate 1ul Birck's solution (Sr loading solution) to almost dryness at $\leq 1.2A$.

Load sample in 1-3ul Birck's solution and evaporate to dryness at $\leq 1.2A$.

Slowly raise the filament current to 1.8A and heat for 1 minute.

Slowly raise the current until the filament 'almost glows' a dull red (~ 2.5 – 3.0A). Heat for ~ 5 seconds.

After the magazine has been assembled it is most important to check that no filament posts are touching their shields for the double filament setup. This can be checked using the circuit tester. If there is a shorting connection, the red diode will glow and that filament will have to be realigned by carefully and judiciously bending the posts. See David Bruce if in doubt.

Mass Spectrometer

Add 1 litre of liquid nitrogen per 8 hour shift. Make sure you are wearing the appropriate personal protection equipment (PPE).

At the start of each day fill in the MAT262 daily checks log sheet and run a Mass calibration.

Daily Mass calibration

- **F2** MS Calib (from Main Menu – ie may need **F8** Return Main Keys)
- **F2** Channel Calib
- **F4** Gain Calib
- **Enter** (Default (V))
- **Enter** (VALVE REMAIN CLOSED)
- Calibration takes about 10 minutes.
- **F5** Channel Supplementary Table, the Rel Gains should be ~ 1. If not, seek assistance.
Baseline [counts] ~ 200. If not, seek assistance.
- **F8** Return Main Keys.

Nd acquisition

- Check that filament currents are zero.
- **F5** MS Control
- **F3** Turn magazine to the desired sample position (Note: **S** first after magazine change or computer crash to initialize the software/magazine location). Then **Enter**.
- Check that the tube valve is closed ie **F2** displays "Open Valve"
- Turn up the Ionisation filament current to ~4.5A, whilst watching the Source vacuum gauge and ensuring the vacuum remains below 1E-6mbar. Allow the vacuum to recover to ~1E-7mbar (a few minutes).

- **F2** open the tube valve and check for beam. (Check that Beam Valve 2 is in AUTOMATIC position from the overnight CLOSED position).
- If there is no beam, turn up filament currents till a beam appears, typically 4.9A on Ionisation filament (or ~10-20mV 187Re) then up to ~1.6A maximum on the Evaporation filament. If no beam, try **F6** Peak Centre and/or focussing (noting any dials settings first). If still no beam, seek assistance.
- At the first sign of 145Nd (1mv or more). **F6** Peak Centre.
- It's now more convenient to go to the Graphical display to focus the beam.
- **F8** Return main key.
- **F6** Graphic/Interplot.
- Maximize the beam using magazine knob. Only move a mm or so in each direction else the electrical contact is broken.
- Use the **Lens 1** and **Lens 2** dials to again maximize the beam. The beam size can often be increased by moving both dials either higher or lower.
- Finally focus using the **Z** dial.
- If there has been a significant change in beam size, a second focus may further optimize the beam.
- Over a few minutes, increase 144Nd (in cup 6) to 300-500mV (Evaporation filament current < ~1.9A, otherwise there is the risk of sample burning off before the measurement can be completed).
- Repeat focussing.
- **F8** Abort
- **F8** Return
- **F1** ACQ
- **F1** Single ACQ. Fill in the details as shown below

ANALYSIS SUPPLEMENTARY TABLE:

ACQ Experiment:	18
ACQ Ident:	Sample Name
ACQ Filename:	Last 3 digits of the run number and the position of the magazine/CRD
ACQ Element (see Configuration Supplementary Table):	ND
ACQ Switch:	3
Minimum pilot level [mV]:	N/A
Analysis:	ND
Comment:	STATIC/DYNAMIC
Printer Report:	No Report
SEQ Startline:	N/A
SEQ Endline:	N/A
ACQ User Program:	N/A

- **F2** Save Supplementary Table.
- **F8** Edit End.
- Top of Form (Y) **Enter**.

When run has finished, set mass 145 in cup 5 (ie **F5** MS Control then **F4** Input Mass).

- **F2** Open valve.
- Peak centre and refocus beam (if necessary).
- Turn up Evaporation filament current to 144Nd 600-1000mV (corresponding 145Nd ~ 370mV).
- Typically 4.8-4.9A Ionization and <~2.1A Evaporation. (Evaporation filament current can go higher but use caution).
- Repeat focussing.
- **F8**
- **F8**

ACQ Experiment:	17
ACQ Ident:	Sample Name
ACQ Filename:	Last 3 digits of the run number and the position of the magazine/CRD
ACQ Element (see Configuration Supplementary Table):	ND
ACQ Switch:	1
Minimum pilot level [mV]:	N/A
Analysis:	ND
Comment:	STATIC/DYNAMIC
Printer Report:	No Report
SEQ Startline:	N/A
SEQ Endline:	N/A
ACQ User Program:	N/A

- **F1** ACQ
- **F1** Single ACQ. Fill in the details as show below
- **F2** Save Supplementary Table.
- **F8** Edit End.
- Top of Form (Y) **Enter**.

Sm acquisition

- Check that filament currents are zero.
- **F5** MS Control
- **F3** Turn magazine to the desired sample position (Note: **S** first after magazine change or computer crash to initialize the software/magazine location). Then **Enter**.
- Check that the tube valve is closed ie **F2** displays “Open Valve”
- Turn up the Ionisation filament current to ~4.5A, whilst watching the Source vacuum gauge and ensuring the vacuum remains below 1E-6mbar.
- Allow the vacuum to recover to ~1E-7mbar (a few minutes).
- **F2** open the tube valve and check for beam. (Check that Beam Valve 2 is in AUTOMATIC position from the overnight CLOSED position).

- If no beam, turn up filament currents till a beam appears, typically 4.9A on Ionisation filament (or ~10-20mV 187Re) then up to ~1.6A maximum on the Evaporation filament. If no beam, try **F6** Peak Centre and/or focussing (noting any dials settings first). If still no beam, seek assistance.
- At the first sign of 149Sm (1mv or more). **F6** Peak Centre.
- It's now more convenient to go to the Graphical display to focus the beam.
- **F8** Return main key.
- **F6** Graphic/Interplot.
- Maximize the beam using magazine knob. Only move a mm or so in each direction else the electrical contact is broken.
- Use the **Lens 1** and **Lens 2** dials to again maximize the beam. The beam size can often be increased by moving both dials either higher or lower.
- Finally focus using the **Z** dial.
- If there has been a significant change in beam size, a second focus may further optimize the beam.
- Over a few minutes, increase 144Nd (in cup 6) to 300-500mV (Evaporation filament current < ~1.9A, otherwise there is the risk of sample burning off before the measurement can be completed).
- Repeat focussing.
- **F8**
- **F8** Fill in the details as shown below

ANALYSIS SUPPLEMENTARY TABLE

ACQ Experiment:	17
ACQ Ident:	Sample Name
ACQ Filename:	Last 3 digits of the run number and the position of the magazine/CRD
ACQ Element (see Configuration Supplementary Table):	ND
ACQ Switch:	1
Minimum pilot level [mV]:	N/A
Analysis:	ND
Comment:	STATIC/DYNAMIC
Printer Report:	No Report
SEQ Startline:	N/A
SEQ Endline:	N/A
ACQ User Program:	N/A

- **F2** Save Supplementary Table.
- **F8** Edit End.
- Top of Form (Y) **Enter**.

Sr acquisition:

- **F8** return MainKeys.
- **F5** MS Control.

- **F3** Turn magazine to the desired sample position (Note: **S** first after magazine change or computer crash to initialize the software/magazine location).
- Check that the tube valve is closed ie **F2** displays “open”
- Turn up the filament current to ~2.6-3.0A or 1200C, whilst watching the Source vacuum gauge and ensuring the vacuum remains below 1E-6mbar. There is typically a surge between ~1 – 2 A filament current. Aim for 1200C with maximum filament current 3A.
- Allow to stand for a few minutes.
- Rb damages the faraday measurement cups and must be STRICTLY AVOIDED so if any appears (mass 85 in cup 5) immediately close the tube valve (**F2**). It will typically burn off before (or simultaneously with) Sr in a few minutes but can be frustratingly persistent.
- Back off the filament current by ~.3 A.
- **F2** open the tube valve (if any 85Rb present, close it again, turn the filament current up to 2.6+A and wait a few minutes for it to burn off).
- If no 85Rb appears slowly turn up the filament current till 88Sr appears. If it hasn't appeared by ~3.3A or 1350C check for a beam ie
- **F5** Input Channel
- **2** Enter
- Then check peak centre **F6** and/or focussing, but note dial positions and return to them if no beam found.
- At the first sign of 88Sr (1mv or more). **F6** peak centre.
- It's now more convenient to go to the Graphical display to focus the beam.
- Maximize the beam using magazine knob. Only adjust a mm or so in each direction otherwise the electrical contact is broken.
- Use the **Lens 1** and **Lens 2** dials to again maximize the beam. The beam size can often be increased by moving both dials either higher or lower.
- Finally focus using the **Z** dial.
- If there has been a significant change in beam size, a second focus may further optimize the beam.
- Over a few minutes, increase the 88Sr to 2000mV (but temperature should be < 1500C and filament current < 4.0A, otherwise there is the risk of sample burning off before the measurement can be completed).
- **F8** Abort
- **F8** Return
- **F1** ACQ
- **F1** Single ACQ. Fill in the details as shown below.

ACQ Experiment:	1
ACQ Ident:	Sample Name
ACQ Filename:	Last 3 digits of the run number and the position of the magazine/CRD
ACQ Element (see Configuration Supplementary Table):	ND
ACQ Switch:	1
Minimum pilot level [mV]:	N/A
Analysis:	ND
Comment:	STATIC/DYNAMIC
Printer Report:	No Report
SEQ Startline:	N/A
SEQ Endline:	N/A
ACQ User Program:	N/A

- **F2** Save Supplementary Table.
- **F8** Edit End
- **Enter** to start the run.

Supplementary Table 12 This shows the parameters that the mass spectrometer operated for the Sr acquisition of each sample.

FILAMENT S	MAG POSITIO N	MAG NO	SAMPLE	MONITOR		FILS CURRENT		EXTP NO	FINSIH
				<i>I</i>	<i>V (mv)</i>	EVAP	ION		
Re	2	1	E13.11	88	.4	3.2	-	2	N
Ta	8	1	E13.12	88	1.0	3.5	-	2	Y
Ta	3	1	E13.18	88	2	3.4	-	2	Y
Ta	4	1	Blank 1694	88	2	3.6	-	2	Y
Ta	1	2	E13.23	88	1.8	3.8	-	2	Y
Ta	2	2	E13.27	88	1.8	3.9	-	2	N
Ta	3	2	E13.19	88	1.5	3.4	-	2	Y

Supplementary Table 13 This shows the parameters that the mass spectrometer operated for the Nd and Sm acquisition of each sample.

FILAMENT S ND	MAG POSTION	MAG NO	SAMPLE	MONITOR		FILS CURRENT		EXTP NO	FINSI H
				<i>I</i>	<i>V (mv)</i>	EVAP	ION		
Ta-Re	1	1	E13.11	144	.05	1.7	4.9	18/17	Y
Ta-Re	2	1	E13.12	144	1.0	1.2	4.9	18/17	Y
Ta-Re	3	1	E13.18	144	2	1.1	4.9	18/17	Y
Ta-Re	4	1	E13.19	144	2	1.7	4.9	18/17	Y
Ta-Re	5	2	E13.23	144	1.8	1.8	4.9	18/17	Y
Ta-Re	6	2	E13.27	144	1.8	2.0	4.9	18/17	N
Ta-Re	7	2	Blank	144	1.5	1.3	4.9	18/17	Y

			1694						
FILAMENT S Sm	MAG POSTION	MAG NO	SAMPLE	MONITOR		FILS CURRENT		EXTP NO	FINSI H
				I	V (mv)	EVAP	ION		
Ta-Re	1	1	E13.11	149	0.3	1.9	4.9	18/17	Y
Ta-Re	2	1	E13.12	149	.2	1.5	4.9	18/17	Y
Ta-Re	3	1	E13.18	149	.2	0.5	4.9	18/17	Y
Ta-Re	4	1	E13.19	149	1.79	1.5	4.9	18/17	Y
Ta-Re	5	1	E13.23	149	1.50	1.9	4.9	18/17	Y
Ta-Re	6	1	E13.27	149	1.50	1.8	4.9	18/17	Y
Ta-Re	7	1	Blank 1694	149	0.08	1.9	4.9	18/17	Y

ICP-MS

1. Weigh 50-100g of rock powder into a clean 15ml Teflon vial or high pressured bomb. The amount of sample is weighed on a 4 to 5 decimal place balance.
2. As soon as the weight is stabilised and can be recorded, carefully squirt 7M HNO₃ to cover the dry powder. This is done to prevent any powder from getting out of the vial due to the static.
3. Remove the vial from the balance and loosely cap it to take into the clean room.
4. Add 4ml of concentrated HF to the vial and evaporate the solution down on the hotplate at 140°C. Add a small amount of 7M HNO₃ shortly before it is dry to help the breakdown of the insoluble fluorides that may have been formed.
5. Once dry add 2ml of 7M HNO₃ and 4ml of concentrated HF and either cap and put it on the hotplate at 140 °C for 3 days or place the bombs and heat in the oven for 5 days at 190°C. Spray inside the metal jacket and on the threads with minimal amount of Ezy Glide (Teflon) spray. Place bomb in the jacket with fittings and screw the top closed tightly
6. After this time evaporate the sample on the hot plate at 140 °C, again adding 7M HNO₃ shortly before it is dry. Add 6M HCL and either cap and heat the hotplate at 140 °C for 2 days or return to the oven at 160 °C for 2 days if using the bombs.
7. After this time, evaporate the sample to dryness on the hotplate at 140 °C.
8. Place 2or 3 mL of 7M nitric acid and evaporate to dryness.
9. After they are dry, allow the vials to cool down to room temperature and add 5MI 5% HNO₃ to the vial whilst on the balance. Record the weight of the acid added,
10. Pour the sample into a clean 2ml centrifuge tube and centrifuge at 13,200 rpm for 5 minutes.

- a. Measure the weight of solution before and after the 1.5mL aliquot is taken.
11. Record the original weight of the ICP-MS tube before adding the solution. Add in 0.5mL of solution with 4.5 mL of 5% nitric acid. This will give an order of 1000X dilution. Ensure that each step is weighed and measured carefully (Other dilutions can be used if needed. 800x and 2000x).
- a. It is also advantageous to create a 5000x dilution of each sample to be able to check for the influence of the rock matrix on the analysis.

Preparation of the rock standards

These are prepared in the same manner as your rock samples however, you will need a final solution at 800x, 1000x, 2000x and 5000x. This will provide 5 calibration points for the curve.

Calculations of the dilutions

Eg: 2000x Dilution

We are already at 100X dilution.

$$\frac{4.5 + x}{x} = 20$$

$$4.5 + x = 20x$$

$$= 0.236$$

NOTE: The dilution does not have to be 2000 exactly. It is just necessary to know what your samples are diluted to. This is done by making sure each section is accurately measured.

Synthetic Standards.

The calibration line created can be used to check against the synthetic solutions. This solution will be 10, 20, 50, 200 and 500 ppb

Solution 'A' and 'B' need to be collected from Adelaide Microscopy. These synthetic standards should be made up just before samples are ready to be run on the ICP.

To make up these solutions approximately 1g of each solution 'A' and 'B' is added to 18g of 5% nitric acid. This will give 20g of solution with a dilution of 500ppb. The solution is then diluted to 200, 100, 50, 20, 10 ppb. A blank is also needed, which is just 5ml of 5% nitric acid.

Dilutions are calculated by utilising $C_1V_1=C_2V_2$

E.g 20ppb

$$500 \times V_1 = 20 \times 5$$

$$= \frac{100}{500}$$

= 0.2ml

Internal Standard

Indium and/or Rhenium is used as an internal standard for the analysis, so 50mL of a 200ppb

Indium/Rhenium solution needs to be made up. This solution is then continually introduced to the ICPMS during the analysis in order to monitor the stability of the instrument and to check that the samples and standards have a good matrix match. To achieve 50 g/ml of 200ppb solution:

1g/ml of Rhenium and 1g/ml of Rhenium is accurately weighed out in 48g/ml of 5% nitric acid.

Once the samples have been prepared they will be analysed using the ICP-MS instrument located at Adelaide Microscopy.

Supplementary Table 1 ICP-MS dilution factor sheet

Description Samples	B - I: Weighing out of rock powder - remember to correct for density variation of the acid					Take 1.5ml, filter it, extract (J,K)0.5ml and make up to (L) 5ml total				
	Sample Weight (g)	Sample + Vial + Acid	Acid Weight (5%HNO3)	Total Weight	Dilution Factor	Weight of ICP- MS Tube (g)	Weight of solution (g)	Weight of 5%HNO3	Dilution Factor	Total Dilution
E13.11 #1	0.052225	21.44786	5.26053	5.312755	101.7281953	2.9758	0.53126	4.65201	9.756559877	992.5172287
E13.11 #2	0.050295	22.07925	4.79191	4.842205	96.27607118	2.975659	0.51452	5.2584	11.22001088	1080.218567
E13.12 #1	0.0517	62.81131	5.2366	5.2883	102.2882012	2.97541	0.51608	4.60122	9.915710743	1014.260215
E13.12 #2	0.05065	62.87775	5.3587	5.40935	106.798618	0	0	0		0
E13.18 #1	0.05263	23.06998	5.52018	5.57281	105.8865666	2.98582	0.51085	4.57677	9.959126945	1054.537759
E13.18 #2	0.05307	21.61689	5.32998	5.38305	101.433013	2.97522	0.51125	4.58744	9.972987775	1011.590199
E13.19 #1	0.05037	21.74732	5.50604	5.55641	110.311892	2.98615	0.51336	4.42857	9.626636279	1061.932461
E13.19 #2	0.051365	21.55225	5.2695	5.320865	103.5893118	2.98641	0.51299	4.59671	9.960623014	1031.814083
E13.23 #1	0.053495	61.56227	5.16117	5.214665	97.47948406	2.99089	0.51152	4.61983	10.03157257	977.8725183
E13.23 #2	0.0525	61.76351	5.17923	5.23173	99.652	2.97565	0.51395	4.61434	9.97818854	994.3464444
E13.27 #1	0.050445	61.55799	5.1497	5.200145	103.0854396	2.97548	0.512	4.5176	9.8234375	1012.653373
E13.27 #2	0.052045	61.88111	5.36641	5.418455	104.1109617	2.97552	0.73533	5.37396	8.308228958	864.9777066
BHV-02 #1	0.05032	23.91987	6.51044	6.56076	130.3807631	2.97568	0.7077	4.60841	7.511812915	979.3959003
BHV-02 #2	0.05018	21.60867	5.17964	5.22982	104.2212037	2.19492	0.59234	4.61141	8.785072762	915.5908576
BCR-2 #1	0.049785	21.40412	5.15282	5.202605	104.5014563	2.97632	0.51211	4.62394	10.02919295	1048.065268
BCR-2 #2	0.05118	21.42683	5.13737	5.18855	101.3784682	2.9864	0.51577	4.76276	10.23427109	1037.534726
G2 #1	0.05025	62.783423	5.110343	5.160593	102.6983682	2.98613	0.51134	4.57141	9.940059452	1020.827885
G2 #2	0.051665	61.446318	5.136368	5.188033	100.4167812	2.99113	0.50691	5.10636	11.07350417	1111.965645

ARGON ARGON DATING:

Two samples from the western Ethiopian Shield for $^{40}\text{Ar}/^{39}\text{Ar}$ dating and separated unaltered, optically transparent, 150 μm -size, muscovite. These minerals were separated using a Frantz magnetic separator, and then carefully hand-picked under a binocular microscope Olympus SZ51. The selected muscovite minerals were further leached in diluted HF for one minute and then thoroughly rinsed with distilled water in an ultrasonic cleaner.

Samples were loaded into 2 large wells of one 1.9 cm diameter and 0.3 cm depth aluminum disc. These wells were bracketed by small wells that included Fish Canyon sanidine (FCs) used as a neutron fluence monitor for which an age of 28.305 ± 0.036 Ma (1σ) was adopted (Renne et al., 2010) based on the calibration by (Jourdan and Renne (2007)). The discs were Cd-shielded (to minimize undesirable nuclear interference reactions) and irradiated in the Hamilton McMaster University nuclear reactor (Canada) in position 5C. The mean J-values computed from standard grains within the small pits range from 0.0026752 ± 0.0000040 (0.15%) to 0.0026644 ± 0.000054 (0.20%) determined as the average and standard deviation of J-values of the small wells for each irradiation disc. Mass discrimination was monitored using an automated air pipette and provided a mean value of 1.00646 ± 0.00238 per dalton (atomic mass unit) relative to an air ratio of 298.56 ± 0.31 (Lee et al., 2006). The correction factors for interfering isotopes were $(^{39}\text{Ar}/^{37}\text{Ar})_{\text{Ca}} = 7.30 \times 10^{-4}$ ($\pm 11\%$), $(^{36}\text{Ar}/^{37}\text{Ar})_{\text{Ca}} = 2.82 \times 10^{-4}$ ($\pm 1\%$) and $(^{40}\text{Ar}/^{39}\text{Ar})_{\text{K}} = 6.76 \times 10^{-4}$ ($\pm 32\%$).

The $^{40}\text{Ar}/^{39}\text{Ar}$ analyses were performed at the Western Australian Argon Isotope Facility at Curtin University, operated by a consortium consisting of Curtin University and the University of Western Australia. The samples were fusion heated using a 110 W Spectron Laser Systems, with a continuous Nd-YAG (IR; 1064 nm) laser rastered over the sample during 1 minute to ensure a homogeneously distributed temperature. The gas was purified in a stainless steel extraction line using three SAES AP10 getters and a liquid nitrogen condensation trap. Ar isotopes were measured in static mode using a MAP 215-50 mass spectrometer (resolution of ~ 500 ; sensitivity of 4×10^{-14} mol/V) with a Balzers SEV 217 electron multiplier mostly using 9 to 10 cycles of peak-hopping. The data acquisition was performed with the Argus program written by M.O. McWilliams and ran under a LabView environment. The raw data were processed using the ArArCALC software (Koppers, 2002) and the ages have been calculated using the decay constants recommended by Renne et al. (2010). Blanks were monitored every 3 to 4 steps and typical ^{40}Ar blanks range from 1×10^{-16} to 2×10^{-16} mol. Individual errors in are given at the 1σ level. Our criteria for the determination of plateau are as follows: plateaus must include at least 70% of ^{39}Ar .

THINSECTIONS:

10 samples were sent to Pontifex and Associates Pty Ltd. Thin-sections were made polished and uncovered. The following method was used.

1. First, a small slab is cut, approximately 25mm x 55mm, x 8mm thick, using a 250mm diameter rock-cutting saw blade with a continuous diamond rim. Two samples were impregnated with epoxy, due to their tendency to fracture.
2. A top surface on the slab, is manually ground flat on a bench-mounted, horizontal diamond grinding wheel Habit-brand, grit size 64.

3. The coarse ground top surface is warmed on a hot plate (at 50°C), and the top coarse-ground surface is impregnated with an epoxy mix of Araldite LC191 resin, with HY951 hardener, ratio 8:1. This surface is then manually more finely ground flat using 600 SiC grit, on a zinc-lap or glass plate, using water as a lubricant. This flat finely ground surface is cleaned, checked manually for “perfection”, (if open porosity is still exposed another veneer of epoxy is applied), is then glued onto a clean, dry glass slide, ground to a known thickness, using a UV curing, cyanoacrylate liquid adhesive “Loctite Impruv 36331”. [Exposure to a UV light of the glued interface through the back of the glass slide cures the adhesive in 2 to 3 minutes. This is a permanent bond, and the rock (or eventual wafer) cannot be ever separated from the glass.
4. The block mounted on glass is then cut off using a trim saw with a thin continuous diamond rimmed sawblade (Diatrenn E2-G), to leave a thickness of about 1mm of the sample slab (glued onto the glass slide), with the top surface exposed for further processing.
5. The 1mm slab thickness is further ground down on a diamond wheel (Habit D76) held within a special jig attachment by vacuum, using water as a lubricant. This reduces the slab thickness stuck on the glass, to a wafer of about 120 micron (0.12mm).
6. The glass slide of known thickness with the glued-on rock wafer is then loaded and held in place on the face of a special jig, and lapped flat on a Logitech machine, to a final petrographic thickness of the rock wafer, of 30 micron, using 600 SiC grit as the grinding abrasive, and water as a lubricant.
7. When the Logitech lapping cycle is finished, the quality of the wafer on the glass is assessed, also optically checked for the required 30 micron thickness, and when confirmed as correct, the section is cleaned and covered with a glass coverslip, using the same UV curing adhesive as listed above. Again this is a permanent fix, i.e. the coverslip cannot be removed. The final thin section is then again cleaned and labelled.

MICROPROBE

Machine used: CAMECA SX 5

Loading a sample:

To place a sample into the microprobe: Sample exchange-Transfer sample into microprobe. Follow the prompts.

Next, turn the extraction handle on the airlock to the extract symbol




Open the airlock (push airlock handle in and swing up). Note that handle locks and rotates slightly. Push extraction handle in all the way, then pull out to remove sample block. Close the airlock (rotate handle and swing down). Note that handle locks and moves out slightly.

Follow the prompts on the screen.

After a minute or so, the airlock is vented. Open the airlock door by depressing the latch button and remove the sample cassette by pushing the sample block onto the extraction handle until it clicks and releases the sample block.

Change the samples as needed on the sample preparation pad.

Place the sample on the sample preparation pad and change samples and standard mounts as necessary. Be sure to document sample placement and identification by filling out the sample mount map in one of the 3 ring binders. Be sure to orient the sample block correctly. The small hole goes to the front of the sample mount. See the sample location chart for the correct orientation.

Place the prepared sample block back in the airlock: When ready, open the airlock door (depress the spring latch) and turn the extraction handle to the insert symbol  Then slide the sample block onto the extraction handle rails until it clicks.

Close the airlock door. During this time, the system may request that the gun valve be turned to position 2. If this is requested, turn the gun valve to position 2 and wait for the Vacuum ready message, if not, then the arlk command can be given immediately. When ready, pump out the airlock: Now open the airlock (push airlock handle in and swing up). Note that handle locks and rotates slightly. Push extraction handle in all the way, then pull the empty extraction handle back out all the way. Close the airlock (rotate handle and swing down). Note that handle locks and moves out slightly. Wait until the system is ready as seen on the screen.

Turn the beam on via the beam and set up tab. Ensuring that the scanning is 'on' focus the beam on both the back scattered image and the reflected light

To navigate use the joystick to move around the slide. To check the composition of the mineral, turn the scanning to 'off'. Click on the EES screen and hit 'Acquire'. Drag the line to the peaks to determine what the mineral is composed of.

Imaging is done via the SEM tab with a frame time of 15.32. Tick the box and press save and display. Once this is done, un-tick the box and return to 0.32 for the frame time.

To store points, ensure that the reflected image is focused. Move the white cross to desired position. On the left hand screen where the software is displayed, click 'digitize'. Type in the name of the file (E13-26 'chrome spinels'). Finally, click add new unknown. Adding a single point is done by clicking 'single point'

Once all points have been selected, select all. Click sample set up, then yes. Finally, to start the acquisition, press the button 'run samples'.

XRF ANALYSES

Major Elements

The samples were dried in an oven at 110° for over two hours to remove the absorbed moisture.

They were then weighed into alumina crucibles and ignited overnight in a furnace at 960°, to yield the Loss on Ignition (LOI) values.

Approximately 1g of the ignited material was then accurately weighed with 4g of flux (commercially available as type 12:22, comprising 35.3% lithium tetraborate and 64.7% lithium metaborate).

The sample-flux mixture was fused using a propane-oxygen flame, at a temperature of approx. 1150°, using Pt-Au crucibles, and cast into a preheated mould to produce a glass disc suiSupplementary Table for analysis.

The samples were analysed with a Philips PW 1480 X-ray Fluorescence Spectrometer, using an analysis program calibrated against several international and local Standard Reference Materials (SRM's). A dual-anode (Sc-Mo) X-ray tube was used, operating at 40kV, 75mA.

Trace Elements

About 5-10g of sample powder was mixed with nominally 1ml of binder solution (Poly Vinyl Alcohol) and pressed to form a pellet.

This was allowed to dry in air and was heated for a further 1 to 2 hours in a 60° oven to ensure that the pellet was completely dry before analysis.

The samples were analysed using a Philips PW 1480 XRF Spectrometer, using several analysis programs covering suites of from 1 to 7 trace elements, with conditions optimised for the elements being analysed. The programs were calibrated against many (30 or more in some cases) local and international SRM's. The dual-anode Sc-Mo tube (operated at sufficient voltage to excite the Mo) and an Au tube were used for the analyses.